Study of Non-Strange Baryon Resonances with Meson Photoproduction

B. Krusche[1] and S. Schadmand[2]
[1]Institut für Physik, Universität Basel, CH-4056 Basel, Switzerland
[2]II Physikalisches Institut, Universität Giessen, D-35392 Giessen, Germany

February 8, 2008

Abstract

Photoproduction of mesons is an excellent tool for the study of nucleon resonances. Complementary to pion induced reactions, photoproduction on the free proton contributes to the determination of the basic properties of nucleon resonances like excitation energy, decay widths, spin, and the coupling to the photon. Photoproduction from light nuclei, in particular from the deuteron, reveals the isospin structure of the electromagnetic excitation of the nucleon. During the last few years, progress in this field has been substantial. New accelerator facilities combined with state-of-the-art detector technologies have pushed the experiments to unprecedented sensitivity and precision. The experimental progress has been accompanied by new developments for the reaction models, necessary to extract the properties of the nucleon states, and for modern hadron models which try to connect these properties to QCD. The emphasis of this review lies on the experimental side and focuses on experiments aiming at precise studies of the low-lying nucleon resonances.

Contents

1 Introduction **2**

2 Photoexcitation of Free and Quasi-free Nucleons **8**

3 The Δ-Resonance Region **15**
3.1 *Quadrupole Strength in the $N \to \Delta$ Transition* 17
3.2 *Helicity Dependence of Pion Photoproduction in the Δ-Range* 24
3.3 *The Magnetic Moment of the Δ-Resonance* 26
3.4 *The Excitation of the Δ-Resonance on the Neutron* 30

4 The Second Resonance Region **36**
4.1 *Single π Photoproduction and the $P_{11}(1440)$ and $D_{13}(1520)$ Resonances* 40
4.2 *η-Photoproduction and the $S_{11}(1535)$-Resonance* 47
4.2.1 *η-Photoproduction from the Proton* 49
4.2.2 *η-Photoproduction from Light Nuclei* 60
4.3 *Double Pion-Photoproduction* 66

5 Conclusion and Perspectives **72**

6 Appendix **76**

1 Introduction

During the last 30 years Quantum Chromo Dynamics (QCD), the formal theory of the color interactions between quarks, emerged as the theory of the strong interaction. The perturbative approach to this theory has been extremely successful in the high energy regime where it has been tested by numerous experiments. However, in the low energy regime, the perturbative approach is meaningless, and a solution of QCD is not known on a scale typical for the mass of the nucleon and its excited states, where the strong coupling constant becomes large. Lattice gauge calculations have provided results for the ground state properties and very recently also for excited states of the nucleon (see e.g. [1]-[4]). However, the prediction of the excitation spectrum of nucleons is still out of reach even for the most powerful computer systems. This situation offers both a challenge and a chance: we do want to understand the physics laws governing the building blocks of matter at low energies, in the regime where we encounter them in nature. On the other hand, it is obvious that the complex many-body system 'nucleon' offers the ideal testing ground for concepts of the strong interaction in the non-perturbative regime.

Perturbative QCD at high energies deals with the interactions of quarks and gluons. However, our picture of the nucleon is more related to effective constituent quarks and mesons that somehow subsume the complicated low energy aspects of the interaction generating the nucleon many-body structure of valence quarks, sea quarks, and gluons. Therefore, the most important step towards an understanding of nucleon structure is the identification of the relevant effective degrees-of-freedom, which naturally must reflect the internal symmetries of the underlying fundamental interaction. This step is attempted in the framework of constituent quark models of baryons, which have contributed substantially to our understanding of the strong interaction. In a sense, these models were the starting point for the development of QCD.

The most basic version of the constituent quark model, using a harmonic oscillator potential, had its origin in the work of Gell-Mann [5], Greenberg [6], Dalitz [7], and collaborators. Copley, Karl, and Obryk [8] and Feynman, Kislinger, and Ravndal [9] gave the first clear evidence for the underlying SU(6)$\otimes$O(3) symmetry of the hadron spectrum. Later, Koniuk and Isgur [10] laid the basis for the description of the electromagnetic and strong decays in the framework of the quark model. The classification of the mesons and baryons into the well-known multiplet structures as derived from the symmetry, and the description of the hadronic excitation spectrum with only few fitting parameters were a striking success of the model. An excellent overview over modern quark models is given by Capstick and Roberts [11]. Most of the models start from three equivalent constituent quarks in a collective potential. The masses of the up and down constituent quarks range from 220 MeV for relativistic models to 330 MeV for non-relativistic models. Here, the quarks are not point-like but have electric and strong form factors. The potential is generated by a confining interaction, for example in the flux tube picture, and the quarks interact via a short range residual interaction. This fine-structure interaction, usually taken as color magnetic dipole-dipole interaction mediated via one-gluon-exchange (OGE), is responsible for the spin-spin and spin-orbit dependent terms.

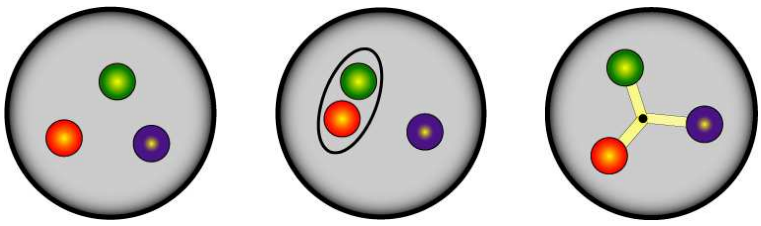

Figure 1: Effective degrees-of-freedom in quark models: three equivalent constituent quarks, quark - diquark structure, quarks and flux tubes?

However, alternative concepts are not a priori ruled out. In fact, models have been proposed which are based on other degrees-of-freedom (see fig.1). One group of models describes the nucleon structure in terms of a quark - diquark ($q - q^2$) cluster (see Anselmino et al. for a review [12]). If the

diquark is sufficiently strongly bound, low lying excitations of the nucleon will not include excitations of the diquark. Therefore, these models predict *fewer* low-lying excited states of the nucleon than the conventional quark models. On the other hand, the number of states would be *increased* in an algebraic model proposed by Bijker et al. [13, 14]. The model is based on collective excitations of string-like objects carrying the quantum numbers of the quarks. Radial excitations arise from rotations and vibrations of these strings. Alternative models are available not only in view of the 'constituents' but also in view of the residual interaction. In conventional models, this interaction is due to OGE. Meanwhile, Glozman and Riska [15] have developed a model where the residual interaction is due to the exchange of Goldstone bosons, taken to be the pseudo-scalar octet mesons. This is a radically different picture since in this case gluons do not contribute at all to the nucleon structure. In addition, this model leads to a quark - diquark clustering effect giving rise to specific selection rules for the decay properties of excited baryons [16].

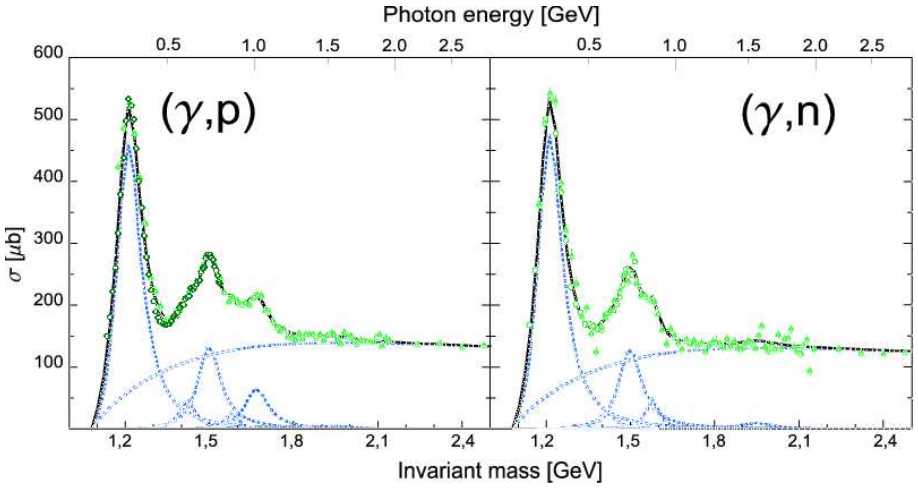

Figure 2: Cross section for total photoabsorption on the proton (left hand side) and the neutron (right hand side) [17]. Points: measured data, curves: fit of Breit-Wigner shapes of nucleon resonances ($P_{33}(1232)$, $P_{11}(1440)$, $D_{13}(1520)$, $S_{11}(1535)$, $F_{15}(1680)$(only for proton), and $F_{37}(1950)$) and a smoothly varying background.

The number of excited states with definite quantum numbers follows directly from the number of effective degrees-of-freedom and their quantum numbers in the models. Consequently, a comparison of the experimentally determined excitation spectrum to the model predictions should allow the determination of the number of degrees-of-freedom. However, from the experimental point of view the situation is quite different from atomic or nuclear physics. The dominant decay channel of nucleon resonances is the hadronic decay via the emission of mesons. Thus, the lifetimes of the excited states are typical for the strong interaction ($\tau \approx 10^{-24}$s) with corresponding widths of a few 100 MeV. The spacing of the resonances is often no more than a few 10 MeV such that the overlap is large. This makes it difficult to identify and investigate individual states, as demonstrated in fig. 2. The figure shows the cross section for total photoabsorption [17], i.e. for the reaction $\gamma N \to NX$ on the proton and the neutron. The latter was measured in quasifree kinematics from the deuteron. In this simple picture the cross section was fitted with a smooth background and Breit-Wigner curves for the excited states which are labeled in the usual notation as $L_{2I2J}(W)$. Here, W is the mass, L=0,1,2,... the angular momentum for the decay into the $N\pi$-channel given in the spectroscopic notation as S,P,D,... and I, J are isospin and spin of the resonances, respectively. Only the lowest lying excited state of the nucleon, the Δ-resonance ($P_{33}(1232)$), corresponds to an isolated peak in the spectrum. At masses around 1500 MeV, several resonances ($P_{11}(1440)$, $D_{13}(1520)$, $S_{11}(1535)$) contribute to the broad resonance structure observed in the spectrum. This energy regime is called the second resonance region. Inclusive measurements like photoabsorption do not allow a detailed investigation of such closely spaced resonances.

Which experimental tools are available for the study of nucleon resonances? The dominant decay of any excited nucleon state is the emission of mesons via the strong interaction. Electromagnetic decays via photon emission have typical branching ratios below the 1% level and are extremely difficult to identify in the presence of large background levels. Meson production in hadron induced reactions

profits from large cross sections and has been intensely used for the study of nucleon resonances.

Beams of stable baryons like protons, deuterons, and α-particles have been used at many accelerators. Recently, the cooler rings at CELSIUS and COSY have been active in this field. Purely baryon induced reactions favor the exploration of the isospin degree of freedom. However, the interpretation is quite involved since initial and final state are governed by the strong interaction. Here, the presence of at least two baryons in the final state gives rise to complex final state interaction effects. Furthermore, due to the large mass of the beam particles, high beam energies must be employed in order to access the resonance regions. Much of the more recent work with baryon beams concentrates on high sensitivity studies of meson production thresholds. An excellent overview over this topic is given by Moskal, Wolke, Khoukaz, and Oelert [18].

The most widely used reactions for the study of nucleon resonances use beams of long-lived mesons. In particular, the elastic scattering of charged pions off the nucleon, and inelastic pion induced reactions, contributed to the experimental data base. Again, the hadronic cross sections are large, and the isospin degree of freedom is accessible. Meanwhile, the final state with only one baryon is less complicated. Sophisticated multipole analyses of pion induced reactions, followed by a parameterization of the partial waves in terms of resonances and background contributions, have been performed by different groups (see e.g. [19]-[26]). These results still form the backbone of nucleon resonance properties. However, the exclusive use of pion induced reactions would bias the data base for resonances coupling weakly to the πN channel. Indeed, a comparison of the excitation spectrum predicted by modern quark models to the experimentally established set of nucleon resonances results in the problem of 'missing resonances': many more states are predicted than have been observed. But is this evidence for inept effective degrees-of-freedom in the models or a simple experimental bias? Already more than 20 years ago, Koniuk and Isgur have argued in a paper [27] entitled 'Where have all the resonances gone?' that the reason for the mismatch is the decoupling of many resonances from the partial wave analysis of pion scattering. These resonances can only be found when other initial and/or final states are investigated. In fact, recent quark models [28], predict a number of the unobserved resonances to have large decay branching ratios for the emission of mesons other than pions. In this case, the nucleon should ideally be excited by scattering of the respective mesons. However, most of them are short lived making the preparation of secondary beams impossible. The use of reactions induced by the electromagnetic interaction offers an alternative.

Detailed tests of quark models cannot be achieved with excitation spectra alone. In this sense, the situation for nucleon physics is similar to nuclear physics. In both cases, the excitation energies and quantum numbers of the states do not provide the most sensitive observables. More crucial tests come from the transitions between the states which reflect their internal structure and are more sensitive to the model wave functions. Photo- and electroproduction of mesons is particularly interesting for this purpose since the rich information connected to the electromagnetic transition amplitudes can be accessed in addition to the dominant hadronic decay modes. The photon couples only to the spin-flavor degrees-of-freedom of the quarks revealing their spin-flavor correlations which are related to the configuration mixing predicted by the models. There is a price to pay for the advantage. The electromagnetic cross sections are naturally much smaller than the hadronic ones. More importantly, photon induced reactions can have significant non-resonant contributions, called 'background'. For example, nucleon Born terms or vector meson exchange complicate the extraction of the resonance properties. Therefore, it is mandatory to use reliable reaction models for the analysis of the photoproduction data. This situation is schematically illustrated in fig. 3. Reaction models are used to extract hadron properties like excitation energies, widths, and branching ratios to different decay channels from the physical observables. QCD inspired models of the hadron are used to make predictions for these properties. More recently, quark models of the nucleon have been developed which directly make predictions for the physical observables (see sec. 2).

The detailed understanding of the elementary process of resonance excitation on the free nucleon

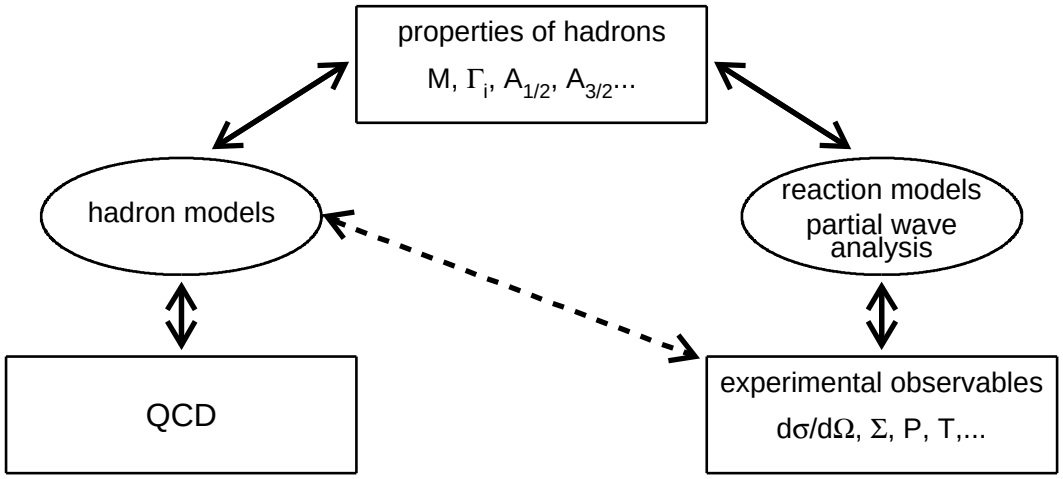

Figure 3: Schematic representation of the relation between experimental observables, baryon properties, and QCD via reaction and hadron models.

is the basis for the investigation of baryon resonances in the nuclear medium. In the case of bound nucleons, even properties like mass and width, which may be influenced by the nuclear medium, are mostly unknown. Such effects arise, for example, from the additional decay channel $RN \rightleftharpoons NN$ and from Pauli blocking of the $R \rightarrow N\pi$ decay where R stands for a $N^\star$ or Δ resonance. However, it came as a surprise when measurements of the total photoabsorption cross section on nuclei indicated a depletion of the resonance structure in the second resonance region [29, 30]. Bianchi et al. [31] reported that, while in the Δ-resonance region strength is only redistributed by broadening effects, strength is *missing* in the $D_{13}(1520)$ region. On the other hand, measurements of exclusive reaction channels like η photoproduction [32] or single π^o photoproduction [33] did not find any effects beyond trivial final state interactions. An overview over the in-medium properties of nucleon resonances will be given elsewhere.

In the present paper, we will review recent progress in the investigation of nucleon resonances with meson photoproduction. The restriction to reactions induced by real photons - as opposed to electron scattering experiments where the nucleon is excited by virtual photons - is not kept strictly. Results from electroproduction experiments are included when the dependence of the observables on the four-momentum transfer Q^2 is directly relevant for the discussion. On the experimental side, the progress made in accelerator and detector technology during the last fifteen years has considerably enhanced our possibilities to investigate the nucleon with different probes. In particular, the new generation of electron accelerators, CEBAF at JLab in Newport News, ELSA in Bonn, ESRF in Grenoble, MAMI in Mainz, and SPring8 in Osaka are equipped with tagged photon facilities and state-of-the-art detector systems. Quasi monochromatic photon beams provided by photon tagging are the working horse of the real photon programs. Two different techniques are used to produce photon beams: bremsstrahlung and Compton backscattering. The principles are sketched in fig. 4. In the first case, the electron beam from the accelerator impinges on a radiator (usually a thin metal foil). Scattered electrons produce bremsstrahlung with the typical $1/E_\gamma$ spectral distribution. In the second case, photons from a laser are scattered from electrons circulating in a storage ring. A certain advantage of this technique is that polarization degrees of freedom are transfered from the laser photons to the Compton back-scattered high energy photons. On the other hand, beam intensities are limited since high intensity laser beams reduce the lifetime of the stored electron beams. In both cases, the energies of the photon and the scattered electron are correlated via the known incident electron (and photon) energy. The scattered electrons are momentum selected with magnetic fields and detected in the focal plane of the magnetic spectrometers. The production detectors are operated in coincidence with the electron detectors so that the incident photon energies are known event-by-event within the resolution of the tagging detector. The bremsstrahlung technique is used at ELSA, JLab (CLAS), and MAMI. Laser backscattering is employed at BNL (LEGS), at ESRF (GRAAL), and at SPring8 (LEPS).

These facilities have opened the way to meson photoproduction experiments of unprecedented sen-

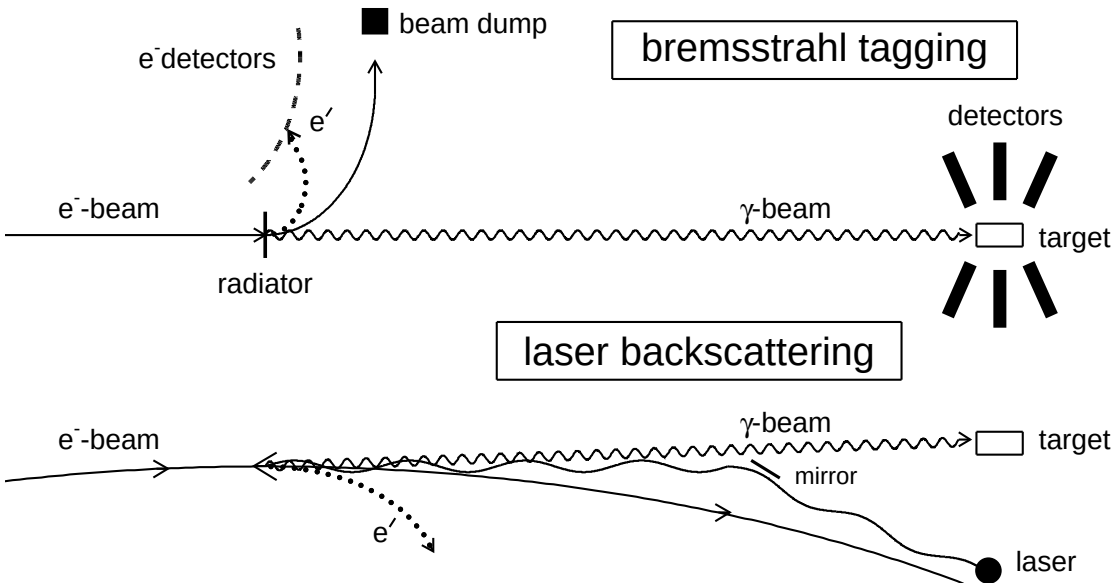

Figure 4: Schematic illustration of tagged photon facilities from bremsstrahlung (upper part) and Compton scattered laser beams (lower part). The solid lines indicate the electron beams, the dotted lines scattered electrons, and the curled lines the photon beams. The scattered electrons are deflected by magnetic fields (not indicated). Position of detectors is only indicated in the upper part. In both cases electron and production detectors are operated in coincidence.

sitivity and precision. In some areas, the cross section of photon induced reactions is currently known more precisely than the cross section of the corresponding pion induced reactions. This is the case for η meson production although the pion induced yields are larger by about two orders of magnitude. The experimental test of nucleon models can proceed along two different roads. The problem of missing resonances can be attacked by a large scale survey investigating many different final states ($N\pi$, $N\pi\pi$, $N\eta$, $N\eta'$, $N\omega$, $N\rho$ etc.) over a large energy range. An instructive discussion of 'Guidelines for identifying new Baryon Resonances' [34] and 'How many $N^\star$ do we need?' [35] is given by Bennhold and Manley. Secondly, the low lying resonances can be studied in great detail providing data for precision tests of the models. Here, the availability of linearly and circularly polarized photon beams and polarized targets has provided access to observables, which are sensitive to specific resonances. The present review concerns itself with the second approach where the results are in a more mature state. This situation reflects the fact that the Mainz MAMI accelerator, which is limited in energy to 880 MeV, has been operational for more than ten years. The investigation of high lying resonances, in particular at JLab and ELSA, started more recently.

The relevant low energy excitation scheme of the nucleon with prominent transitions via meson emission is summarized in fig. 5. Most resonances have comparable branching ratios into the $N\pi$ final state, so that their contribution to pion photoproduction is mainly determined by their photon couplings. Single pion production will be discussed in detail in sec. 3 where new precise studies of the properties of the $P_{33}(1232)$-resonance are presented. In the second resonance region, single pion production is dominated by the decay of the $D_{13}(1520)$-resonance, which is discussed in sec. 4.1.

Even in this low energy region, the emission of heavier mesons is important for some states. The most selective channel is the photoproduction of η-mesons which is dominated by the excitation of the $S_{11}(1535)$-resonance. This selectivity comes partly from the fact that Δ-resonances cannot decay to the nucleon ground state via emission of the isoscalar η. More importantly, the $P_{11}(1440)$- and $D_{13}(1520)$-resonances have very small decay branching ratios into $N\eta$ since they need to decay with relative orbital angular momentum $l = 1, 2$. Close to threshold, these l-values are strongly suppressed as compared to the s-wave decay of the $S_{11}(1535)$. The $P_{11}(1440)$-resonance even lies below the η-production threshold

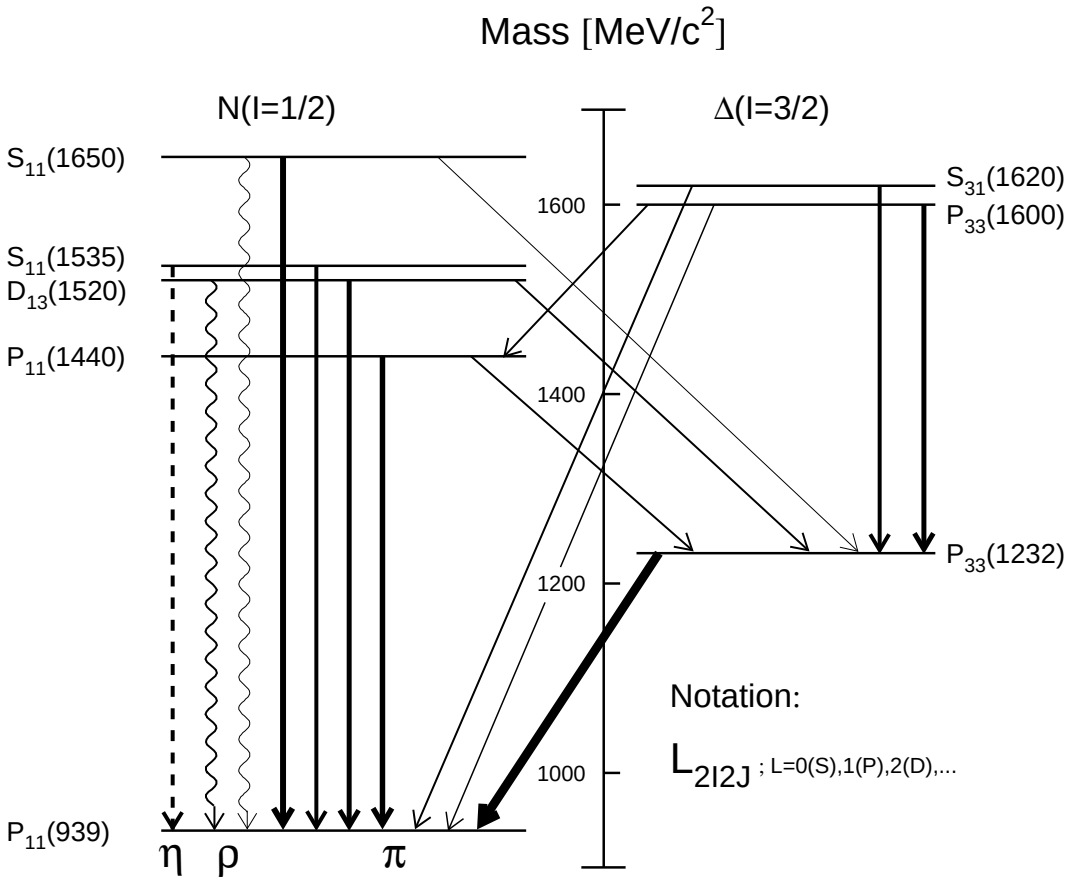

Figure 5: Low lying excited states of the nucleon [36] with isospin I=1/2 (left hand side) and isospin I=3/2 (right hand side). The arrows indicate the decays via pion emission (solid), η-emission (dashed) and ρ-emission (curled). The thickness of the arrows scales with the branching ratios of the respective decays. Weak decay branchings have been omitted.

so that only its high energy tail could contribute. On the other hand, the large difference in the $N\eta$ decay branching ratios of the first and second S_{11}-resonance must reflect a different structure of the states. Recent results for the photoproduction of η mesons are discussed in 4.2.

In addition to single pion and η emission, double pion production contributes to resonance decays in this energy region. The pion emission of some resonances does not only lead to the nucleon ground state, but also to higher lying states, in particular to the $P_{33}(1232)$ which subsequently decays via emission of a second pion. The other contribution comes from decays into the $N\rho$ channel with a final state pion pair from the ρ meson decay. The detailed experimental study of the double pion production reaction, allowing to a large extend the extraction of resonance contributions, is discussed in 4.3.

At excitation energies above the second resonance region further meson production thresholds open. ω mesons are produced off the free proton above E_γ=1108 MeV, η' mesons above 1447 MeV, and Φ mesons above 1573 MeV. In addition, the thresholds for open strangeness production open around 1 GeV (915 MeV for $K\Lambda$ and 1052 MeV for $K\Sigma$). Here, final states with open strangeness can couple to intermediate non-strange nucleon resonances. These couplings carry important information about the internal structure of the states. Finally, sequential decay chains of resonances, such as $\Delta^* \to \Delta\eta \to N\eta\pi$ will become important. Progress in this field is rapid, and we will give examples of recent results and ongoing efforts in the Conclusions and Outlook section. The main part of this review concentrates on the low lying states in view of the fact that the available data base for pion, double pion, and η-photoproduction is by far superior.

2 Photoexcitation of Free and Quasi-free Nucleons

The most prominent decay channel of excited states of the nucleon is the emission of light mesons belonging to the ground state nonets of pseudo-scalar and vector mesons. Photoproduction of pions is by far the best explored channel. However, as already mentioned, it is difficult to isolate the contributions from individual resonances if only pion production is studied, and bias arises for resonances which couple only weakly to $N\pi$. For this reason, the study of photoproduction reactions involving heavier mesons or multiple meson production has attracted a lot of attention. The properties of the relevant mesons are summarized in app. 6.1.

The formalism of the photoproduction of pseudo-scalar mesons from nucleons is well known. Detailed reviews can be found in [37, 39]. Here, only a brief description is given in order to establish the notation of the observables which will be used for the discussion of the results. The most general Lorentz and gauge invariant amplitude for the photoproduction of a pseudo-scalar particle from a nucleon can be written in the Chew-Goldberger-Low-Nambu (CGLN) parameterization [41]:

$$\mathcal{F} = iF_1 \cdot \vec{\sigma} \cdot \vec{\epsilon} + F_2(\vec{\sigma} \cdot \vec{q})(\vec{\sigma} \cdot (\vec{k} \times \vec{\epsilon})) + iF_3(\vec{\sigma} \cdot \vec{k})(\vec{q} \cdot \vec{\epsilon}) + iF_4(\vec{\sigma} \cdot \vec{q})(\vec{q} \cdot \vec{\epsilon}) \tag{1}$$

where $\vec{k}$, $\vec{q}$ are momentum unit vectors of the photon and meson, $\vec{\epsilon}$ is the polarization vector for a real photon of helicity $\lambda_\gamma = \pm 1$, and $\vec{\sigma}$ are the nucleon's spin matrices. A different parameterization of the amplitude exists in terms of the helicities of the initial and final state particles (see app. 6.2).

The differential cross section in the center of momentum (cm) frame for an unpolarized target and an unpolarized photon beam is given in terms of the CGLN-amplitudes by:

$$\begin{aligned} \frac{k^\star}{q^\star}\frac{d\sigma}{d\Omega} &= [|F_1|^2 + |F_2|^2 + \frac{1}{2}|F_3|^2 + \frac{1}{2}|F_4|^2 + Re(F_1 F_3^\star)] \\ &+ [Re(F_3 F_4^\star) - 2Re(F_1 F_2^\star)]cos(\Theta^\star) \\ &- [\frac{1}{2}|F_3|^2 + \frac{1}{2}|F_4|^2 + Re(F_1 F_4^\star) + Re(F_2 F_3^\star)]cos^2(\Theta^\star) \\ &- [Re(F_3 F_4^\star)]cos^3(\Theta^\star) \end{aligned} \tag{2}$$

where $q^\star$, $k^\star$ are meson and photon cm momenta, respectively, and $\Theta^\star$ is the cm polar angle of the meson (throughout the paper a '$\star$' at kinematical variables indicates the cm system, but note that for the amplitudes it means 'complex conjugated'). The expressions for all polarization observables in terms of the F_i or the helicity amplitudes H_i can be found in [42, 37, 43].

The amplitude involves four complex functions (the F_i), and consequently complete information about the reaction requires the determination of seven independent real quantities (the overall phase is arbitrary) at each incident photon energy and each meson emission angle. A 'complete' experiment does not only require the measurement of the differential cross section $d\sigma/d\Omega$, the photon beam asymmetry Σ, the target asymmetry T, and the recoil nucleon polarization R (referred to as $\mathcal{S}$-type experiments). In addition, several double polarization observables which are characterized as $\mathcal{BT}$- (beam-target), $\mathcal{BR}$- (beam-recoil), and $\mathcal{TR}$- (target-recoil) type have to be determined. The question which set of observables allows a unique determination of the amplitudes is not trivial and has been intensely discussed in the literature. Barker, Donnachie, and Storrow [42] showed that in the transversity representation (see app. 6.2) the four $\mathcal{S}$-type experiments determine the magnitude of the amplitudes. The additional measurement of at least three double polarization observables, not all from the same group, determines the phases up to discrete ambiguities. Furthermore, they argued that the measurement of five double polarization observables with no more than three from one of the groups $\mathcal{BT}$, $\mathcal{BR}$, $\mathcal{TR}$ is sufficient for a unique determination of all amplitudes (BDS-rule). Thus, nine measurements are required in total. However, Keaton and Workman [44] have shown that certain combinations of double polarization observables, which satisfy the BDS-rule, do not resolve all discrete ambiguities. On

the other hand, Chiang and Tabakin [45] have proven that in addition to the $\mathcal{S}$-type experiments, already four appropriately chosen double spin observables are sufficient for a unique determination of the amplitudes. This means that the 'complete' experiment requires at least eight measurements. However, in general it is impractical to do this ideal experiment. Therefore, the analysis of meson photoproduction data often relies on reaction models. In particular, close to production thresholds, where only few partial waves contribute, differential cross sections alone often provide valuable information.

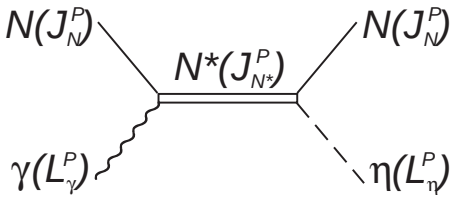

Figure 6: Photoproduction of mesons via excitation of nucleon resonances.

We are primarily interested in the photoproduction of mesons via the intermediate excitation of resonances. This process is sketched in fig. 6 for η-production (the discussion is valid for any pseudo-scalar meson). It is advantageous to decompose initial and final state into multipole components since the intermediate resonance has definite parity and angular momentum. In the initial state, the photon with spin $\vec{s}_\gamma$ ($s = 1$), orbital angular momentum $\vec{l}$ relative to the target nucleon, and total angular momentum $\vec{L}_\gamma = \vec{l} + \vec{s}_\gamma$ couples electromagnetically to the nucleon with spin $\vec{J}_N$ ($J = 1/2$) and parity $P_N = 1$ to produce a resonance with spin $\vec{J}_{N^\star}$ and parity $P_{N^\star}$.

The usual multipole expansion of the photon field gives rise to electric EL- and magnetic ML-multipoles with angular momentum L and parity $P_\gamma = (-1)^L$ for the electric and $P_\gamma = (-1)^{L+1}$ for the magnetic case. This process obeys the following selection rules:

$$|L_\gamma - J_N| = |L_\gamma - 1/2| \leq J_{N^\star} \leq |L_\gamma + 1/2| = |L_\gamma + J_N| \qquad (3)$$
$$P_{N^\star} = P_N \cdot P_\gamma = P_\gamma \ .$$

The resonance subsequently decays by strong interaction to the nucleon ground state via emission of the meson with spin 0, parity $P_\eta = -1$ and relative orbital angular momentum L_η. The respective selection rules must be fulfilled:

$$|L_\eta - J_N| = |L_\eta - 1/2| \leq J_{N^\star} \leq |L_\eta + 1/2| = |L_\eta + J_N| \qquad (4)$$
$$P_{N^\star} = P_N \cdot P_\eta \cdot (-1)^{L_\eta} = (-1)^{L_\eta + 1} \ .$$

Consequently, we have

$$\begin{aligned} P_\gamma &= P_{N^\star} &&= (-1)^{L_\eta + 1} \qquad (5) \\ L_\gamma \pm 1/2 &= J_{N^\star} &&= L_\eta \pm 1/2 \ , \end{aligned}$$

where the two '$\pm$' are independent. Parity and angular momentum conservation allow two possibilities:

$$EL: \quad L = L_\eta \pm 1 \qquad (6)$$
$$ML: \quad L = L_\eta \ . \qquad (7)$$

The corresponding photoproduction multipoles for pseudo-scalar mesons are denoted as $E_{l\pm}$ and $M_{l\pm}$, where E, M stands for electric or magnetic photon multipoles, l ($l = L_\eta$ in the above example) denotes the relative orbital angular momentum of the final meson - nucleon system, and '+' or '−' indicates whether the spin 1/2 of the nucleon must be added to or subtracted from l to give the total angular momentum $J_{N^\star}$ of the intermediate state.

With the exception of $J_{N^\star}$=1/2 resonances, which can only be excited by one multipole (E_{0+} for negative parity states and M_{1-} for positive parity states), each resonance can be excited by one electric and one magnetic multipole. Examples for the lowest order multipoles are given in tab. 9, app. 6.3.

The partial wave decomposition of the CGLN-amplitudes into the multipole amplitudes corresponding to definite parity and angular momentum states is given by:

$$\begin{aligned}
F_1(\Theta^\star) &= \sum_{l=0}^{\infty}[lM_{l+} + E_{l+}]P'_{l+1}(cos(\Theta^\star)) + [(l+1)M_{l-} + E_{l-}]P'_{l-1}(cos(\Theta^\star)) \\
F_2(\Theta^\star) &= \sum_{l=0}^{\infty}[(l+1)M_{l+} + lM_{l-}]P'_{l}(cos(\Theta^\star)) \\
F_3(\Theta^\star) &= \sum_{l=0}^{\infty}[E_{l+} - M_{l+}]P''_{l+1}(cos(\Theta^\star)) + [E_{l-} - M_{l-}]P''_{l-1}(cos(\Theta^\star)) \\
F_4(\Theta^\star) &= \sum_{l=0}^{\infty}[M_{l+} - E_{l+} - M_{l-} - E_{l-}]P''_{l-1}(cos(\Theta^\star))
\end{aligned} \tag{8}$$

where the P'_l, P''_l are derivatives of Legendre polynomials. The angular distributions reflect the quantum numbers of the excited state when the cross section is dominated by a resonance. The most familiar example from pion photoproduction is the excitation of the $P_{33}(1232)$-resonance (Δ-resonance) via the M_{1+}-multipole which exhibits the characteristic $(5 - 3cos^2(\Theta^\star))$ angular distribution (see fig. 10). Therefore, the analysis of resonance contributions to pion photoproduction uses a parameterization of the cross section in terms of the multipole amplitudes. However, the differential cross sections by themselves do not allow a unique extraction of the multipoles. This is obvious from table 9 because the entries for the angular distributions exhibit a certain symmetry. They depend on the combination of the spin of the resonance and the order of the photon multipole but not on the combination of the parities of resonance and multipole. For example, the excitation of a $5/2^+$ resonance by an electric quadrupole has the same angular dependence as the excitation of a $5/2^-$ resonance by a magnetic quadrupole. This ambiguity can be resolved with polarization observables.

The case of vector meson production is much more complicated. The general formalism of polarization observables in vector meson photoproduction and their multipole analysis was discussed by Tabakin and coworkers (see e.g. [47]-[49]). The spin of the mesons contributes three additional degrees-of-freedom, and 12 independent amplitudes have to be considered. This corresponds to the determination of 23 independent real quantities for each incident photon energy and each meson emission angle since the overall phase is again not needed. At the same time the number of observables increases. In the case of pseudo-scalar mesons, 12 double polarization observables are defined (see e.g. [42]) apart from the four $\mathcal{S}$-type observables. For vector mesons, the number of observables increases to 8 (independent) single, 51 (non-zero) double, 123 triple, and 108 quadruple polarization observables [83, 46, 47]. The extraction of resonance parameters will have to rely on model dependent analyses even more than in the case of the pseudo-scalar mesons. A 'complete' measurement is certainly out of reach. In contrast to the pseudo-scalar case, the measurement of all $\mathcal{S}$-type observables does not even allow to fix the magnitude of the amplitudes.

So far, we have ignored one complication of meson photoproduction, namely the treatment of isospin. For a resonance excitation process, as depicted in figure 6, isospin must be conserved at the hadronic vertex. As a consequence only $N^\star$ resonances are allowed as intermediate states in η-photoproduction. For pion photoproduction, Δ-resonances may also contribute. On the other hand, the electromagnetic interaction violates isospin conservation so that the production vertex is complicated by the presence of isoscalar (ΔI =0) and isovector (ΔI =0,$\pm$1) components of the electromagnetic current. Each multipole amplitude has to be reconstructed from the various isospin contributions. If the transition operator is split into an isoscalar part $\hat{S}$ and an isovector part $\hat{V}$, three independent matrix elements are obtained for the photoproduction of isovector mesons from the nucleon [50] in the notation $\langle I_f, I_{f3}|\hat{A}|I_i, I_{i3}\rangle$:

$$A^{IS} = \langle\frac{1}{2}, \pm\frac{1}{2}|\hat{S}|\frac{1}{2}, \pm\frac{1}{2}\rangle \qquad \mp A^{IV} = \langle\frac{1}{2}, \pm\frac{1}{2}|\hat{V}|\frac{1}{2}, \pm\frac{1}{2}\rangle \qquad A^{V3} = \langle\frac{3}{2}, \pm\frac{1}{2}|\hat{V}|\frac{1}{2}, \pm\frac{1}{2}\rangle\ . \tag{9}$$

The multipole amplitudes of the four possible photoproduction reactions can be expressed in terms of this isospin amplitudes as [51] (see also app. 6.4):

$$\begin{aligned} A(\gamma p \to \pi^+ n) &= -\sqrt{\frac{1}{3}}\, A^{V3} + \sqrt{\frac{2}{3}}(A^{IV} - A^{IS}) \\ A(\gamma p \to \pi^o p) &= +\sqrt{\frac{2}{3}}\, A^{V3} + \sqrt{\frac{1}{3}}(A^{IV} - A^{IS}) \\ A(\gamma n \to \pi^- p) &= +\sqrt{\frac{1}{3}}\, A^{V3} - \sqrt{\frac{2}{3}}(A^{IV} + A^{IS}) \\ A(\gamma n \to \pi^o n) &= +\sqrt{\frac{2}{3}}\, A^{V3} + \sqrt{\frac{1}{3}}(A^{IV} + A^{IS})\ . \end{aligned} \tag{10}$$

The situation is simpler for isoscalar mesons like the η meson. Here, the isospin changing part $V3$ cannot contribute, and all amplitudes X can be written as:

$$A(\gamma p \to \eta p) = (A^{IS} + A^{IV}) \qquad A(\gamma n \to \eta n) = (A^{IS} - A^{IV})\ . \tag{11}$$

The complication of isospin means, that a complete characterization of the photoproduction amplitudes for isovector as well as for isoscalar mesons requires measurements off the neutron which must rely on meson photoproduction from light nuclei. This introduces additional uncertainties due to nuclear effects. In principle, two possibilities exist to learn about the isospin composition via photoproduction from nuclei. Photoproduction from bound nucleons in quasifree kinematics can be used to extract the production cross section on the neutron. Here, the meson is produced on one nucleon which is subsequently knocked out of the nucleus. The other nucleons act only as spectators. The small binding energy and the comparatively well understood nuclear structure single out the deuteron as an exceptionally important target nucleus. However, for better control of systematic effects it is desirable to study the reaction for more strongly bound nuclei as well. Here, the extreme case is ^{4}He. The different methods for the extraction of the neutron cross section will be discussed in detail for the example of η-photoproduction in 4.2. Additional information may be obtained from coherent meson photoproduction, where the reaction amplitudes from all nucleons add coherently and the nucleus remains in its ground state. Nuclei with different ground state quantum numbers may be used as spin/isospin filters of the production amplitude. The light nuclei ^{2}H (J=1, I_z=0), ^{3}H (J=1/2, I_z=$-$1/2), ^{3}He (J=1/2, I_z=+1/2), and ^{4}He (J=0, I_z=0) provide a selection of the relevant quantum numbers, although the ^{3}H case is basically unexplored due to complications in the usage of tritium targets. Furthermore, with the exception of pion photoproduction, coherent cross sections are small due to the nuclear form factors. Incoherent excitations of the nuclei, where the final state nucleus is in an excited state, could provide even more flexible spin/isospin filters. These reactions have been even less exploited due to the small size of the cross sections.

Two obvious difficulties arise when extracting the properties of nucleon resonances from meson photoproduction data: in general, it is impractical to carry out a 'complete' experiment which allows the unique determination of the photoproduction amplitudes and in most cases, important non-resonant background contributions must be separated from resonance excitations. As an example, fig. 7 shows the most important contributions to the low energy photoproduction of η-mesons. Born terms and vector meson exchange terms are expected to contribute in addition to nucleon resonance excitations. Therefore, reaction models are needed which allow the extraction of the resonant multipoles in the presence of the background from incomplete data sets. More model assumptions are necessary for the analysis when fewer observables have been measured. Therefore, such models have been developed from different concepts and for different levels of sophistication.

In the following, we will give an overview of the different methods which is certainly not complete. More detailed discussions for specific reactions will be given in the following sections. Partial wave

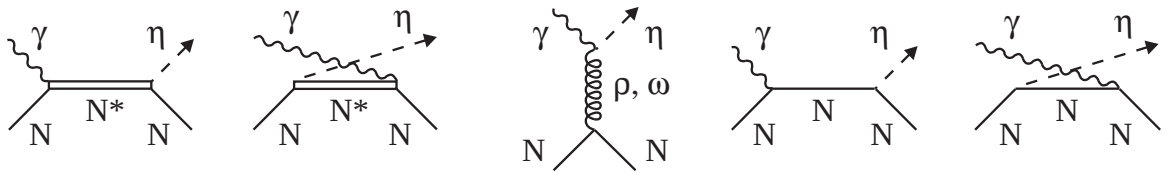

Figure 7: Tree level diagrams contributing to η-photoproduction from the nucleon.

analyses, trying to extract the photoproduction amplitudes without making assumptions about production processes, have mostly been limited to pion photoproduction. In this case, resonant contributions can be extracted in a second step by fitting the multipole amplitudes with resonance parameterizations and backgrounds. Fixed-t dispersion relations have frequently been used for such multipole analyses (see e.g. [52, 53] and ref. therein). Recently Hanstein et al. [54] have updated this type of analysis for the now available extended and more precise data base at low incident photon energies ($E_\gamma < 450$ MeV). An extensive analysis of the world data base for pion photoproduction up to 2 GeV is given in the T-matrix formalism by Arndt and coworkers [55]-[57]. The most recent update of this work [58], includes the new precise data, in particular the polarization observables in the data base. This is the SAID partial wave analysis [59]. The results, also for other reaction channels, are available online [60].

All other models start from a separation of the amplitudes into resonance and background contributions. The first group of models, called Isobar Analyses, parameterizes the electric and magnetic multipole amplitudes in terms of Breit-Wigner curves for the resonances and smoothly varying phenomenological forms of the background amplitudes. The simplest of these analyses was used for the total photoabsorption data in ref. [17] (see fig. 2). Breit-Wigner curves for the resonances and a phenomenological background were fitted to the total cross section data. Different reaction channels contribute to total photoabsorption where the total cross section is the only recorded observable. A more sophisticated analysis does not seem to be practical. Reliable, precise resonance properties cannot be extracted in this way. The interference between the contributions from the different resonances and the background, which in most cases is important, is not accounted for. These terms were included in early isobar analyses of pion- and η-photoproduction data [51, 61, 62], where observables like angular distributions and polarization degrees-of-freedom were reconstructed from the multipole amplitudes. The advantage of the isobar models is that they have a simple, physically transparent form which is well suited to analyze the data. On the other hand, the models usually involve fits of many parameters, and the background terms are not treated in a very sophisticated manner.

Both problems were attacked in the framework of the Effective Lagrangian Approach (ELA). In these models, all contributions to the photoproduction reaction are derived on an equal footing from the effective Lagrangian densities corresponding to the interaction vertices. In this way, the number of fit parameters is reduced to a smaller set of coupling constants which can partly be compared to or taken from other reactions. The analysis of pion- and η-photoproduction in this framework was mostly developed by N.C. Mukhopadhyay and coworkers [63, 39] building on the work of Olsson and Osypowski [64]. An ELA-model for pion photoproduction was also proposed by Garcilazo and Moya de Guerra [65]. A certain drawback of most of these models is their complexity and difficulty in handling. This holds in particular for nuclear applications like photoproduction from few nucleon systems which aim at the isospin structure of resonance excitations. In practice, the model of Blomqvist and Laget [66], which is a non-relativistic reduction of the Olsson - Osypowski [64] model, was used much more extensively for such applications. Modern versions of isobar models constitute a compromise. For pion and η-photoproduction [43, 67, 68] the effective Lagrangian parameterizations for the background processes have been adopted while keeping the Breit-Wigner forms for the resonances. Online versions of these models are available at the MAID homepage [69].

In general, inclusion of the background terms at the tree level violates unitarity in the ELA-models

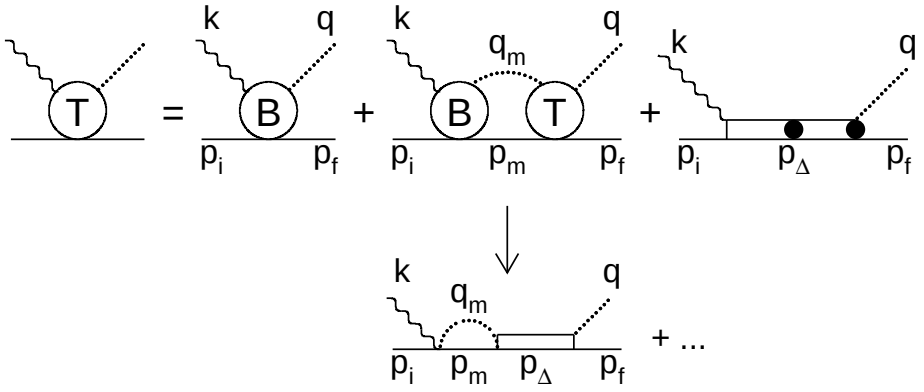

Figure 8: Schematic representation of the scattering equation used in [73] for the calculation of pion photoproduction from the nucleon (upper part). The lower part shows one of the diagrams from the rescattering contributions.

as well as in the isobar models. It was argued (see e.g. [39]) that this does not pose a severe problem for η-photoproduction, since the background terms are small, and the coupling of the η-meson to the nucleon is weak. On the other hand, Sauermann et al. [70] found important effects in η-photoproduction due to unitarity corrections. However, unitarity effects are much more important for pion photoproduction. The pion-nucleon coupling is large, and it is well known that background multipoles can have large imaginary parts, building up from pion-nucleon re-scattering contributions. Models for pion photoproduction like the Unitary Isobar Model of Drechsel et al. [67] need a careful adjustment of the phases of the background and resonance contributions to the corresponding pion-nucleon scattering phase shifts.

For a precise comparison of resonance properties to quark model predictions, a further, subtle difficulty arises from the separation of resonance and background contributions. Let's consider, as an example, the properties of the $\gamma N\Delta$-vertex studied via pion photoproduction, to be discussed in detail in 3.1. Once sufficient observables have been measured, the reaction models as discussed above can be used to separate resonance from background contributions at the tree level. However, off-shell rescattering effects are neglected in the models. Usually, quark models predict the properties of the 'bare' $\gamma N\Delta$-vertex in the absence of re-scattering contributions. However, the data analysis in the framework of the reaction models cannot separate the bare interaction from contributions where an off-shell pion is produced in a non-resonant reaction (e.g. nucleon Born term) and then is re-scattered off the nucleon to produce a Δ-resonance (see lower part fig. 8). The reaction models are thus sensitive to the properties of the 'dressed' vertex which includes the re-scattering terms. The solution to this problem requires that either the hadron models make predictions for the dressed vertex or the reaction models manage to extract the properties of the bare vertex from the data. The reaction models attacked this problem with dynamical models of pion photoproduction. These models build on the experience from purely hadronic systems. On account of the strong interaction, a reasonable description with lowest order contributions is not possible and multiple scattering processes where carefully treated. The models developed by Tanabe and Otha [71], Yang [72], with later extension by Nozawa, Blankleider, and Lee [73] include the final state πN interaction explicitly so that unitarity is ensured. They treat the πN interaction via the well-known meson exchange contributions and phenomenological two-body separable potentials for multiple scattering. A schematic description of the scattering equation used in [73] is shown in fig. 8. Sato and Lee [74] have further developed a consistent meson-exchange description of the πN scattering and pion photoproduction which allows to extract the bare vertex couplings. However, all of these models are quite involved and have so far been almost exclusively applied to pion photoproduction in the Δ-resonance region.

The approaches discussed above analyze individual meson production reactions and use input from other channels only in indirect ways, e.g. as constraints for resonance parameters or coupling constants. The resonance properties like excitation energy, total width and the couplings to the photon - nucleon or meson - nucleon states do not depend on the individual reactions. More efficient use of the available data is made in the framework of coupled channel analyses. These models simultaneously fit photon- and pion-induced meson production reactions for many different final states ($N\pi$, $N\pi\pi$, $N\eta$, $N\eta'$, $N\rho$,

$K\Lambda$, $K\Sigma$,...). The models have been developed based on different concepts for the treatment of the individual reaction channels. Recent results from three approaches incorporate unitarity but differ in the background treatment, the parameterization of the resonance contributions, and the use of theoretical constraints like gauge invariance, analyticity, and chiral symmetry. The results are compared in [75]. The Giessen model [76]-[78] is based on the Bethe-Salpeter equation in the K-matrix approximation. The s-, u-, and t-channel contributions are parameterized via effective Lagrangians. Pion and photon induced reactions to the final states πN, $2\pi N$, ηN, $K\Lambda$, $K\Sigma$, and ωN are included in the latest version. The strength of this field theoretical approach is that constraints from gauge invariance and chiral symmetry can be included in a natural way. The starting point of the Pitt-ANL model [26] is an analytic, unitary representation of the s-channel resonances. This model gives a particularly good description of the inelastic threshold openings, but t-channel contributions must be added by hand, and gauge invariance is not guaranteed. Finally, the KSU model [79] uses a multi-channel Breit-Wigner approach with a phenomenological background parameterization. The comparison of the results from the three models showed satisfactory agreement for the first resonance in each partial wave, but already for the second resonance, properties like decay branching ratios and photon couplings varied widely.

The models discussed above all are reaction models in the sense that they try to extract the properties of the excited states of the nucleon from the physical observables which then can be compared to the predictions of hadron models. There is an obvious drawback of this approach. Each nucleon resonance which is accounted for, introduces parameters into the models, and the number of parameters grows quickly with increasing incident photon energy. A direct connection between the quark degrees-of-freedom and photoproduction observables, largely reducing the number of parameters, was constructed by Zhenping Li and collaborators for pseudo-scalar and vector mesons [80]-[84]. Their model for pseudo-scalar mesons [82] starts from the effective low energy chirally invariant QCD Lagrangian proposed by Manohar and Georgi [85]:

$$\mathcal{L} = \bar{\psi}[\gamma_\mu(i\partial^\mu + V^\mu + A^\mu) - m]\psi + ... \tag{12}$$

which involves the interaction of the quark field in SU(3) symmetry $\psi = (\psi(u), \psi(d), \psi(s))^T$ with the field of the pseudo-scalar mesons from the ground state octet treated as Goldstone bosons:

$$\pi = \begin{vmatrix} -\frac{1}{\sqrt{2}}\pi^0 - \frac{1}{\sqrt{6}}\eta & \pi^+ & K^+ \\ -\pi^- & \frac{1}{\sqrt{2}}\pi^0 - \frac{1}{\sqrt{6}}\eta & K^0 \\ K^- & \bar{K}^0 & \sqrt{\frac{2}{3}}\eta \end{vmatrix} \tag{13}$$

via vector and axial currents:

$$V^\mu = \frac{1}{2}(\zeta^\dagger\partial_\mu\zeta + \zeta\partial_\mu\zeta^\dagger) \qquad A^\mu = i\frac{1}{2}(\zeta^\dagger\partial_\mu\zeta - \zeta\partial_\mu\zeta^\dagger), \qquad \zeta = e^{i\pi/f} \tag{14}$$

where f is a decay constant. Then, the CGLN amplitude for the seagull term is constructed as well as the u- and s-wave contributions of the SU(6)$\otimes$O(3) quark model configurations for π, η- and K-photoproduction from the proton and the neutron in terms of only a few constants. Since SU(6)$\otimes$O(3) symmetry is broken, additional parameters must account for the configuration mixing in the physically observed states. In a similar approach the helicity amplitudes for the photoproduction of vector mesons are constructed from a chirally invariant low energy Lagrangian in [83].

Finally, we would like to note that a special working group, the Baryon Resonance Analysis Group (BRAG [86]), has been formed. The formation of the group has been triggered by the large amount of new data from electromagnetic and hadronic facilities worldwide; it tries to organize and coordinate the efforts. Among the goals of this group are a standardized data base for all reactions investigated, a better understanding of the systematic uncertainties of multipole analysis, and of the extraction of resonance properties in the framework of the different models. The systematic effects are studied via analyses of 'benchmark' data sets (see e.g. [87]).

3 The Δ-Resonance Region

The Δ(1232) resonance is the best known exited state of the nucleon. It has been investigated via many different reactions on the free proton and on bound nucleons, in particular in the πN-final state. The total photoproduction cross section and the angular distributions for the reactions $\gamma p \to p\pi^o$ and $\gamma p \to n\pi^+$ are summarized in figs. 9 and 10. The angular distributions have been fitted with the ansatz

$$\frac{d\sigma}{d\Omega} = \frac{q^\star}{k^\star}[a + b\ cos(\Theta^\star) + c\ cos^2(\Theta^\star)] \tag{15}$$

where a, b, c are free parameters (full curves in fig. 10), and are compared to the $(5-3cos^2(\Theta^\star))$ behavior expected for the excitation of the Δ resonance via the M_{1+}-multipole (dashed curves).

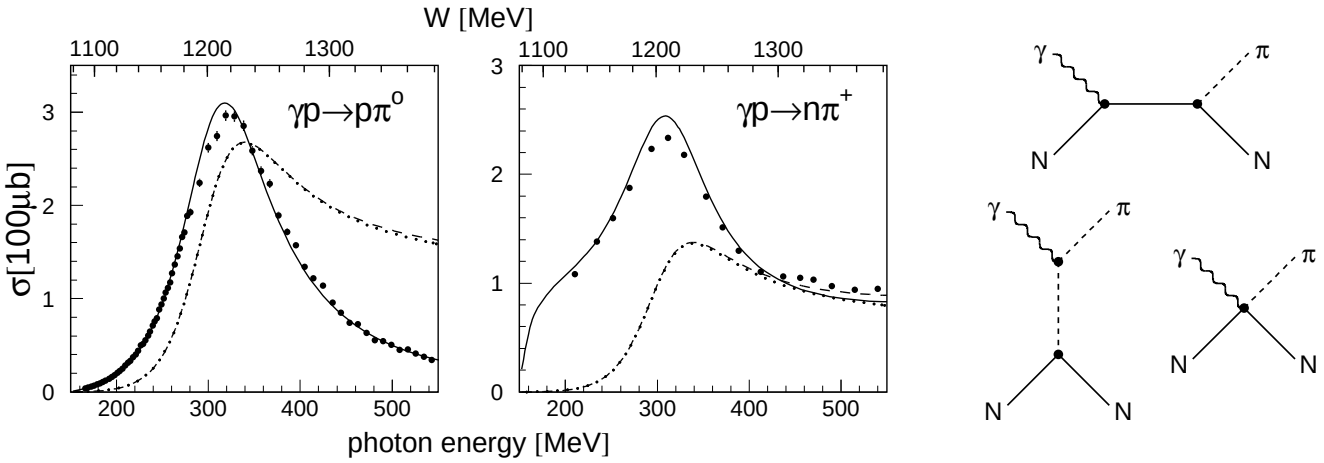

Figure 9: Total cross section of neutral (left hand side) and charged (middle) pion production from the proton in the Δ-resonance region. Data: [88, 89] ($\pi^o p$) and [90] ($\pi^+ n$). Curves: MAID2000 [67], Solid: all contributions, dashed: without background but with higher resonances, dotted: only $P_{33}(1232)$ (dashed and dotted curves almost identical). Right hand side: background contributions, upper part: nucleon Born term, lower part: pion-pole and Kroll-Rudermann (contact) term (only for charged pions).

The large difference between the neutral and charged channel is demonstrated in the figures. The energy dependence of the cross section for $\gamma p \to p\pi^o$ approximates the shape of a Breit-Wigner resonance more than in the case of charged pions. Furthermore, the angular distribution of π^o-photoproduction close to the resonance position at $E_\gamma \approx$330 MeV is in excellent agreement with the expectation for the M_{1+}-multipole transition. The photoproduction of charged pions deviates from this behavior already

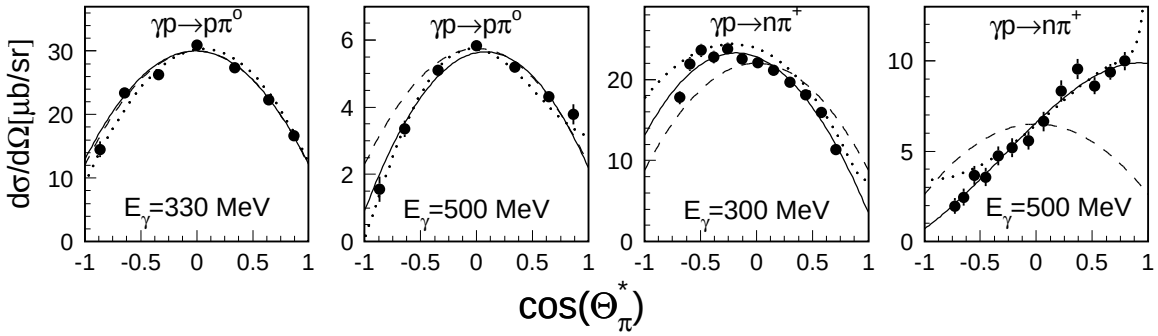

Figure 10: Angular distributions for neutral and charged pion photoproduction from the proton. Data are from [89, 90]. Solid curves: fits to the data, dashed curves: expected distribution for excitation of the Δ (see text), dotted curves: MAID2000 model [67] (full calculation including all terms).

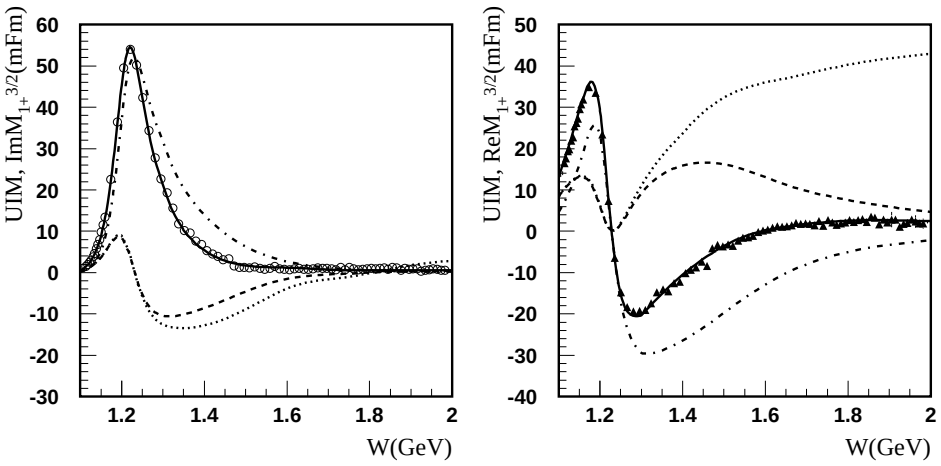

Figure 11: Imaginary and real parts of the M_{1+} multipole for $\gamma p \to p\pi^o$ in the UIM of Aznauryan [91]. Full curves: full model, dashed-dotted: resonance contribution, dashed: background. Circles and triangles: SAID multipole analysis [57]. Dotted curves: background in the UIM of Drechsel et al. [67]

at the resonance position and has a completely different shape at higher incident photon energies. The reason is that non-resonant background contributions are suppressed for the neutral channel. The Kroll-Rudermann (KR) term and the pion-pole term cannot contribute since the photon does not couple to the neutral pion, so that only nucleon Born terms mix with the resonance excitation (see diagrams in fig. 9). On the other hand, photoproduction of charged pions close to threshold is dominated by background terms, in particular the Kroll-Rudermann term. At higher incident photon energies, the KR-term and the pion-pole term are still important.

The relative importance of the background contributions is illustrated by a comparison of the data to the results of the Unitary Isobar Model (UIM) from Drechsel et al. [67]. The full calculation is shown in fig. 9 (also in fig. 10), along with the calculation with non-resonant background excluding other resonances, and the result for the Δ resonance without any other contributions. As expected, contributions from resonances other than the Δ are negligible in this energy range. The only eligible candidate would be the tail of the $P_{11}(1440)$ 'Roper' resonance. The cross section ratio of $\approx$2 for the two reactions, when only the excitation of the Δ is considered, simply reflects the isospin Clebsch-Gordan coefficients for the strong $\Delta^+ \to \pi^o p$ and $\Delta^+ \to \pi^+ n$ decays (see eqs. (10)). Only the amplitude A^{V3} can change the isospin and excite the Δ.

The non-resonant background is substantial for charged pions. At the resonance position the contribution from the Δ agrees with the data for π^o-production but underestimates it for π^+-production by roughly a factor of two. Unexpectedly, the experimental $\gamma p \to p\pi^o$ cross section deviates significantly at higher incident photon energies from the Δ contribution in the UIM of Drechsel et al. [67] since the resonance curve has a very pronounced high energy tail. In the model, the large resonance contributions to the total cross section are cancelled by background terms. However, the separation of resonance and background terms in the models is by no means unique. Due to the unitarization, modifications in one sector will also affect the rest. The background in the UIM of ref. [67] is constructed from s- and u-channel nucleon Born terms and t-channel π-, ρ-, and ω-exchange. Recently, it was argued by Aznauryan [91] that this background becomes too large at higher incident photon energies, which is artificially compensated in [67] by the large high energy tail of the Δ. In a modified version of the UIM, Aznauryan included Regge-pole type background amplitudes in order to account for t-channel contributions of heavier mesons which are neglected in [67]. The background contributions to the $M_{1+}^{3/2}$ multipole in the UIM's from refs. [67, 91] (see fig. 11) show indeed a very different high energy behavior which in turn results in different resonance contributions. It should be noted however, that very good agreement is found at energies close to the resonance position. We have discussed this behavior in some detail since the background contributions are very important for the following discussion. The message is that background contributions are small close to the resonance position for π^o-photoproduction but substantial for π^+-photoproduction. In both cases they are reasonably well under control albeit with some model dependency at higher incident photon energies.

One might wonder what can be learned from photoproduction in the Δ-resonance region beyond the basic resonance properties like excitation energy, width, and electromagnetic coupling which are well known [36]. In fact, the recent experimental progress has opened the possibility for new, detailed studies of this resonance. We will discuss four examples: the $E2$ admixture in the electromagnetic excitation amplitude, the helicity dependence of the cross section, the magnetic moment of the Δ, and the isospin dependence of the excitation.

3.1 *Quadrupole Strength in the $N \to \Delta$ Transition*

The standard picture for the excitation of the Δ-resonance on the nucleon is the spin-flip of a single quark. In the electromagnetic case, the spin-flip is induced via the absorption of a magnetic dipole $M1$-photon which for pion production corresponds to the M_{1+}-multipole. However, from the quantum numbers, the excitation can also proceed via the absorption of an electric quadrupole photon $E2$, corresponding to the E_{1+} multipole. In nuclear physics, electric quadrupole transitions are an important tool for the study of quadrupole moments related to deformations of the nuclei. In many nucleon models, a tensor force in the hyperfine interaction, first suggested by De Rujula, Georgi, and Glashow [92], arises from one gluon exchange between the quarks, and leads to a d-state admixture in the ground state. This is similar to the tensor force in the nucleon - nucleon interaction which gives rise to a d-state admixture in the deuteron ground state and results in the prolate deformation of the deuteron.

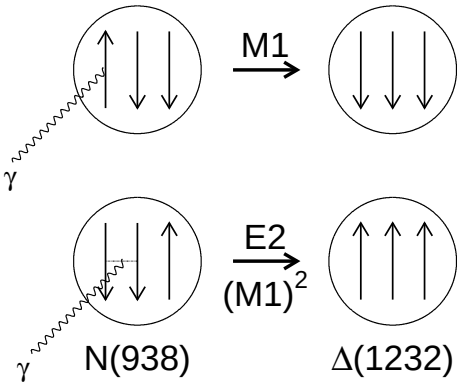

Figure 12: Upper part: excitation of the Δ-resonance via the spin-flip of a single quark from absorption of a magnetic dipole photon. Lower part: absorption of an electric quadrupole photon on a quark pair correlated by gluon or meson exchange currents, resulting in a spin-flip of the pair.

The situation for the nucleon is different in so far as an intrinsic quadrupole deformation cannot be directly measured for particles with spin less than one but may reveal itself in transitions between the ground and the excited states. Therefore, the idea is to look for an $E2$-admixture in the Δ-excitation. In the quark picture, such an admixture can occur in two different ways. An electric quadrupole photon can induce the spin-flip on a quark, with the initial or final state $L = 2$, when either the nucleon or the Δ has a d-state admixture in its wave function. This scenario is related to a possible deformation of the baryons. However, it was pointed out by Buchmann and collaborators [96]-[99] that $E2$ admixtures in the absence of d-state components in the wave functions may stem from the coupling of the photon to mesonic or gluonic exchange currents. Indeed they predict that this process provides a large contribution to the observed $E2$ strength. As illustrated in fig. 12, it results in the simultaneous spin-flip of two quarks which are both in s-states and correlated via gluon or meson exchange. Therefore, care has to be taken in the interpretation of possible $E2$ admixtures. Nevertheless, it is indisputable that the $E2$ admixture in the amplitude is sensitive to the internal structure of the nucleon, and its measurement provides a stringent test of baryon model predictions. The quantity of interest is the ratio:

$$R_{EM} = \left.\frac{E_{1+}^{(3/2)}}{M_{1+}^{(3/2)}}\right|_{W=M_\Delta} = \left.\frac{\mathrm{Im}E_{1+}^{(3/2)}}{\mathrm{Im}M_{1+}^{(3/2)}}\right|_{W=M_\Delta}, \tag{16}$$

where the index $(3/2)$ indicates the isospin I of the πN-system. The Fermi-Watson theorem guarantees that $E_{1+}^{(3/2)}/M_{1+}^{(3/2)}$ is a real number, at least up to the two-pion threshold. However, the ratio depends on the photon energy, and the resonance position is taken to be the energy where the phase is 90^o.

Predictions for this ratio are available from many different nucleon models. SU(6)-symmetry, as employed in the MIT bag model, requires R_{EM}=0. Constituent quark models predict values in the range -3.5%< R_{EM} <0% [10],[93]-[96] while relativized quark models [100, 101] yield small values around -0.1%. The cloudy bag model [102, 103] produces results in the range -3.0%< R_{EM} <-2.0% while Skyrme models [104] tend to give larger values between -2.5% and -5%. First results from QCD lattice calculations ($R_{EM} = (+3 \pm 8)\%$) [105] presently have rather large uncertainties.

The experimental determination of R_{EM} is difficult. The $E2$ admixture is small, and photoproduction reactions are dominated by the magnetic M_{1+} multipole. Furthermore, we have already seen that photoproduction in the Δ range has significant contributions from background processes. Multipole analyses of data prior to 1999 as in [57] made a first step towards the extraction of the resonant $E_{1+}^{(3/2)}$-amplitude. As pointed out in [107], systematic errors in the data base have a large influence on the result. This is so because the older experimental results, often obtained with untagged bremsstrahlung beams, came from a number of experiments with different systematic error sources. When combined, even the shapes of angular distributions are affected by different normalization errors. Observables, like angular distributions and polarization degrees-of-freedom or observables from different isospin channels, were often not consistent. The analysis of inconsistent data sets is problematic for weak multipoles which may be completely obscured by such effects. Therefore, attempts were made to explore new experimental possibilities for a sensitive search for the $E_{1+}^{(3/2)}$ admixture. The experiments determined all relevant observables simultaneously, so that systematic uncertainties were minimized. Two independent measurements were carried out at the MAMI accelerator in Mainz [106, 107] and at the LEGS laser backscattering facility at BNL [108, 109]. Both experiments established angular distributions and photon beam asymmetries for the reactions $\gamma p \to p\pi^o$ and $\gamma p \to n\pi^+$. In addition, the LEGS experiment determined the same observables for Compton scattering. There are two reasons why the choice of reactions and observables comes naturally.

The measurement of the two isospin channels allows the extraction of the I=3/2 contribution in the final state. From eqs. (89,91) follows that all multipole amplitudes M_{1+}, E_{1+},... denoted as $\mathcal{M}_{l\pm}$ can be decomposed into the isospin 1/2 components ${}_p\mathcal{M}_{l\pm}^{(1/2)}$ and the isospin 3/2 components $\mathcal{M}_{l\pm}^{(3/2)}$ via:

$$\mathcal{M}_{l\pm}(p\pi^o) =_p \mathcal{M}_{l\pm}^{(1/2)} + \frac{2}{3}\mathcal{M}_{l\pm}^{(3/2)} \qquad \mathcal{M}_{l\pm}(n\pi^+) = \sqrt{2}\left({}_p\mathcal{M}_{l\pm}^{(1/2)} - \frac{1}{3}\mathcal{M}_{l\pm}^{(3/2)}\right) . \tag{17}$$

The amplitudes $\mathcal{M}_{l\pm}^{(I)}$ are complex functions of the incident photon energy. The phases can be related to the corresponding pion - nucleon scattering phase shifts $\delta_{l\pm}^{(I)}$ via the Fermi-Watson theorem [110]:

$$\mathcal{M}_{l\pm}^{(I)} = \left|\mathcal{M}_{l\pm}^{(I)}\right| e^{(i\delta_{l\pm}^{(I)} + n\pi)} , \tag{18}$$

where n is an integer. This relation is strictly valid only below the two-pion photoproduction threshold at $E_\gamma \approx$310 MeV. It is valid approximately well above the two-pion threshold since the πN inelasticities in the P_{33} partial wave are small even at energies around 400 MeV.

The importance of the photon beam asymmetry Σ stems from the fact that it contains an interference term proportional to the product of the small E_{1+} term with the leading M_{1+} multipole (see below). The beam asymmetry is defined by:

$$\Sigma(\Theta) = \frac{d\sigma_\perp(\Theta) - d\sigma_\parallel(\Theta)}{d\sigma_\perp(\Theta) + d\sigma_\parallel(\Theta)} . \tag{19}$$

$\sigma_\perp(\Theta)$ and $\sigma_\parallel(\Theta)$ are the cross sections perpendicular and parallel to the plane defined by the photon polarization and momentum vectors of a 100% linearly polarized photon beam. It is related to the differential cross section via:

$$\frac{d\sigma(\Theta,\Phi)}{d\Omega} = \frac{d\sigma_o(\Theta)}{d\Omega}\left[1 - P\Sigma(\Theta)cos(2\Phi)\right] \tag{20}$$

where P is the degree of linear polarization of the photon beam and Φ is the angle with respect to the polarization plane. The photon beam at the LEGS facility [111] is produced via the scattering of laser photons at a high energy electron beam. Linear or circular polarization of the laser beam is transferred to the backscattered photon beam where the highest transfer of linear polarization (100%) is achieved for photons scattered at 180^o, corresponding to the highest photon beam energies. The MAMI tagged photon facility [112] works with bremsstrahlung tagging. Here, linear polarization can be produced with coherent bremsstrahlung off a diamond crystal [113]. The energy region with the highest degree of polarization can be varied with the orientation of the crystal. Reasonable polarization cannot be achieved at photon energies larger than $\approx 2/3$ of the maximum photon energy. This is not a disadvantage for the presently discussed experiment since the MAMI-B facility provided a photon beam with energies up to 800 MeV while the LEGS facility reaches 330 MeV only. The MAMI experiment covered the complete range of the Δ-resonance, while the LEGS experiment measured only up to the maximum of the Δ-peak. An example for the experimental differential cross sections and the photon beam asymmetry is shown in fig. 13.

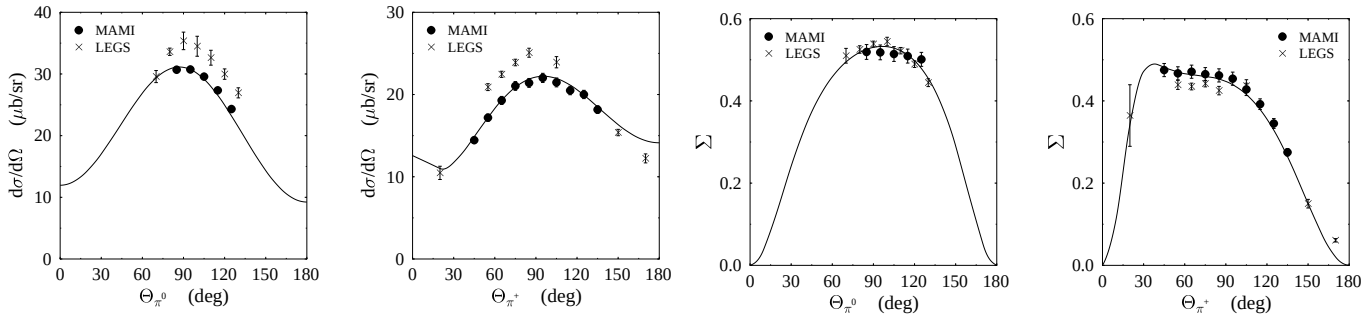

Figure 13: Differential cross sections $d\sigma/d\Omega$ and photon asymmetry Σ for the reactions $p(\vec{\gamma},\pi^o)p$ and $p(\vec{\gamma},\pi^+)n$ for $E_\gamma = 320$ MeV from the LEGS [108, 109] and the MAMI experiment [106, 107]. The curves correspond to the energy dependent analysis of the MAMI data. (Fig. from [107].

The shape and the absolute scale of the differential cross sections published by the two groups do not agree for photon energies close to the resonance maximum. The agreement is somewhat better at lower incident photon energies [107]. Close to the resonance peak, a disagreement at the 10% level is observed for both channels, which is well outside the claimed systematic uncertainties on the 3% level. Recently, the same problem has emerged for Compton scattering, where an experiment performed at MAMI [114, 115] finds systematically smaller cross sections than the LEGS-experiment. The LEGS-group has investigated this issue in [116] where the calibration procedures are discussed in detail. The authors emphasize that they do not find any source of additional systematic errors. The $p\pi^o$ final channel has been investigated at MAMI using two different detection systems, the DAPHNE-detector [106, 107] as well as the TAPS-detector [89, 107]. Both results are consistent. In addition, the Mainz results are consistent with previous measurements at Bonn, for both the $\pi^o p$ [117, 118] and the $\pi^+ n$ [119],[90] channels. In summary, there seems to be a yet unexplained systematic difference in the cross section results from Bonn/Mainz versus LEGS on the 10% level, which is clearly unsatisfactory. However, the extraction of the $E2$-admixture involves mainly ratios where the results from Mainz and LEGS for R_{EM} are still marginally consistent within their uncertainties.

The first result for R_{EM} from the MAMI data was obtained from an analysis of the $\pi^o p$ final state [106] only. We will shortly discuss this analysis, which is instructive in view of the importance of the polarization degree-of-freedom while involving some approximations. As long as only s- and p-waves contribute, the differential cross sections can be written as:

$$\frac{d\sigma_x(\Theta^\star)}{d\Omega} = \frac{q^\star}{k^\star}\left[A_x + B_x cos(\Theta^\star) + C_x cos^2(\Theta^\star)\right] , \tag{21}$$

where x indicates the unpolarized (0), parallel ($\parallel$) and perpendicular ($\perp$) components. The largest sensitivity to the E_{1+}-multipole due to an interference term with the leading M_{1+} is carried by the parallel component [107]:

$$\begin{aligned} A_\parallel &= |E_{0+}|^2 + |3E_{1+} - M_{1+} + M_{1-}|^2 \\ B_\parallel &= 2\mathrm{Re}\left[E_{0+}(3E_{1+} + M_{1+} - M_{1-})^*\right] \\ C_\parallel &= 12\mathrm{Re}\left[E_{1+}(M_{1+} - M_{1-})^*\right] \end{aligned} \tag{22}$$

$$\text{with:} \qquad R \equiv \frac{1}{12}\frac{C_\parallel}{A_\parallel} = \frac{\mathrm{Re}\left[E_{1+}(M_{1+} - M_{1-})^*\right]}{|E_{0+}|^2 + |3E_{1+} - M_{1+} + M_{1-}|^2} \; . \tag{23}$$

It is then argued that at the resonance position $\mathrm{Re}(M_{1+} - M_{1-})$, $|E_{0+}|^2$, and $9\,|E_{1+}|^2$ can be neglected so that [107]:

$$R = \frac{R_{\pi^o}}{1 - 6R_{\pi^o}} \qquad \text{with:} \qquad R_{\pi^o} = \frac{\mathrm{Im}E_{1+}}{\mathrm{Im}M_{1+} - \mathrm{Im}M_{1-}} \approx \frac{\mathrm{Im}E_{1+}}{\mathrm{Im}M_{1+}^{(3/2)}} \; . \tag{24}$$

In the last approximation, the imaginary part of the non-resonant M_{1-}-multipole and the isospin $I = 1/2$ component of the M_{1+}-multipole, which resonates in the $I = 3/2$ component, are neglected. In this approximation, R_{π^o} equals R_{EM} (see eq. (16)) up to corrections for isospin $I = 1/2$ contributions to the E_{1+}-multipole. In the first analysis in [106], the $3E_{1+}$-term in the denominator of eq. (23) was neglected. The above approximations and the neglect of higher partial waves are discussed in detail in [120, 121, 122, 107]. The energy dependence of $R \equiv C_\parallel/12A_\parallel$ is shown in fig. 14 (right hand side), and the value obtained for R at resonance [106, 107] is $R = (-2.5 \pm 0.2_{stat})\%$ which, without corrections for $I = 1/2$ contributions to the E_{1+}-multipole, corresponds to $R_{EM} = -2.95\%$. Including corrections for Born-terms of the order of 10 - 20% for $\mathrm{Im}E_{1+}^{(1/2)}/\mathrm{Im}E_{1+}$, Beck et al. quote [107]:

$$R_{EM} = (-2.5 \pm 0.2_{stat} \pm 0.2_{syst})\% \; . \tag{25}$$

This analysis benefits from the fact that, at the resonance position at 340 MeV, π^o-photoproduction is practically free of background contributions, as we have already seen in the discussion of the unpolarized cross section (see figs. 9,10). Therefore, a full multipole analysis is not necessary. On the other hand, the contribution of the isospin 1/2 final state to the multipoles is not determined, and can only be estimated from model predictions. The clean separation of the isospin $I = 1/2$ and $I = 3/2$ components requires a combined analysis of the $\pi^o p$ and $\pi^+ n$ final states. Since the latter is strongly affected by background contributions, a much more involved analysis is necessary. Such analyses have been performed for the LEGS and the Mainz data.

The LEGS-data were analyzed in an energy dependent way, using a parameterization of the energy dependence of the (γ, π) multipole amplitudes of the following type [108]:

$$\mathcal{M}_{l\pm}^i = \left[\mathcal{M}_B^I(E_\gamma) + \alpha_1\epsilon_\pi + \alpha_2\epsilon_\pi^2 + \alpha_3\Theta_{2\pi}(E_\gamma - E_\gamma^{2\pi})^2\right] \times \left(1 + iT_{\pi N}^l\right) + \beta T_{\pi N}^l \; , \tag{26}$$

where E_γ and ϵ_π are photon beam energy and pion kinetic energy. $\mathcal{M}_B^I$ are pseudo-vector Born amplitudes including ρ and ω t-channel exchange. The $\alpha_i\epsilon^j$ terms are a phenomenological parameterization of non-Born background contributions, and the $\alpha_3\Theta_{2\pi}(E_\gamma - E_\gamma^{2\pi})^2$ term with the unit Heavyside step function ($\Theta_{2\pi} = 1$ for $E_\gamma > E_\gamma$=309 MeV) accounts for s-wave double pion production (used only for the E_{0+} multipole). The πN scattering matrix elements $T_{\pi N}^l$ were taken from the SAID multipole analysis [57]. The first term of eq. (26) parameterizes the background contributions and the $\beta T_{\pi N}^l$ term the resonance contributions. For a single resonance decaying into a single channel, the latter has the usual energy dependence of a Breit-Wigner curve. The ansatz satisfies the Watson theorem below

the 2π threshold and maintains unitarity at higher energies in a model dependent way. The multipoles up to the f-waves were included, and Born terms were kept up to l=19. The imaginary parts of the Compton amplitudes are connected to the (γ,π) multipoles via unitarity and their real parts were evaluated with dispersion integrals. The calculation of the latter requires (γ,π) multipoles outside the range of the analysis of the LEGS data, which were estimated from other sources (see [108] for details). The parameters of the (γ,π) multipoles where then fitted to the cross section data from the $p(\vec{\gamma},\pi^o)p$, $p(\vec{\gamma},\pi^+)n$, and $p(\vec{\gamma},\gamma)p$ reactions and additional data for beam- [123], target- , and recoil polarization [128, 124, 125] and for double polarization observables [126, 127]. Only ratios of the additional polarization data were used in order to minimize normalization uncertainties. The $E2$ admixture of the Δ excitation is determined as the ratio of the β coefficients of the $E_{1+}^{(3/2)}$ and $M_{1+}^{(3/2)}$ multipoles. In the fit, this ratio equals the ratio of the imaginary parts of the two multipoles. Systematic model uncertainties from higher partial waves, the πN phase shifts, relative energy calibrations and assumptions used for the calculation of the Compton dispersion integrals are included. The authors quote a final result of [108] $R_{EM} = (-3.0 \pm 0.3_{stat+syst} \pm 0.2_{model})\%$. After a more refined analysis using an enlarged data base the final result is [116]:

$$R_{EM} = (-3.07 \pm 0.26_{stat+syst} \pm 0.24_{model})\% \; . \tag{27}$$

The combined results for the differential cross sections and photon beam asymmetries of the $\pi^o p$ and $\pi^+ n$ channels from the Mainz experiment [107] were analyzed with an energy dependent and an energy independent multipole analyses. For the energy independent analysis of the MAMI data alone, 8

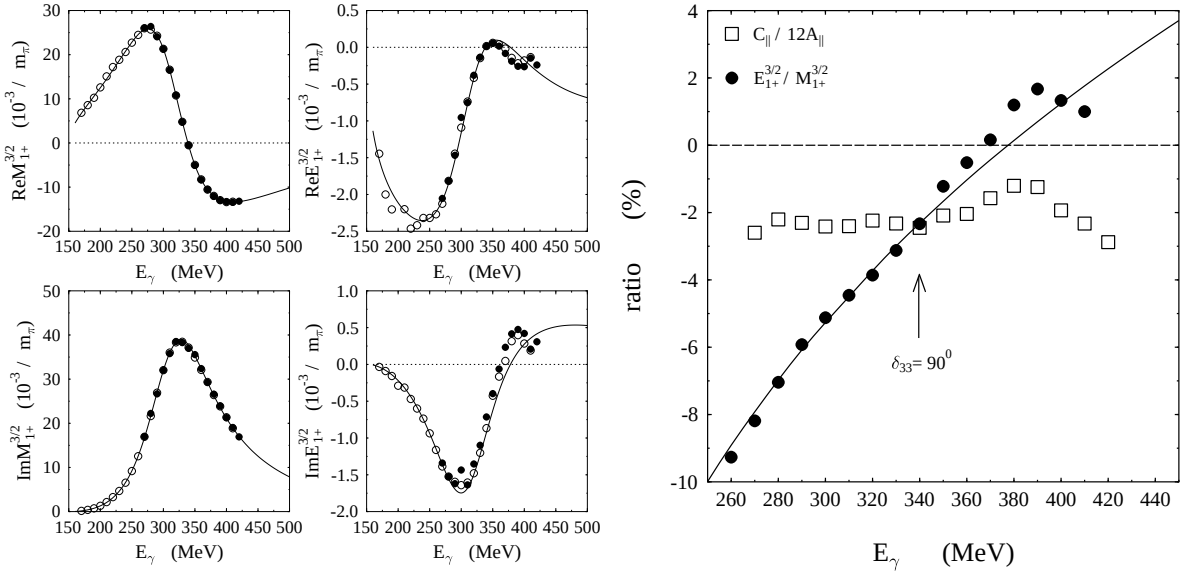

Figure 14: Extraction of R_{EM} [107]. Left hand side: Real and imaginary parts of the $I = 3/2$ components of the M_{1+} and E_{1+} amplitudes. Solid circles: energy independent fits of the MAMI data alone. Line and open circles: energy dependent and energy independent fixed-t dispersion analysis of a larger data base [54]. Right hand side: energy dependence of the ratio $E_{1+}^{(3/2)}/M_{1+}^{(3/2)}$. Solid circles (energy independent) and solid line (energy dependent) results of the fixed-t dispersion analysis [54]. Open squares: energy dependence of $R \equiv C_\parallel/12A_\parallel$.

parameters (the s- and p-wave multipole amplitudes $E_{0+}^{(I)}$, $M_{1+}^{(I)}$, $E_{1+}^{(I)}$ and $M_{1-}^{(I)}$, I=1/2,3/2) were fitted to the data independently for 16 energy intervals between 270 and 420 MeV incident photon energy. Higher partial waves were taken into account for the Born-terms. The result for the imaginary and real parts of the two multipoles of interest are shown as solid dots in fig. 14. The data were furthermore analyzed with fixed-t dispersion relations based on Lorentz invariance, isospin symmetry, unitarity, and

crossing symmetry [54]. This second analysis also included more recent Mainz data for the differential cross sections of the $\pi^o p$ final state [88, 89], data from Bonn for the target asymmetry [90, 128, 129], and differential cross sections for π^- photoproduction off the neutron [130, 131]. The results for the multipoles of the two analyses are shown in fig.14 (left hand side, open circles and line). All three analyses agree very well, and the ratio of the $E_{1+}^{(3/2)}$ and $M_{1+}^{(3/2)}$ multipoles is shown in fig. 14 (right hand side). The combined final result from the three analyses is quoted as [107]:

$$R_{EM} = (-2.5 \pm 0.1_{stat} \pm 0.2_{syst})\% \ , \tag{28}$$

which is lower than the LEGS result, but still consistent within the combined uncertainties.

The data from [107, 108] have also been analyzed by other groups. Davidson and Mukhopadhyay [120], and Workman [121] found quite different results for R_{EM}. Davidson and Mukhopadhyay used their effective Lagrangian model [63] for an analysis of the data from [106], and found a value of R_{EM} = (-3.19 ± 0.24)%. Workman, using the SAID-multipole analysis [57], found a much smaller value of R_{EM} = (-1.5 ± 0.5)% [121]. However, as pointed out in [107], these discrepancies can be traced to the data bases employed. In case of the effective Lagrangian analysis, the inclusion of the Mainz $\pi^+ n$-data in the data base lowered the result to R_{EM} = (-2.64 ± 0.25)%. The small value obtained in the VPI multipole analysis is due to the inclusion of older data sets. Removal of the $\pi^o p$ data prior to 1980 from the SAID data base raises R_{EM} into the range of the other analyses [107, 132]. In summary, the extraction of the R_{EM} value seems to be almost model independent as long as the same data basis is used. The main systematic discrepancy which remains unresolved is the scale difference between the differential cross section data from Mainz and LEGS which results in a R_{EM} value close to -3% for LEGS, and close to -2.5% for Mainz.

Apart from systematic effects in the extraction of R_{EM}, another aspect is important for the comparison of the experimental result to quark model predictions. The very definition of the $E2/M1$ ratio and its relation to quantities predicted by models has to be considered. R_{EM} is defined to correspond to the $E2/M1$ ratio at the K-matrix pole on the real energy axis. Recently, it has been argued (see e.g. [133]), that the T-matrix pole in the complex plane, which can be evaluated with the 'speed-plot' technique, is a more fundamental quantity. However, the $E2/M1$ ratio at the T-matrix pole is a complex quantity and is not easily related to the real predictions of the quark models. Finally, as already discussed above, the value extracted from the data applies to the 'dressed' resonance, while models in general will predict it for the 'bare' resonance. Kamalov and Yang [134] have investigated this problem with a dynamical model using a scattering equation of the type shown in fig. 8. Fitting the data with this model, they indeed find a large difference between the 'dressed' and 'bare' values. The resulting $E2/M1$-ratio for the 'dressed' resonance of (-2.5 ± 0.14)% agrees nicely with the other analyses, but the result for the 'bare' resonance of ($+0.25\pm0.19$)% is positive and compatible with zero. It is thus concluded that the 'bare' Δ is nearly spherical and the $E2/M1$ mixing for the 'dressed' resonance can be attributed to the pion cloud, i.e. to pion re-scattering effects. In a similar analysis, Sato and Lee [135] also find a significant difference between the 'dressed' (-2.7%) and 'bare' (-1.3%) values of $E2/M1$. However, in their dynamical model the 'bare' value is negative and has a larger magnitude than in the model of Kamalov and Yang. Recently, the predictions of the two models for a different observable have been tested experimentally [136]. The experiment determined the beam-helicity asymmetry $\rho_{LT'}$ in the electroproduction of π^o-mesons with longitudinally polarized electrons ($p(\vec{e}, e'\pi^o)$p). The MAID model [67] as well as the two dynamical models correctly predict the negative sign of the measured asymmetry and agree fairly well with the angular dependence. However, all fail to reproduce the absolute magnitude. The MAID model, and the dynamical model of Kamalov and Yang *overestimate* the magnitude by roughly 30% while the model of Sato and Lee *underestimates* it by almost the same value. These results seem to indicate that the pion cloud effects are not yet well under control in the models. In this sense, any comparison of the experimental value for R_{EM} to model predictions must be regarded with care.

For some issues, electron scattering results obtained at finite momentum transfer Q^2 are closely related to the topic of this review, and we find it necessary to include them. In the case of virtual photons, the $C2$ Coulomb quadrupole excitation, which corresponds to the S_{1+}-multipole, can additionally contribute. The $C2$ analog to the R_{EM}-ratio for the $E2$-admixture is the R_{SM}-ratio defined via:

$$R_{SM} = S_{1+}^{(3/2)}/M_{1+}^{(3/2)} \ . \tag{29}$$

Perturbative QCD (pQCD) predicts [137]-[139] that, in the limit of very high Q^2, only helicity conserving amplitudes survive. In particular, the $A_{3/2}$ and $A_{1/2}$ helicity amplitudes for the electromagnetic excitation of the Δ scale like [137]:

$$A_{3/2} \propto Q^{-5} \qquad A_{1/2} \propto Q^{-3} \tag{30}$$

for large Q^2. Consequently, the $A_{1/2}$-amplitude dominates the Δ-excitation for large Q^2. This means, that pQCD predicts an asymptotic R_{EM} value of +100% (see eqs. (36,37)). The prediction for R_{SM} at large Q^2 is a constant value. Therefore, investigating the R_{EM} value as function of Q^2, the transition from the constituent quark model to the region of pQCD can be studied.

At Bates, Bonn (ELSA), JLab, and Mainz (MAMI), efforts to measure the Q^2-dependence of R_{EM} and R_{SM} have been undertaken [140]-[145]. The results are summarized and compared to older data in fig. 15. It is evident from the figure, that the recent experiments have improved the data base significantly. The scattering of the data prior to 1990 was substantial. In the case of R_{EM}, not even a clear tendency towards positive or negative values was visible. Meanwhile, the new data establish the Q^2-dependence for both ratios more firmly. The result for R_{EM} are small, negative values showing no pronounced Q^2-dependence up to 4 GeV^2 while R_{SM} seems to drop as function of Q^2. Since pQCD predicts R_{EM}=+100% and a constant R_{SM}-value, it is obvious that up to momentum transfers squared of 4 GeV^2 an onset of pQCD behavior is not visible. For a more detailed interpretation of the results

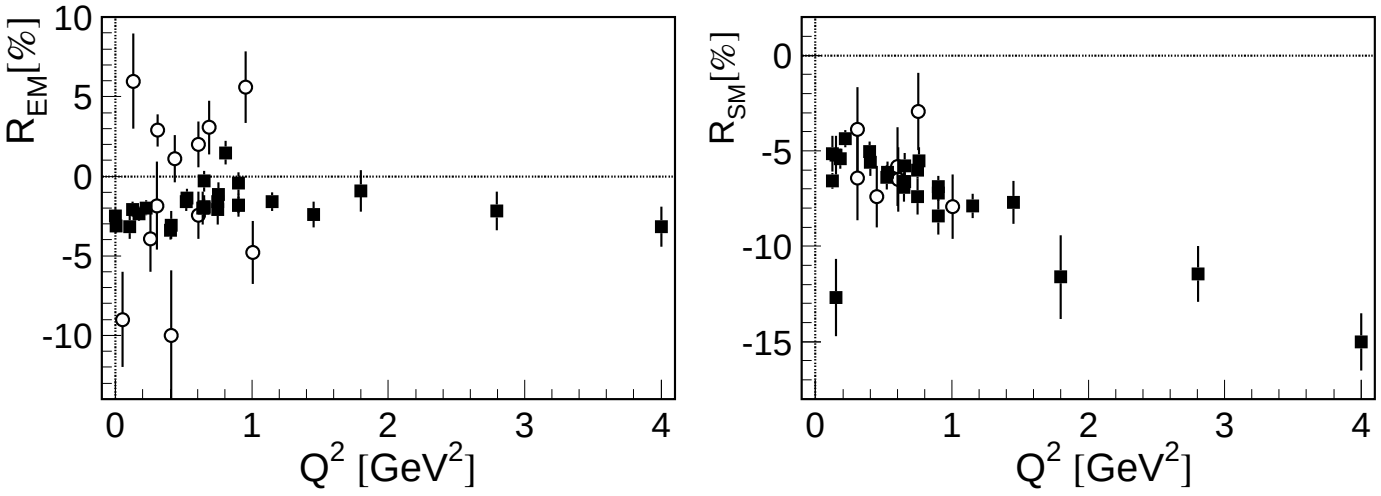

Figure 15: Q^2-dependence of R_{EM} (left hand side) and R_{SM} (right hand side). Photon point values (Q^2=0): refs. [107, 116], values for $Q^2 > 0$: [140]-[146] and ref. therein. Open symbols: pre-1990 data.

one should keep in mind that the extraction of the R_{EM} and R_{SM} ratios is not completely model independent. The problem is connected to the non-resonant background contributions which we have already discussed for the measurements at the photon point and which are less well under control for high Q^2. The measurement of a rather large induced proton polarization p_n in π^o electroproduction at Bates [147] was interpreted as evidence for background contributions larger than those predicted by models. However, in principle this observable and R_{SM} extracted from the double polarization measurement $p(\vec{e}, e'\vec{p})p$ [145] can involve different combinations of multipole amplitudes. In particular, while p_n is sensitive to the real part of the background amplitudes, R_{SM} is only sensitive to the imaginary part [147, 145], so that it is difficult to judge the influence of the background amplitudes on R_{SM}.

3.2 *Helicity Dependence of Pion Photoproduction in the Δ-Range*

The initial photon - nucleon state is characterized by the helicities, i.e. the spin projections onto the momentum axis (see app. 6.2). For a real photon with $\lambda = \pm 1$ and the nucleon with $\nu_i = \pm 1/2$, two different possibilities exist which are schematically shown in fig. 16. They correspond to the photoproduction cross sections $\sigma_{1/2}$ and $\sigma_{3/2}$ with total helicities 1/2 and 3/2.

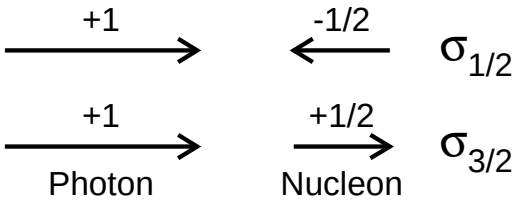

Figure 16: Definition of $\sigma_{1/2}$, $\sigma_{3/2}$. The arrows symbolize the spin projections of the photon and nucleon onto the momentum axis of the incoming photon.

In 1966, Gerasimov [148] and independently Drell and Hearn [149] derived the Gerasimov-Drell-Hearn (GDH) sum rule which relates the difference of the two helicity components of the total photoabsorption cross section to static properties of the nucleon via the GDH-integral:

$$\int_{m_\pi}^{\infty} \frac{\sigma_{3/2}(\omega) - \sigma_{1/2}(\omega)}{\omega} d\omega = \frac{\pi e^2}{2m_N^2}\kappa^2 \ , \qquad (31)$$

where $\omega = E_\gamma$ is the incident photon energy in the lab frame, m_π the mass of the pion, m_N the mass of the nucleon, and κ the anomalous magnetic moment of the nucleon.

During the last few years, the GDH collaboration has undertaken a joint effort towards the experimental verification of the sum rule, measuring the difference of the helicity components in total photoabsorption. The experiment is divided into two parts, the first for the energy range from the pion threshold up to 800 MeV carried out at the Mainz MAMI accelerator and the second in the energy range 600 MeV - 3 GeV at the Bonn ELSA accelerator. The experiment requires a measurement with a circularly polarized photon beam and a longitudinally polarized proton target. Circularly polarized photon beams are produced via backscattering of circularly polarized laser beams (LEGS, GRAAL) or via bremsstrahlung of longitudinally polarized electron beams (MAMI, ELSA). Both are now available at most electron beam facilities. For the longitudinally polarized protons, a butanol (C_4H_9OH) frozen spin target was developed [150]. The recent advance in the technology of polarized targets (see [151] for a review) was essential for the success of the experiment. First results for the GDH integral have been published [152, 153]. Here, we will not discuss the sum rule itself but emphasize another aspect.

The low energy part of the experiment has not only determined the helicity dependence of the total absorption cross section, but also provided results for the helicity difference for exclusive channels [153]-[155]. These observables provide valuable new constraints for the multipole analysis of photoproduction reactions. As an example, we consider the single pion photoproduction reactions $\vec{\gamma}\vec{p} \to p\pi^o$ and $\vec{\gamma}\vec{p} \to n\pi^+$. The measured helicity difference $\Delta\sigma = \sigma_{3/2} - \sigma_{1/2}$ for these reactions [152] is shown in fig. 17. The total cross section for each channel is given by $\sigma_{tot} = (\sigma_{3/2} + \sigma_{1/2})/2$ and the cross sections corresponding to the helicity 3/2 and 1/2 states can be reconstructed from:

$$\sigma_{3/2} = \sigma_{tot} + \frac{1}{2}\Delta\sigma \qquad \sigma_{1/2} = \sigma_{tot} - \frac{1}{2}\Delta\sigma \ . \qquad (32)$$

The results for the two cross sections are shown in the lower part of fig. 17. The total cross section for both reactions was taken from the MAID parameterization [67] (see also fig. 9). If only the Δ excitation were to contribute to the observed cross sections, the ratio of the helicity 3/2 and 1/2 components would give directly the ratio of the $A_{3/2}$ and $A_{1/2}$ helicity amplitudes of the Δ. However, it is obvious from fig. 17 that the helicity 1/2 component for the $n\pi^+$ channel has significant background contributions. So far, background contributions for all observables investigated have been weak for the $p\pi^o$ channel at the Δ position of 340 MeV incident photon energy. It is interesting to check which ratio of the helicity amplitudes would follow from the experimental π^o cross sections at $E_\gamma = 340$ MeV, assuming

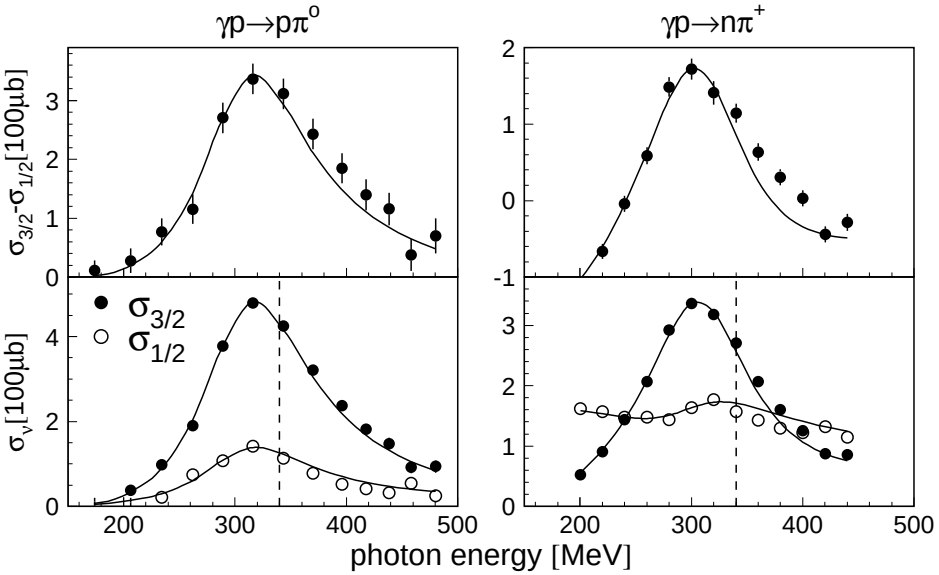

Figure 17: Helicity dependent pion photoproduction cross sections in the Δ range (left hand side: $p\pi^o$, right hand side: $n\pi^+$ final states). Top part: cross section difference of the two helicity states [153]. Bottom part: helicity dependent cross sections (full symbols: $\sigma_{3/2}$, open symbols: $\sigma_{1/2}$). Curves: MAID results [67]. Dashed lines: Δ resonance position.

background is negligible. The result (up to a sign) is:

$$\frac{A_{3/2}}{A_{1/2}} \approx \sqrt{\frac{\sigma_{3/2}(\gamma p \to p\pi^0, W = M_\Delta)}{\sigma_{1/2}(\gamma p \to p\pi^0, W = M_\Delta)}} = (1.94 \pm 0.15_{stat} \pm 0.10_{syst}) \; . \tag{33}$$

This value compares very well with recent results for the helicity amplitudes obtained from the full multipole analyses of the differential cross sections and photon beam asymmetries as discussed in the previous section:

$$\frac{A_{3/2}}{A_{1/2}} = \frac{-(251.0 \pm 1.0)(10^{-3}\sqrt{\text{GeV}})}{-(131.0 \pm 1.0)(10^{-3}\sqrt{GeV})} = (1.916 \pm 0.016) \; , \qquad \text{ref. [107]} \tag{34}$$

$$\frac{A_{3/2}}{A_{1/2}} = \frac{-(266.9 \pm 8.0)(10^{-3}\sqrt{\text{GeV}})}{-(135.7 \pm 3.9)(10^{-3}\sqrt{\text{GeV}})} = (1.967 \pm 0.082) \; , \qquad \text{ref. [116]} \; . \tag{35}$$

The ratio of the helicity amplitudes is connected to the $E2$ admixture in the Δ excitation. For a pure $M1$ transition it would be given by the ratio of the Clebsch-Gordan coefficients for the 3/2 and 1/2 states which is $\sqrt{3} = 1.73$. One can check using the MAID model [67] that the cross section ratio $\sigma_{3/2}/\sigma_{1/2}$ for π^o-photoproduction at $E_\gamma = 340$ MeV is predicted to be very close to the Clebsch-Gordan (1.70) when the $E2$-contribution is switched off but all background contributions are kept. This is another indication that this ratio seems to be almost unaffected by background contributions.

The connection between the helicity and multipole amplitudes for the Δ excitation in the presence of a non-vanishing $E2$ admixture is given by:

$$R_A = \frac{A_{3/2}}{A_{1/2}} = \left. \frac{\sqrt{3}\left(M^\Delta_{1+} - E^\Delta_{1+}\right)}{(M^\Delta_{1+} + 3E^\Delta_{1+})} \right|_{W=M_\Delta} \; . \tag{36}$$

The ratio of the helicity amplitudes and the R_{EM} value are related by:

$$R_{EM} = \left. \frac{E^\Delta_{1+}}{M^\Delta_{1+}} \right|_{W=M_\Delta} = \frac{\sqrt{3} - R_A}{3R_A + \sqrt{3}} \; , \tag{37}$$

which results in R_{EM}=−2.75%, in agreement with refs. [107, 116]. It must be emphasized that possible background contributions have been neglected. The extracted R_{EM} value is therefore less well founded than the results obtained from the multipole analysis. However, it demonstrates that the results obtained from the differential cross sections and photon beam asymmetries are consistent with the outcome of the helicity dependent cross sections.

3.3 *The Magnetic Moment of the Δ-Resonance*

The anomalous magnetic moments of proton and neutron [156] gave the first hint for a substructure of the nucleon. As is the case in nuclear physics, magnetic moments depend sensitively on the details of the wave functions. The magnetic moments of the octet baryons (N, Λ, Σ, Ξ) are known precisely from spin precession measurements [36]. However, the lifetimes of the decuplet baryons are so short that a direct measurement of the magnetic moment was only possible for the Ω^-. The Δ-resonance is a particularly interesting case for which models assume a quark structure similar to the nucleon ground state but with spin and isospin of the quarks coupled to 3/2 instead of 1/2. In the case of SU(3) flavor symmetry, the mass of the nucleon ground state and the Δ would be degenerate, and the magnetic moments would be related by $\mu_\Delta = Q_\Delta \mu_p$. Here, Q_Δ is the charge of the Δ and μ_p the magnetic moment of the proton. This would imply in particular that $\mu_{\Delta^+} = \mu_p$, and $\mu_{\Delta^o} = 0$. Predictions for the Δ-magnetic moments are available from a variety of nucleon models (see table 1). Experimentally, estimates have only been obtained for the Δ^{++}.

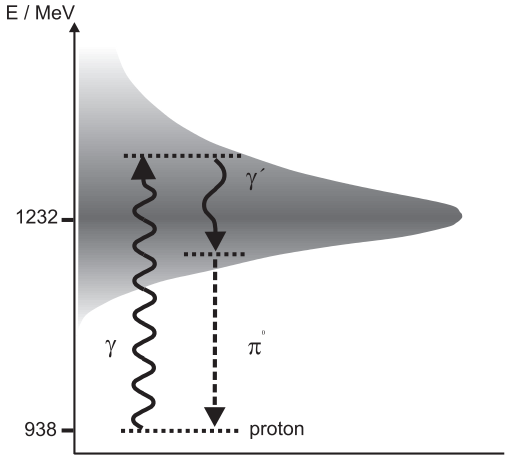

Figure 18: Principle of the determination of the Δ magnetic moment from the reaction $p(\gamma, \pi^o\gamma')p$.

The experimental value for $\mu_{\Delta^{++}}$ is based on two measurements of the hadron induced reaction $\pi^+ p \to \pi^+\gamma' p$ carried out at the University of California, Los Angeles (UCLA) [164, 165] and at the Paul Scherrer Institut, Switzerland [166]. The value quoted by the Particle Data Group (PDG) is $\mu_{\Delta^{++}}$= (3.7 - 7.5)μ_N. This large uncertainty comes mainly from a model dependence of the extraction of the magnetic moment from the data. The problem is that π^+-bremsstrahlung in the initial and final state makes a large contribution to the $\pi^+ p \to \pi^+\gamma' p$ cross section. Although kinematic conditions with maximum destructive interference between the bremsstrahlung contributions were chosen in the experiments, the model dependence of the analysis was significant. Different analyses of the UCLA experiment came up with values ranging from (3.7 - 4.2)μ_N to (6.9 - 9.8)μ_N [167]-[171].

Recently, a first attempt was made to measure the magnetic moment of the Δ^+ via the photon induced reaction $\gamma p \to \pi^o\gamma' p$. The principle of the experiment is the same as for the pion induced reaction and was first suggested by Kontratyuk and Ponomarev [172]. It is schematically depicted in fig. 18. The Δ-resonance is excited by a real photon, and decays within its final width via an electromagnetic $M1$ realignment transition, which is sensitive to the magnetic moment. Finally, the resonance de-excites by emission of a π^o-meson to the nucleon ground state. The small values of the $E2/M1$ admixture in the excitation of the Δ, as discussed in the previous section, indicate that the quadrupole deformation of the Δ must be small. Furthermore, electric quadrupole realignment transitions vanish in the limit of zero photon energy because of time reversal symmetry [179]. The next higher magnetic octupole is suppressed by two additional powers of photon momenta so that the re-alignment transition is dominated by the $M1$ multipole which couples to the magnetic dipole moment.

A pilot experiment [173, 174] was performed using the TAPS detector [175, 176] at the MAMI-B accelerator. In a fully exclusive measurement, the momenta of the recoil proton, the realignment photon, and the photons from the $\pi^o \to 2\gamma$ decay were measured. The π^o mesons were reconstructed via a standard invariant mass analysis. Additional kinematic cuts ensured the unique identification of the reaction and the rejection of background arising mainly from double π^o photoproduction events, where one photon had escaped detection due to the limited solid angle coverage of the detector.

Table 1: Model predictions for the magnetic moment of the $P_{33}(1232)$ resonance in units of the nuclear magneton $\mu_N = e\hbar/2m_p$. Models: relativistic quark model (RQM), chiral bag model (χB), chiral quark-soliton model (χQSM), chiral perturbation theory (χPT), QCD sum rules (QCDSR), light cone QCD sum rules (LCQSR), lattice QCD (LQCD).

Method	$\mu_{\Delta^{++}}/\mu_N$	$\mu_{\Delta^{+}}/\mu_N$	$\mu_{\Delta^{o}}/\mu_N$	$\mu_{\Delta^{-}}/\mu_N$
Experiment [36]	3.7 - 7.5			
SU(3)	5.58	2.79	0	-2.79
RQM [157]	4.76	2.38	0	-238
χB [158]	3.59	0.75	-2.09	-1.93
χQSM [159]	4.73	2.19	-0.35	-2.9
χPT [160]	4.0±0.4	2.1±0.2	-0.17±0.04	-2.25±0.25
QCDSR [161]	4.13±1.30	2.07±0.65	0	-2.07±0.65
LCQSR [162]	4.4±0.8	2.2±0.4	0	-2.2±0.4
LQCD [163]	4.91±0.61	2.46±0.31	0	-2.46±0.31

The contribution of bremsstrahlung processes to the $\gamma p \to \pi^o \gamma' p$ reaction is less important than for the $\pi^+ p \to \pi^+ \gamma' p$ reaction since the latter has the charged pions in the initial and final state. Nevertheless, the contributions are still significant, and a reaction model is necessary for the extraction of the magnetic moment. First calculations of the resonant $\Delta \to \Delta\gamma'$ process have been performed in the effective Lagrangian formalism by Machavariani, Faessler, and Buchmann [177] and by Drechsel, Vanderhaeghen, and Giannini [178]. The experimental data cannot be reproduced since the bremsstrahlung contributions are neglected in the calculations, and merely a first estimate of the size of the cross section is provided. Recently, Drechsel and Vanderhaeghen [179] included background diagrams from bremsstrahlung, non-resonant Born graphs, and vector meson exchange. A useful feature of this model is that the $\gamma p \to p\pi^o$ reaction can be calculated as a first step. Then, in a second step, the additional

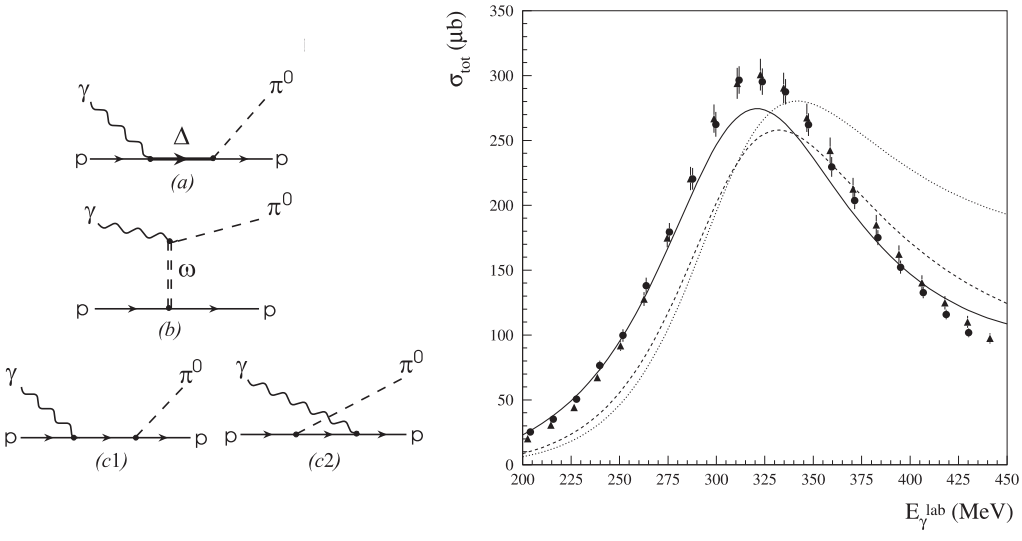

Figure 19: Left hand side: diagrams included in the model for $p(\gamma, \pi^o)p$ [179]. Right hand side: comparison of the model prediction to the measured total cross section of $p(\gamma, \pi^o)p$. Dotted: only Δ excitation, dashed: Δ and ω exchange, full: all contributions.

photon from the realignment transition and from bremsstrahlung contributions can be added. The diagrams included in the calculation of pion production and the comparison of the model result for the total cross section to data for π^o photoproduction are shown in fig. 19. At energies below the maximum of the Δ-resonance, the agreement is good but worsens at higher incident photon energies. This discrepancy is probably due to pion re-scattering contributions which have not yet been included in the model.

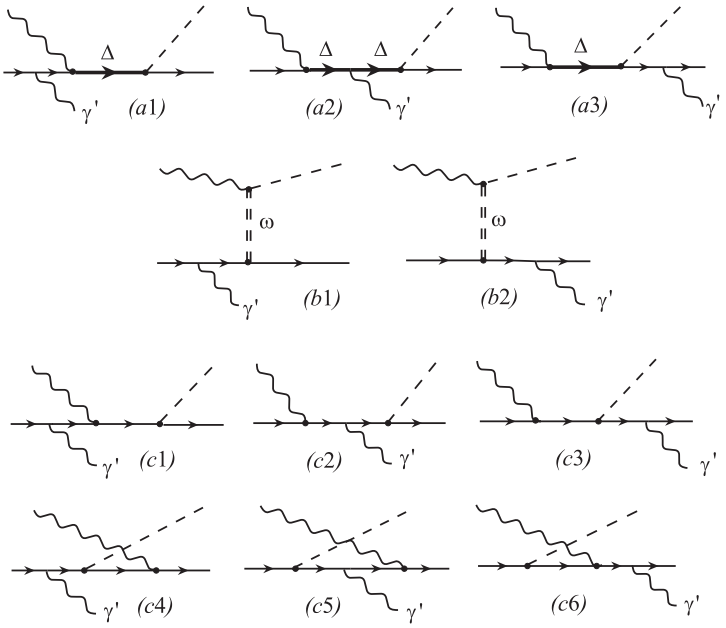

Figure 20: Diagrams included for the calculation of the $\gamma p \to p\pi^0\gamma'$ reaction [179]. The process of interest for the Δ-magnetic moment is diagram (a2).

The diagrams for the modeling of the $\gamma p \to p\pi^0\gamma'$ reaction are shown in fig. 20. The only new free parameter compared to the calculation for pion photoproduction is the magnetic moment μ_{Δ^+} of the Δ resonance in diagram (a2) which is expressed in terms of the anomalous magnetic moment κ_{Δ^+} via:

$$\mu_{\Delta^+} = (1 + \kappa_{\Delta^+})\frac{m_N}{m_\Delta}\mu_N \qquad (38)$$

where μ_N is the nuclear magneton, and m_N, m_Δ are the nucleon and Δ masses. A comparison of the model prediction for different values of κ_{Δ^+} to the data, shown in fig. 21, can be used for the extraction of the magnetic moment.

The energy distributions of the γ' photon for low energy incident photons show the typical $1/E_{\gamma'}$ behavior of bremsstrahlung. At higher incident photon energies an additional structure develops which is partly due to the Δ radiation. The shape of the distributions is rather well reproduced by the model predictions. However, for the highest incident photon energy, the absolute values do not agree for any reasonable value of κ_{Δ^+}. Since the model already fails for π^o photoproduction at the high energy side of the Δ, apparently, systematic effects are not yet under control. The systematic uncertainty of the data may add to the discrepancy.

A rough correction of the effects is attempted in [174] via a renormalisation of the data and the model predictions to the soft photon limit which relates the cross sections for the $\pi^o\gamma' p$ and $\pi^o p$ final states in the limit of vanishing $E_{\gamma'}$ [174]:

$$\lim_{E_{\gamma'}\to 0}\left(\frac{d\sigma}{dE_{\gamma'}}\right) = \frac{1}{E_{\gamma'}}\sigma_o \ , \qquad (39)$$

where

$$\sigma_o = \int d\Omega_{\pi^o}\left(\frac{d\sigma}{d\Omega_{\pi^o}}\right)\frac{\alpha}{2\pi}\mathcal{F}(t) \qquad (40)$$

with a kinematic function $\mathcal{F}$ depending on the four momentum transfer t between initial photon and π^o-meson:

$$\mathcal{F}(t) = 4\left[-1 + \left(\frac{v^2+1}{2v}\right) ln\left(\frac{v+1}{v-1}\right)\right] \ , v = \sqrt{1 - \frac{4m_p^2}{t}} \ . \qquad (41)$$

Model predictions and data were divided by $\sigma_o/E_{\gamma'}$. For the model, σ_o was taken from the model prediction for neutral pion production, and for the data the integral for σ_o was evaluated with measured angular distributions. In this way, systematic effects are reduced, and a value of:

$$\mu_{\Delta^+} = (2.7^{+1.0}_{-1.3} \pm 1.5)\mu_N \qquad (42)$$

is extracted from the data. The first error is the statistical and the second the systematic error which, however, does not include systematic effects in the model calculations. The uncertainty of the above

result is too severe for precise tests of hadron models. A second generation experiment is in preparation which will use a 4π detector at the MAMI-B accelerator promising to improve the statistical quality of the data. In parallel, theoretical efforts are continuing to improve the model by including the presently neglected re-scattering contributions. Furthermore, the model calculations [179] have demonstrated that the 5-fold differential cross section $d\sigma/(dE_\gamma d\Omega_\gamma d\Omega_\pi)$ has a larger sensitivity to μ_{Δ^+} for special kinematic regions than the distributions measured previously. Also, photon beam asymmetries are predicted to have a higher sensitivity to the magnetic moment. These observables will be exploited in the follow-up experiment.

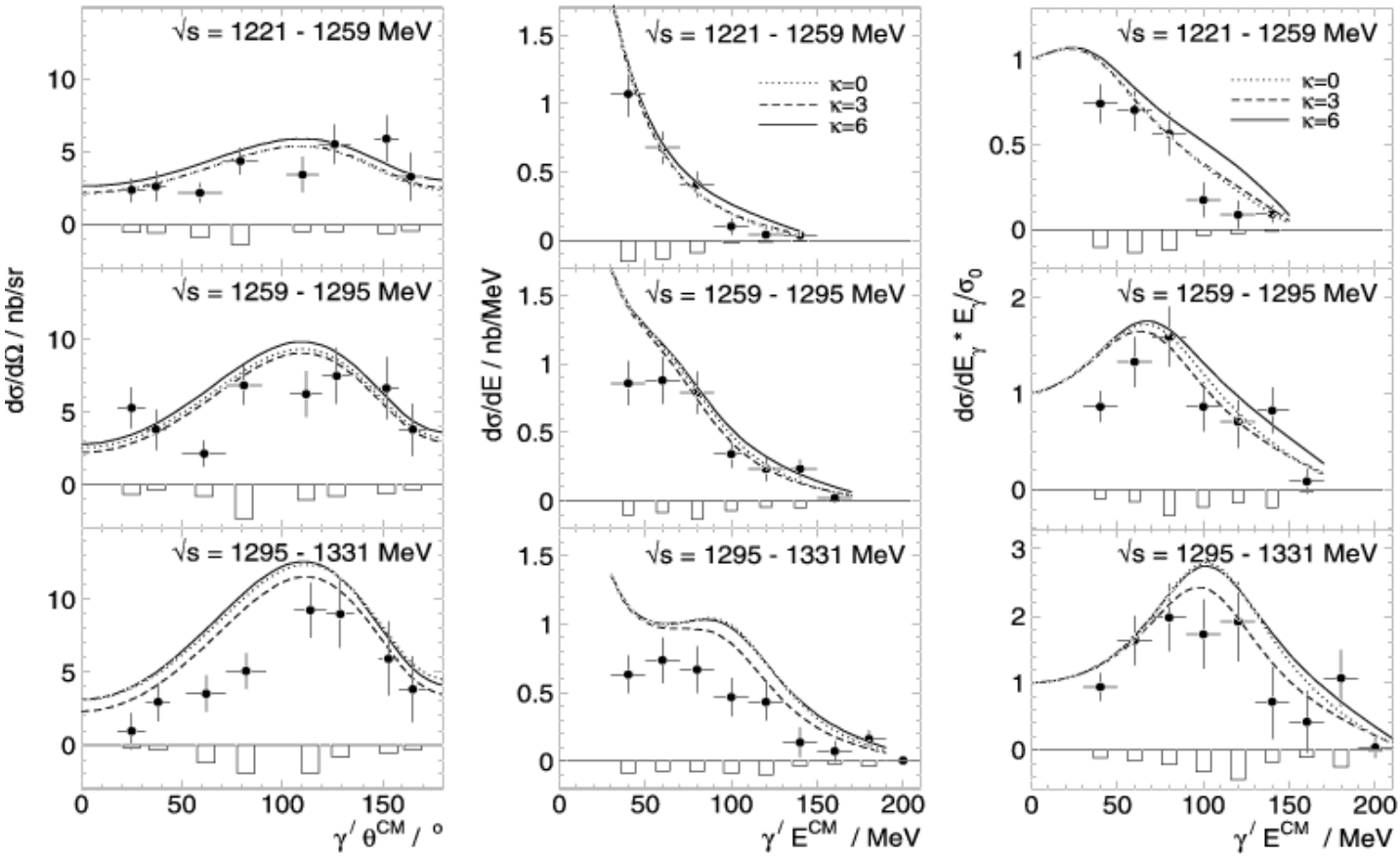

Figure 21: Differential cross sections [174] for three ranges of incident excitation energies in the cm frame. The systematic errors are shown as the bar chart. The left column shows the angular distribution of the alignment photon, the middle column its energy. The energy distributions on the right hand side have been normalized for both data and calculations to the soft photon limit. The calculations correspond to magnetic moments with κ_{Δ^+}=0,3,6.

The method is in principle not restricted to the Δ. However, the reaction $\gamma p \to p\pi^o\gamma'$ is probably not well suited for the extraction of magnetic moments of higher lying resonances. Even if background from reactions with higher pion multiplicity could be eliminated, it would seem to be almost hopeless to disentangle the contributions from different, overlapping resonances in the presence of large non-resonant backgrounds. However, at higher energies other meson production reactions can be exploited. A measurement of the magnetic moment of the $S_{11}(1535)$ resonance via the reaction $\gamma p \to p\eta\gamma'$ seems to be promising. In this case, background from other reactions is negligible, and in the relevant range, η-photoproduction is dominated by the excitation of the first S_{11} resonance. First model calculations for this reaction have been presented by Chiang et al. [180].

3.4 *The Excitation of the Δ-Resonance on the Neutron*

A full multipole analysis including the isospin structure of the amplitudes requires the measurement of meson photoproduction from the neutron. Targets of free neutrons do not exist, and the cross section must be extracted from measurements on neutrons bound in nuclei. One obvious choice of the target nucleus is the weakly bound deuteron. A number of experiments using deuteron targets have recently been and are currently performed, aiming at the investigation of nucleon resonance properties as well as tests of the GDH sum rule on the neutron. In the following, we will discuss pion photoproduction off the deuteron in the Δ-range. The situation is particularly simple when only the Δ-resonance is excited. Only the total isospin changing part A^{V3} of the amplitude can contribute, and one can directly read off from eqs. (10):

$$\sigma(\gamma p \to p\pi^o) = \sigma(\gamma n \to n\pi^o) = 2\sigma(\gamma p \to n\pi^+) = 2\sigma(\gamma n \to p\pi^-) \tag{43}$$

The contribution of background terms will modify these simple relations. It is obvious that experimental information about the reaction on the neutron would be very useful for the separation of the background and resonance contributions. The relations of eq. (43) hold as long as isospin violating terms with $\Delta I \geq 2$ can be neglected. The investigation of pion photoproduction off the neutron thus can be used to search for isotensor contributions in the Δ excitation, provided the background contributions can be sufficiently controlled.

The charged final state $p\pi^-$ had been investigated 30 years ago in a bubble chamber measurement of the $\gamma d \to pp\pi^-$ reaction by the ABHHM collaboration [181], at Frascati [182], and later at higher energies by the TAGX-collaboration [183]. The result for the total cross section is compared to the

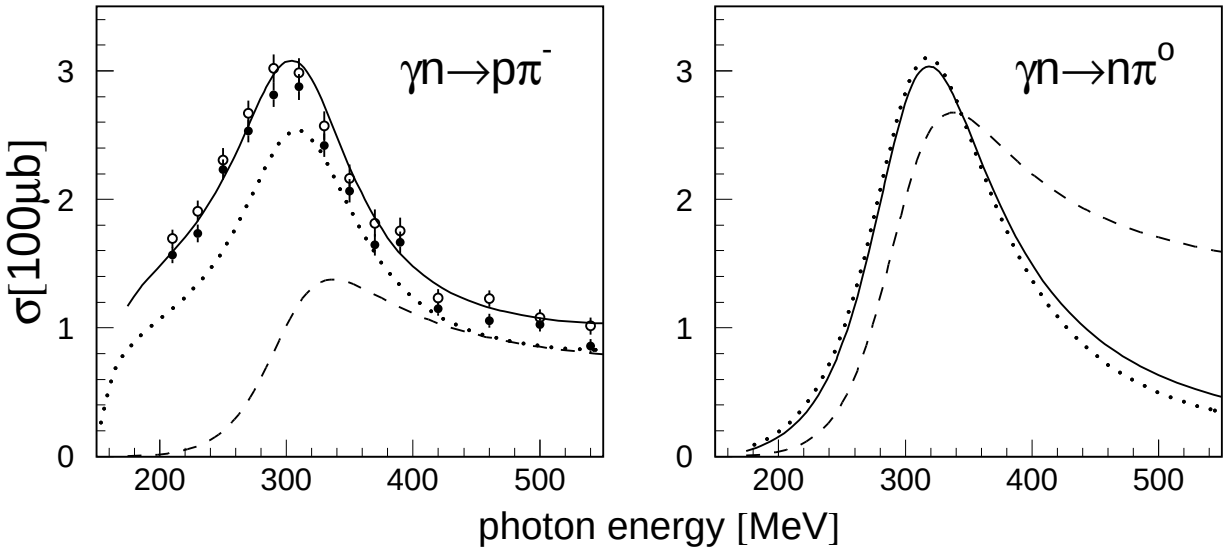

Figure 22: Pion photoproduction in the Δ-region from the neutron. Left hand side: $p\pi^-$ final state, right hand side: $n\pi^o$ final state. Data for $\gamma n \to p\pi^-$ are from ref. [181], full and open symbols represent two different extraction procedures of the cross section from a measurement of the $\gamma d \to pp\pi^-$ reaction. The full (all contributions) and dashed (only Δ-resonance) curves are the MAID predictions [67]. The dotted curves are the MAID results for $\gamma p \to n\pi^+$ (left hand side) and $\gamma p \to p\pi^o$ (right hand side).

MAID model in fig. 22 (left hand side). The agreement is good, and as is the case for the $\gamma p \to n\pi^+$ reaction, the influence of background contributions is large. The MAID prediction for the neutral final state is shown on the right hand side of the figure. Here, the model predicts that the cross sections including resonance and background terms are practically identical for π^o-production on the proton and on the neutron. The remarks concerning the separation of resonance and background contributions for the reaction on the proton apply here, too.

Until very recently, data for π^o photoproduction off the deuteron in the Δ range were scarce. Clifft et al. [184] measured the cross section ratio of the $p\pi^o$ and $n\pi^o$ final states in quasifree photoproduction off the deuteron, albeit with large statistical uncertainties. Some results were obtained for coherent π^o photoproduction on the deuteron mainly for backward angles [185]-[188]. However, during the last few years, precise data from threshold up to the second resonance region have been obtained [189]-[191]. The experiment at the Saskatchewan Accelerator Laboratory (SAL) [189] covered only the threshold region (below 160 MeV incident photon energy), with very good statistics. Here, the motivation was to test the predictions of chiral perturbation theory. The measurement of ref. [191], which was originally motivated as a search for a dibaryon state, covered incident photon energies between threshold and 300 MeV, and ref. [190] the range from 200 - 800 MeV. The latter two experiments which were carried out at MAMI with similar detector setups, agree very well in the overlap region from 200 - 300 MeV. The results from ref. [189, 191] agree in the immediate threshold region. The total cross section from the SAL experiment seems to be systematically higher by some per cent around 160 MeV, although the statistical uncertainties from ref. [191] are of the same order.

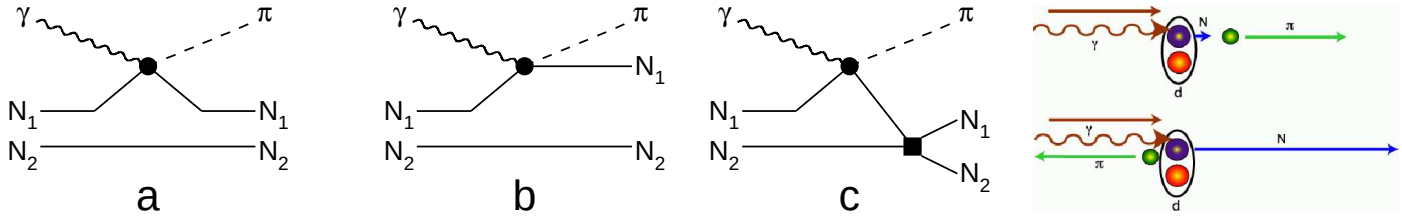

Figure 23: Contributions to neutral pion photoproduction off the deuteron: (a) coherent, (b) break-up, (c) break-up process followed by NN FSI. Right hand side: relative momenta of nucleons.

In comparison to photoproduction of charged pions from the deuteron, an additional complication arises for neutral pions since, as sketched in fig. 23, the process involves two different reaction mechanisms. In case of coherent photoproduction with the $d\pi^o$ final state (diagram a) the amplitudes for π^o-production off both nucleons add coherently. In the simplest approximation of the breakup reaction (diagram b) with the $np\pi^o$ final state, one nucleon acts as participant, and the other can be regarded as spectator. This is the quasifree production, and one might expect that this process offers the ideal tool for the investigation of the $n(\gamma,\pi^o)n$ reaction. However, the plane wave impulse approximation (PWIA) is not a good approximation for the $d(\gamma,\pi^o)np$ reaction in the Δ range because the third diagram (c) in fig. 23, with final state interaction of the two nucleons, gives an important contribution. The NN FSI leads to a relation between the coherent and the quasifree process since it may (coherent) or may not (breakup) bind the two nucleons in the final state. The size of the NN FSI effect depends strongly on the meson emission angle. This can be qualitatively understood in the following way. As sketched in fig. 23 the two nucleons in the final state will have a large relative momentum when the pion is emitted at backward angles, but only a small relative momentum for pions emitted at forward angles. Therefore, NN FSI will be important and tend to bind the two nucleons for forward emission of the pion leading to an enhancement of the coherent part and a suppression of the breakup part. The opposite happens for backward angles.

Based on the connection between coherent and breakup contributions, Kolybasov and Ksenzov [202], using the completeness relation, have argued that the effect of FSI in the breakup process is just counterbalanced by the coherent process so that the sum of the cross sections for the coherent and the breakup part with FSI equals the cross section of the pure quasifree process without FSI. In this case, the semi-inclusive cross section of the $d(\gamma,\pi^o)X$ reaction, i.e. the sum over coherent and breakup parts, is best suited for the extraction of the neutron cross section. This recipe has been employed by Siodlaczek et al. [191] for a modeling of the cross sections with a coalescence model. The relative momentum of the two nucleons determines the NN FSI which in turn pushes the reaction into the

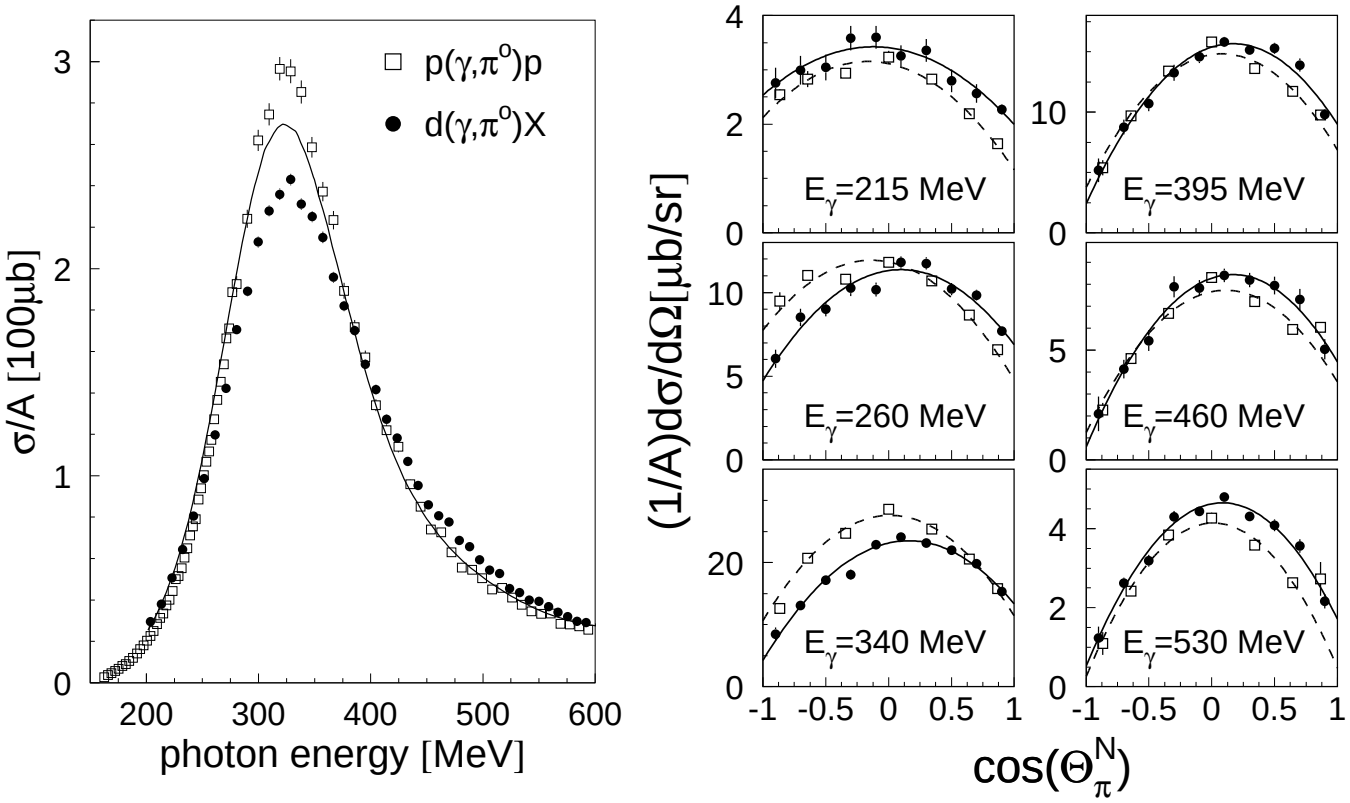

Figure 24: Inclusive π^o photoproduction from ^{2}H in the Δ range [190]. Left: total cross sections of $p(\gamma,\pi^o)p$ (open squares) and $d(\gamma,\pi^o)X$ (filled dots) normalized by the mass number. Curve: free proton cross section folded with momentum distribution of bound nucleons. Right: angular distributions in the cm frame of the photon and a nucleon at rest (symbols as on left side). Curves: fits with eq. (15).

coherent or breakup final state. This simple model reproduces the shape of the angular distributions quite well, but the absolute scale of the breakup part is not in agreement with the data [191].

According to the argument that the inclusive cross section equals the quasifree cross section without FSI effects, the neutron cross section would simply follow from a comparison of the elementary cross sections folded with the nucleon momentum distribution to the measured semi-inclusive deuteron cross section. Total cross sections and angular distributions [190] of the semi-inclusive $d(\gamma,\pi^o)X$ reaction, where both final states ($d\pi^o$ and $np\pi^o$) were accepted, are compared in fig. 24 to the results for the free proton. The angular distributions are shown for the photon - proton cm system for the free proton case, and for the cm system of a photon and a nucleon at rest (with zero Fermi momentum) for the deuteron case. In comparison with the free nucleon case the angular distributions for quasifree pion production from the deuteron should be smeared out only slightly by Fermi motion. The distributions for the proton and the deuteron are indeed quite similar. As discussed above, the amplitude for the excitation of the Δ on the free proton and on the free neutron must be identical as long as isotensor components can be neglected. The MAID model predicts that the π^o-photoproduction cross section including all background terms is nearly identical for the proton and the neutron (see fig. 22). However, fig. 24 shows that the experimental total cross section close to the peak position of the Δ from the deuteron does not equal twice the Fermi smeared proton cross section. Curing this disagreement with a modification of the free $\gamma n \to n\pi^o$ cross section would result in a reduction of $\approx$25% at the peak position [191], while it would remain unchanged in the wings of the Δ-peak. Since we know that the Δ-excitation should contribute equally for the proton and the neutron, this would mean that non-resonant backgrounds contribute very differently for proton and neutron. However, this simple model does not allow to draw such far-reaching conclusions. A more sophisticated treatment of the FSI effects is necessary.

For the extraction of the free neutron cross section, one should ideally have reaction models for the coherent and the breakup reaction off the deuteron and find agreement with the data for the same free neutron cross section. On the experimental side, coherent and breakup contributions have been separated in ref. [190, 191] via their different reaction kinematics. Total and differential cross sections are summarized in figs. 25,26 and compared to model predictions. It should be noted that the model results are really predictions in the sense that they were made before the data were available. In particular, the calculations from Laget [193] predated the experimental results by almost 20 years. The experimental angular distributions show the anticipated FSI effects: they are peaked at forward angles for the coherent process while the breakup distributions are suppressed at forward angles.

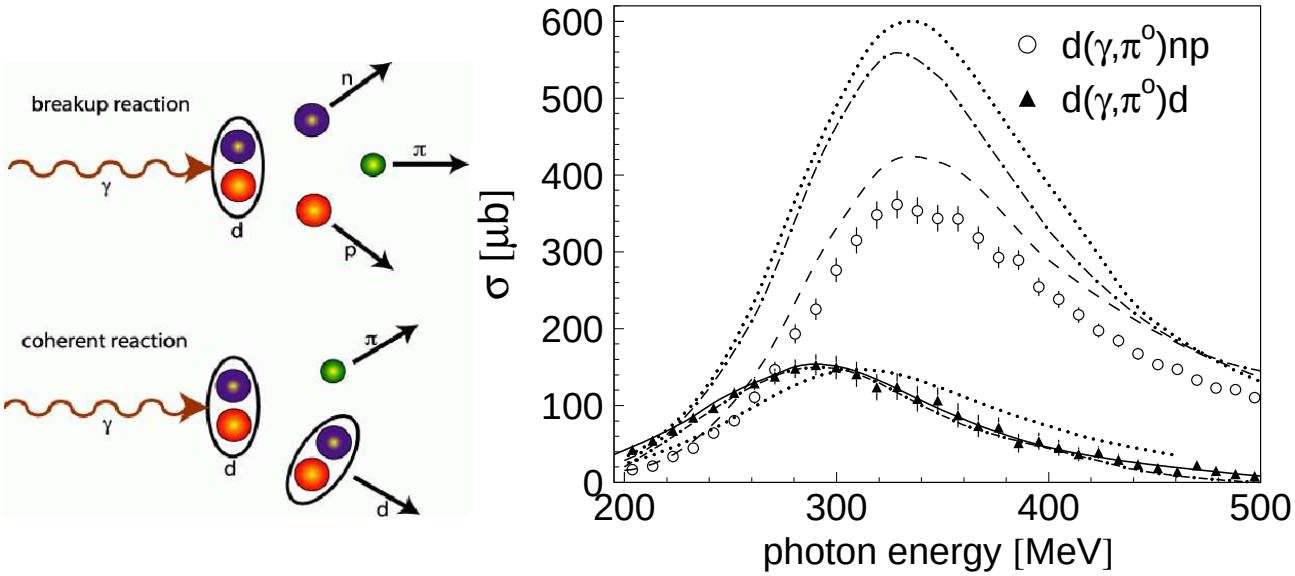

Figure 25: Total cross sections for the reactions $d(\gamma, \pi^o)np$ (open circles) and $d(\gamma, \pi^o)d$ (filled triangles) [190]. Solid, dash-dotted, and dotted curves for the coherent cross section: predictions from models of Kamalov et al. [192], Laget [193], and Wilhelm et al. [194]. Break-up reaction: dash-dotted and dashed curves predictions from Laget [193] with (dashed) and without (dash-dotted) np FSI, dotted curve: the PWIA prediction from Schmidt et al. [195].

The models for the coherent process are similar as far as the elementary production process is concerned, but differ in the treatment of re-scattering effects. The calculations by Laget [193] and Kamalov et al. [192] treat the final state interaction in multiple scattering theory. Both results are in excellent agreement with the data. Blaazer et al. [196] studied re-scattering corrections to all orders by solving the Faddeev equations of the πNN-system. Their results (not shown in the figures) are in agreement with the data. Wilhelm and Arenhövel have developed a dynamical model [194] for the coupled $N\Delta$, $NN\pi$, and NN-systems, which does not reproduce the energy dependence of the total cross section as well as the simpler models (see figure 25). All models suggest the presence of pion re-scattering effects but a common conclusion about their importance is presently not possible since the various models even disagree qualitatively (see [190, 195] for a detailed discussion). Kamalov et al. [192] claim that in the Δ-range the main mechanism of FSI is elastic pion scattering, while the contribution from charge exchange reactions is small and their final state interaction increases the cross section. Wilhelm and Arenövel [194], on the other hand, argue that charge exchange contributions produce a sizeable effect and their FSI lowers the cross section. Unfortunately, the effects in the models are most pronounced for the extreme forward angles, where the systematic uncertainty of the data is largest (see ref. [190] for a detailed comparison of the data to the different model predictions). Therefore, a systematic uncertainty remains for the extraction of the elementary neutron cross section from the data. However, it is fair to say that most model predictions are close to the data and that an indication for

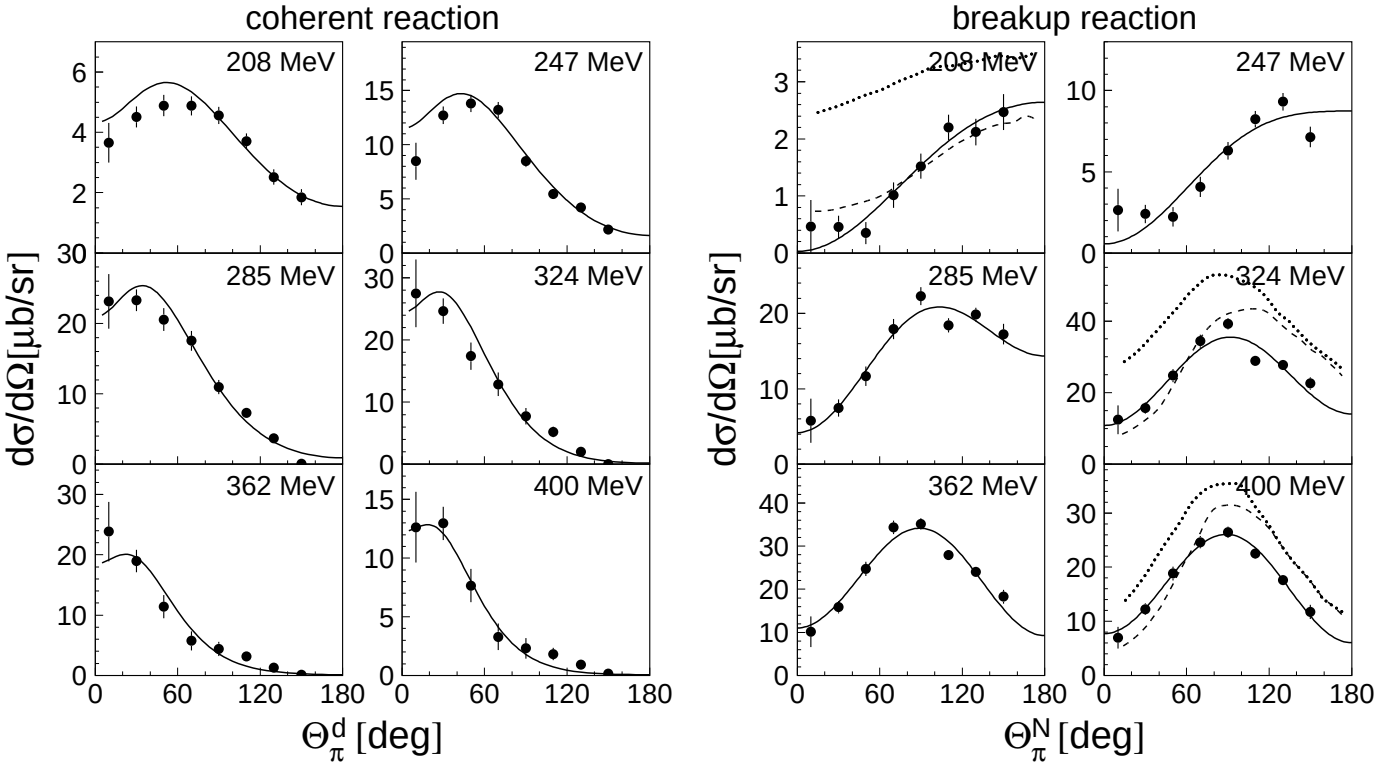

Figure 26: Angular distributions for the reactions $d(\gamma,\pi^o)d$ (left hand side) and $d(\gamma,\pi^o)np$ (right hand side) for different bins of incident photon energy. The coherent cross sections are shown in the photon - deuteron cm system, the break-up cross sections in the photon - nucleon cm system. Coherent part, full curves: predictions from [192]. Break-up part: full curves: fits to the data with eq. (15), dashed and dotted curves: predictions from ref. [193] with and without NN FSI.

a deviation of the elementary cross section on the neutron from the model inputs is not observed. It is interesting to note, that for heavier nuclei the DWIA approximations fail, and significant modifications of the Δ excitation appear [197]-[199].

The situation is different for the breakup channel. Here, final state interaction effects, in this case NN FSI, are more important than for the coherent channel. As can be seen in figs. 25,26, the PWIA calculations strongly overestimate the data. However, even after inclusion of FSI the data are still overestimated. This problem was already apparent in [193] where Laget noted that his calculations reproduced the available data for the charged channels and coherent π^o-production quite well but the sum of the cross section from all channels overestimated the experimental total photoabsorption cross section. He suggested that the total photoabsorption data [200] might suffer from systematic effects, but in the meantime those data have been remeasured [201], yielding the same result. Thus, most of the discrepancy comes from the π^o breakup channel, which was obviously not well understood in the models. The question is whether the failure of the models is connected to the input for the elementary π^o production off the neutron or to nuclear effects.

Very recently, new detailed model calculations for the breakup reactions $\gamma d \to np\pi^o$, $\gamma d \to pp\pi^-$, and $\gamma d \to nn\pi^+$ have been presented by Levchuk et al. [203] and Darwish et al. [204]. In both calculations, care is taken that the elementary cross section on the nucleon is modeled as realistically as possible. The earlier calculation by Laget [193] used the well-known Blomqvist-Laget parameterization [66] of the pion photoproduction amplitude which reproduces the charged channels quite well but is known to give a less good description of the $\gamma p \to p\pi^o$ reaction. Levchuk et al. [203] use CGLN amplitudes taken from the SAID [57] and MAID [67] multipole analyses. Darwish et al. [204] use the effective Lagrangian model of Schmidt et al. [195] and check with a detailed comparison to cross section

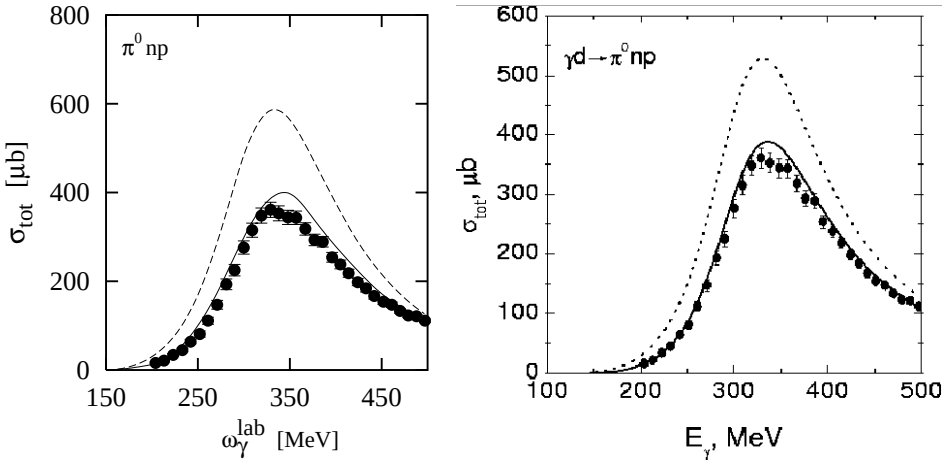

Figure 27: Total cross section for $\gamma d \to np\pi^o$, compared to the calculation of Darwish et al. [204] (left hand side) and Levchuk et al. [203] (right hand side) (dashed, respectively dotted lines: PWIA, solid lines: full calculations). Data are from [190].

data and the SAID and MAID multipoles that the elementary reactions are well reproduced. Levchuk et al. consider only NN FSI, while Darwish et al. include FSI in all two-body subsystems. They find however, that only NN FSI is important while $N\pi$ FSI is negligible.

The results of the two calculations are similar and in better agreement with data than previous models. The predictions for the total cross section of the $np\pi^o$ channel are compared in fig. 27. Both models almost reproduce the data, and the over-prediction of the cross section in the Δ peak is reduced to below 10%. FSI effects are important in both models. However, a closer inspection shows still some difference in the models. The PWIA prediction of Darwish et al. is slightly higher than the one of Levchuk et al., which seems to indicate a difference in the elementary production operator. The angular distributions are similar in the models. Typical results from [204] for the $np\pi^o$ and $pp\pi^-$ final states are summarized in figure 28. The figure highlights the difficulties of the investigation of the Δ excitation on the neutron from quasifree pion production on the deuteron: FSI effects are large for neutral pions, so that substantial model input is necessary for the nuclear effects. FSI effects are small for the production of π^- mesons since the competing coherent channel does not exist in this case. However, like in case of π^+ production from the proton, the strong forward peaking of the angular distributions is an indication for significant non-resonant background in the elementary process. Indeed, Darwish et al. [204] find strong contributions of nucleon Born terms.

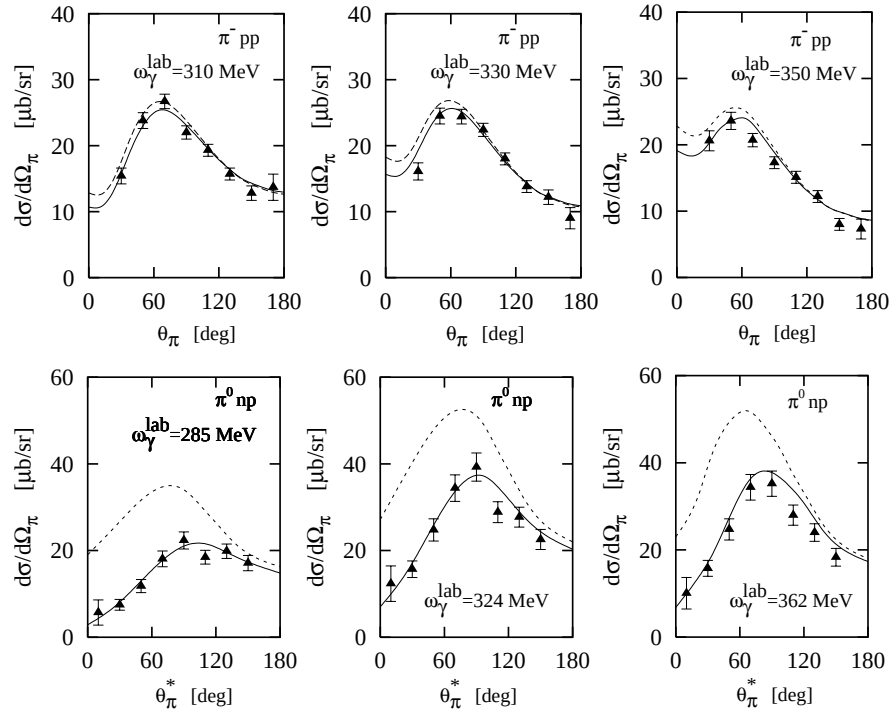

Figure 28: Angular distributions for the reactions $\gamma d \to \pi^- pp$ (upper part, data from ref. [181]) and $\gamma d \to \pi^o np$ (lower part, data from ref. [190]) in the Δ range compared to model calculations from [204]. Solid lines: full model, dashed lines: without FSI.

In summary, the more elaborate model calculations, having become available during the last few years, agree with precision data to a degree which demonstrates that the elementary amplitudes for pion production in the Δ range are reasonably well under control for all isospin channels.

4 The Second Resonance Region

The excitation function of total photoabsorption on the nucleon shows a broad structure above the energy range of the Δ resonance at incident photon energies between 500 and 900 MeV, corresponding to resonance invariant masses between 1350 and 1600 MeV. This bump in the spectrum is called the 'second resonance region'. The structure is more complicated than the peak corresponding to the Δ resonance. As discussed below, three overlapping nucleon resonances, the tail from the Δ, tails from additional higher lying resonances, and background terms contribute. Furthermore, the total photoabsorption cross section in the Δ range stems entirely from single pion production. In the second resonance region, the kinematical particle thresholds allow the production of two pions and η mesons. This is demonstrated in fig. 29, where the total photoabsorption cross section is decomposed into the

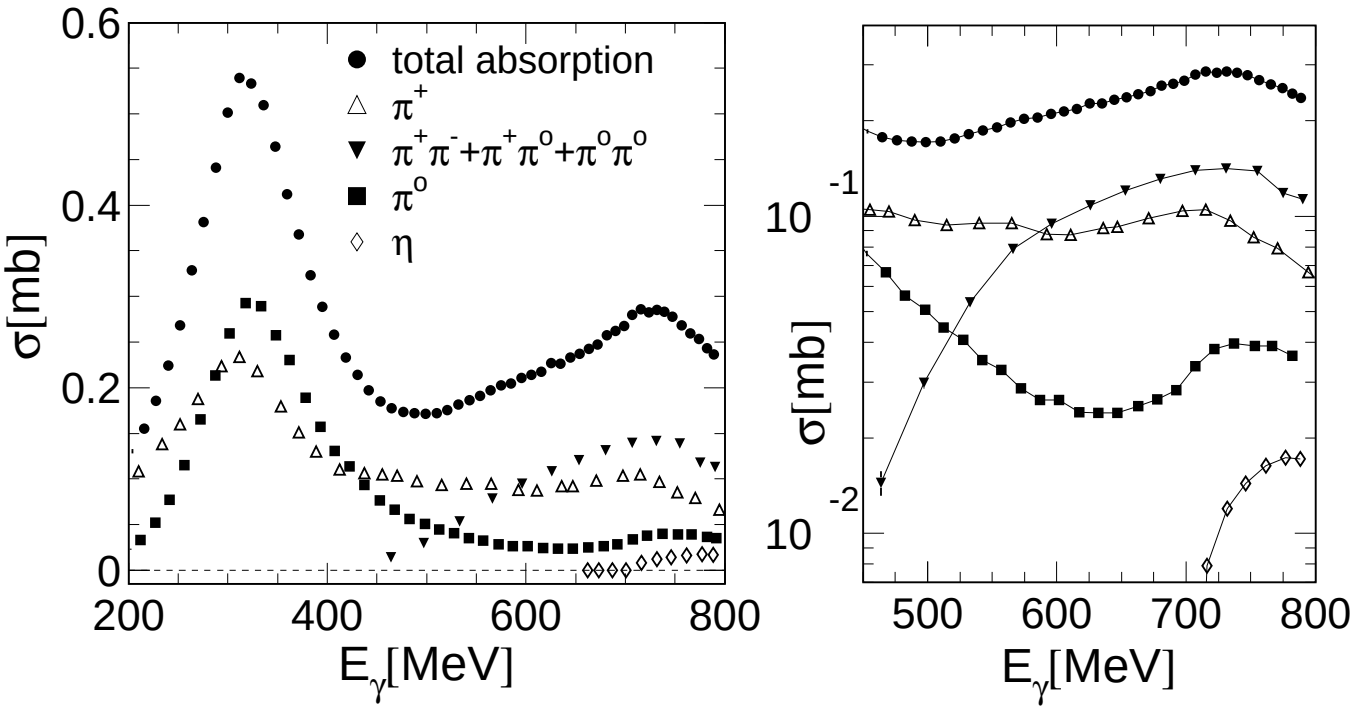

Figure 29: Total photoabsorption and partial cross sections for photoproduction off the proton. Data are from [201] (total absorption), [201, 90] ($\gamma p \to \pi^+ n$), [89] ($\gamma p \to \pi^o p$), [281, 282] (double pion production), and [205] ($\gamma p \to \eta p$). Right hand side: second resonance region in logarithmic scale, symbols as on left side, lines are only to guide the eye.

contributions from the partial channels. The cross sections have been measured over the past ten years with the DAPHNE [207] and TAPS detectors [175, 176] at the MAMI accelerator. The partial channels add up exactly to the total photoabsorption cross section. It is evident, that the resonance bump consists of a complicated superposition of the different reaction channels which differ in their energy dependence. The neutral and charged single pion production channels behave quite differently. Most of the rise of the cross section from the minimum around 500 MeV to the maximum around 700 MeV comes from double pion production. Fitting the total photoabsorption cross sections with Breit-Wigner curves for the resonances plus some background as in fig. 2 would certainly be an oversimplification. It should be noted that an understanding of this peak structure requires a thorough investigation of the three double pion production channels. This is not only important for the discussion of resonance excitations on the free nucleon but also forms the basis for discussing the experimentally observed strong depletion of the bump structure in photoabsorption from nuclei. As we will see in section 4.3, the interpretation of the double pion production channels is complicated. Only the combined progress of experiments and reaction models during the last few years has shed light on the dominant reaction mechanisms. The

photoproduction of η-mesons contributes only little to the total absorption cross section. However, as discussed in detail in sec. 4.2, it plays a crucial role in the investigation of the $S_{11}(1535)$ resonance.

In the following, we will discuss briefly the nucleon resonances expected to contribute in the second energy region. A schematic representation of the lowest lying nucleon states in the constituent quark model with three quarks in a harmonic oscillator potential is given in fig. 30. The pictorial representation, which neglects the flavor degree of freedom, is a strong simplification of the properly anti-symmetrized wave functions of the model (see [11]). Furthermore, mixing of the basis states with equal quantum numbers is expected due to spin-orbit interactions. An example are the two S_{11} states.

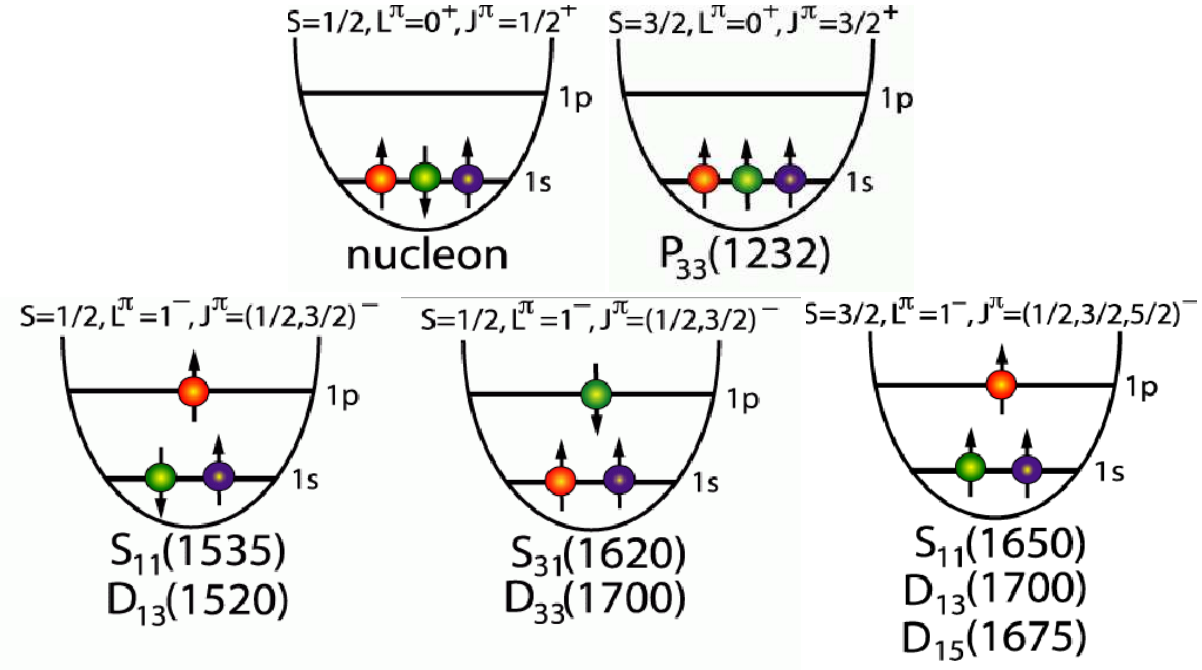

Figure 30: Schematic representation of the $0\hbar\omega$, $1\hbar\omega$ excitations of the nucleon in the naive constituent quark model. The labels correspond to the lowest lying experimentally observed states with the respective quantum numbers.

Experimental evidence for the existence of the low-lying excited states is provided by pion-nucleon scattering reactions. The relevant partial amplitudes from elastic pion scattering, taken from the SAID multipole analysis [57], are summarized in fig. 31. Three partial waves in the isospin 1/2 channel, the P_{11}, the S_{11}, and the D_{13}, show clear signals at invariant masses around 1500 MeV. The isospin 3/2 channel is not shown but does not contribute to the second resonance region. However, the correspondence between the quark model expectations and experimental findings is different for various quantum numbers. The lowest lying D_{13}, the $D_{13}(1520)$, is almost as close to a textbook case as the Δ. The imaginary part shows a strong peak while the real part is crossing zero. The same is true for the higher-lying lowest D_{15} excitation.

The S_{11} channel shows two structures related to the $S_{11}(1535)$ and ß resonances, which will be discussed further in connection with η-photoproduction. However, the situation for the lowest lying S_{11} is less obvious. This resonance is close to the kinematical production threshold of the long-lived η meson which can be produced off the nucleon in an s-wave. The sharp structure in the real part at 1485 MeV corresponds to the cusp induced in the pion production amplitude by the η threshold. Some authors, using the speed plot technique [208, 209], have argued that the evidence for the $S_{11}(1535)$ in pion scattering is not convincing. It is claimed that the entire structure could be attributed to the threshold cusp. Other authors [210, 211] try to explain the unusually large branching ratio of the $S_{11}(1535)$ resonance into $N\eta$ by suggesting that the structure in the η photoproduction cross section

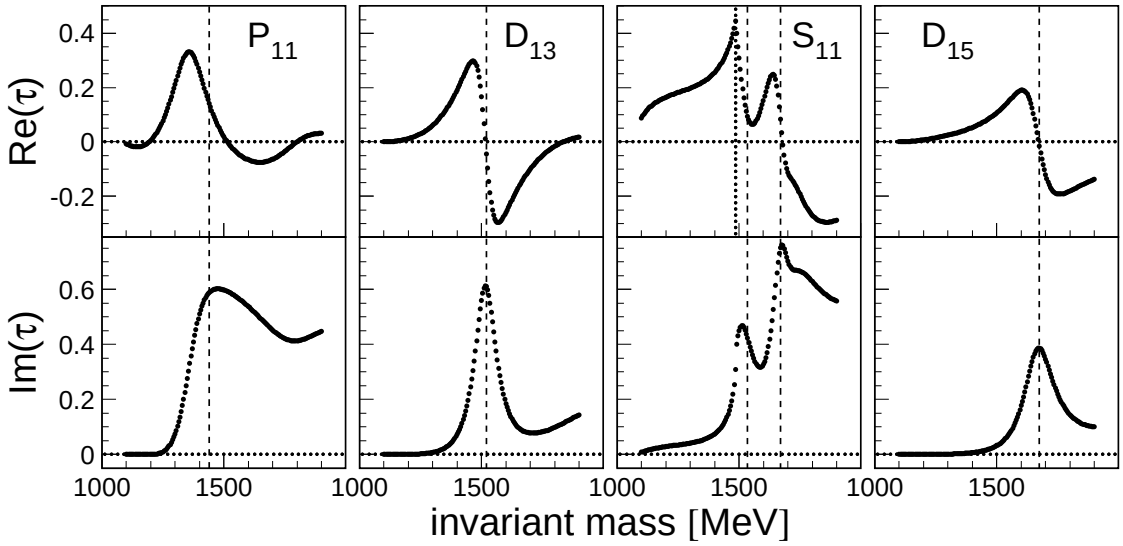

Figure 31: Real and imaginary parts of the $I = 1/2$ partial amplitudes for $\pi N \to \pi N$ throughout the second resonance region (taken from the SAID analysis [57, 60]). Dashed lines: resonance positions, vertical dotted line: η production threshold.

might be attributed to a molecular-like $K\Sigma$ state. This scenario would correspond to a quasi-bound state rather than to a three-quark excited state of the nucleon. Thus, the structure and the very existence of this resonance are subject to debates in the literature even though it is assigned a four-star rating in the Particle Data Booklet [36]. As we will see in sec. 4.2, recent η photoproduction experiments have contributed significantly to the discussion.

In addition, the P_{11} partial wave, too, shows a prominent structure close to 1500 MeV. This is surprising since a P_{11} excitation corresponds to a 1s→2s transition in the constituent quark model. Thus, it would be expected at higher excitation energies than the states shown in fig. 30. Howver, on the contrary, it is centered at a lower energy than any of the $1\hbar\omega$ states and it has a much larger width. This low-lying P_{11} state is the Roper resonance. Non-relativistic constituent quark models do not offer a natural description of this state even if the harmonic confinement is replaced by a more realistic linear confinement. The state is better described in a relativistic quark model with instanton-induced quark forces proposed by Löring, Metsch, and Petry [212]-[215]. It also decreases in energy in the quark model of Glozman and Riska [15] which adds a chirally invariant meson exchange interaction of the quarks to the harmonic confinement. A monopole excitation is found as the lowest lying state in the Skyrmion model [216] which treats the nucleon structure as a mesonic field. However, possible 'exotic' structures of this resonance have also been discussed. Burkert and Li [217] have argued that the Q^2 dependence of the $A_{1/2}$ helicity coupling in electroproduction is in better agreement with a model that treats the Roper as a q^3G hybrid, with a gluonic excitation admixed to the three quark state. On the other hand, Krehl, Hanhart, Krewald, and Speth have [218] generated the resonance structure dynamically without a q^3 core. In this coupled channel meson exchange model for pion-nucleon scattering, the Roper resonance appears in the σN channel. Here, σ is understood as a correlated pion pair in the scalar-isoscalar state. Finally, based on a comparison of αp and πN scattering experiments, Morsch and Zupranski [219] have suggested that the structure in the P_{11} channel would be composed of two resonances with different internal structures. Many aspects of the Roper excitation in hadron induced reactions have been summarized in the proceedings of the COSY Workshop on Baryon Excitations [220].

In summary, the second resonance region of the nucleon is a structure formed by the three overlapping resonances $P_{11}(1440)$, $D_{13}(1520)$, $S_{11}(1535)$. Their properties are listed in table 2. Surprisingly, the structure of the $P_{11}(1440)$ and $S_{11}(1535)$ is controversial although these are the lowest lying isospin 1/2 excitations of the nucleon, and all three states hold a four-star status in the Particle Data Booklet.

Table 2: Properties of nucleon resonances forming the second resonance region [36]. (The decay branching ratios into $N\rho$ and $\Delta\pi$ are partial channels of $N\pi\pi$).

state	I	J^P	mass [MeV]	width Γ [MeV]	$A^p_{1/2}$, $A^n_{1/2}$ / $A^p_{3/2}$, $A^n_{3/2}$ [10^{-3}GeV$^{-1/2}$]	decays (%)	
$P_{11}(1440)$	$\frac{1}{2}$	$\frac{1}{2}^+$	1430 - 1470	250 - 450	-65 ± 4 $+40\pm10$	$N\pi$	60 - 70
						$N\pi\pi$	30 - 40
						$N\rho$	<8
						$\Delta\pi$	20 - 30
						$N\eta$	?
$D_{13}(1520)$	$\frac{1}{2}$	$\frac{3}{2}^-$	1515 - 1530	110 - 135	-24 ± 9 -59 ± 9	$N\pi$	50 - 60
					$+166\pm5$ -139 ± 11	$N\pi\pi$	40 - 50
						$N\rho$	15 - 25
						$\Delta\pi$	15 - 25
						$N\eta$	0 - 1
$S_{11}(1535)$	$\frac{1}{2}$	$\frac{1}{2}^-$	1520 - 1555	100 - 200	$+90\pm30$ -46 ± 27	$N\pi$	35 - 55
						$N\pi\pi$	1 - 10
						$N\rho$	<4
						$\Delta\pi$	<1
						$N\eta$	30 - 55

The experimental investigation of the resonance properties, in particular the electromagnetic couplings and partial decay widths, is complicated by their large overlapping widths. The situation in meson photoproduction reactions is sketched in fig. 32. The figure shows the expected contribution of the three resonances and the tails of other resonances to π^o and η photoproduction off the proton. The contribution is approximated from the resonance positions, widths, photon couplings, and decay branching ratios. The D_{13} resonance dominates single pion production, and is also important for the understanding of double pion production reactions, as we will discuss in sec. 4.3. The other two resonances contribute only weakly to single pion production. Photoproduction of the η meson is dominated by the $S_{11}(1535)$, and this fact enables detailed studies of the resonance in the η channel. In contrast, the P_{11} is not favored in any reaction over the other resonances. For the P_{11} resonance, it is mandatory to establish precise experimental cross sections and polarization observables in order to define the relevant multipole amplitudes. The situation is reflected in the results discussed in the following sections. Many new results have become available for the S_{11} via η production. The role of the D_{13} not only in single but also in double pion production and even in η production was investigated in detail. Much less new material is available for the P_{11}.

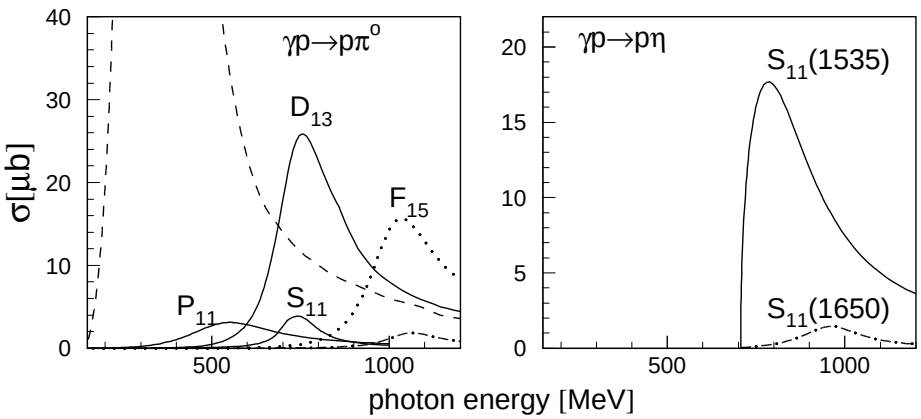

Figure 32: Contribution of resonances to π^o and η photoproduction (not quantitative). Full curves labelled P_{11}, D_{13}, and S_{11} correspond to the $P_{11}(1440)$, the $D_{13}(1520)$, and the $S_{11}(1535)$ resonances. The dashed curve corresponds to the Δ, the dash-dotted curves to the ß, and the dotted curve to the $F_{15}(1680)$.

4.1 *Single π Photoproduction and the $P_{11}(1440)$ and $D_{13}(1520)$ Resonances*

Single pion photoproduction is the standard method for the investigation of the electromagnetic resonance couplings, being one of the most important testing grounds for hadron models. Partial wave analyses of pion production data up to 2 GeV incident photon energy are available (see [57, 58] and ref. therein). Dispersion relations and unitary isobar models [54, 67, 91] have been used for the analysis of the data, and predictions for the photoproduction amplitudes have been made in the framework of quark models [84]. A review of all available pion photoproduction data and analyses would go far beyond the scope of this article. Instead, we will discuss recent advances using the second resonance region as an example.

During the last ten years, the data base for pion photoproduction has been improved considerably with respect to two aspects. Many of the older bremsstrahlung measurements have been replaced by more precise tagged photon beam experiments. An increasing number of polarization observables have been measured for the first time. As noted in the most recent pion multipole analysis [58], in 1994 bremsstrahlung data comprised still 85% of the then available data. These results were often plagued by poorly understood systematic uncertainties causing inconsistencies in the data base. The few data sets that were available from tagged photons generally came from low statistics measurements. The situation changed due to experimental programs running at modern tagged-beam facilities at MAMI-B (Mainz), GRAAL (Grenoble), and LEGS (Brookhaven) and will further improve with the upcoming results from CLAS (JLab). Progress was fastest in the energy range below 800 MeV incident photon energy, since the MAMI-B facility produced over 20% of the $\pi^+ n$ data after 1995, and almost 90% of the new $\pi^o p$ data [58]. In parallel with the improvement in data quality, measurements of previously unexplored polarization observables produced crucial constraints for the analyses. Such results in the Δ range were already discussed in secs. 3.1, 3.2. In the medium energy range, the $\pi^+ n$ beam asymmetry (Σ) was measured at GRAAL (E_γ=550 - 1500 MeV) [224, 225] and the $\pi^o p$ beam asymmetry (E_γ=500 - 1100 MeV) at Yerevan [226]. Target asymmetry (T) measurements for $\pi^o p$ and $\pi^+ n$ (E_γ=220 - 800 MeV) have been reported from ELSA at Bonn [128, 227]. The difference of the helicity components $\sigma_{3/2} - \sigma_{1/2}$ has been measured for $\pi^o p$ with the GDH experiment in Mainz [154].

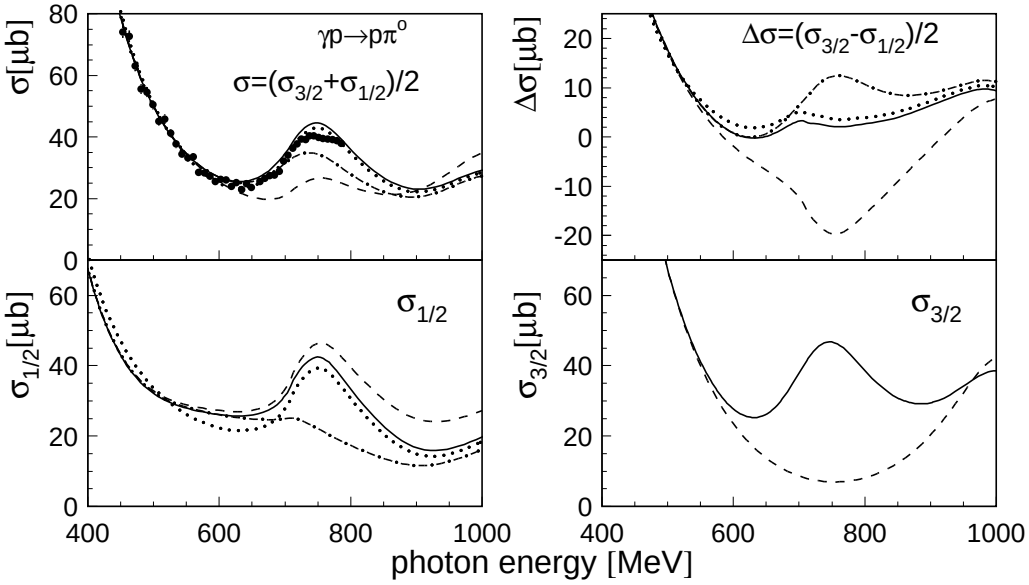

Figure 33: Unpolarized and helicity dependent total cross sections for $p(\gamma, \pi^o)p$ The curves are the MAID results [67] for the full model (solid), without D_{13} (dashed), without S_{11} (dash-dotted), and without P_{11} (dotted). The data for the unpolarized cross section are from [190].

Helicity dependent cross section data are particularly useful for the separation of contributions from the $J = 1/2$ (P_{11} and S_{11}) states and the $J = 3/2$ D_{13} resonance. This is demonstrated in fig. 33 for the reaction $\gamma p \to \pi^o p$. The figure shows the unpolarized cross section, the two helicity components and their difference, calculated from the MAID analysis [67] for the full model, and for three truncated versions each excluding one resonance. The D_{13} has a strong effect on the difference

of the helicity components. The resonance structure in the helicity $\nu = 3/2$ component is entirely due to the D_{13} state since the $J = 1/2$ resonances cannot contribute. A measurement of $\sigma_{3/2}$ would thus put stringent constraints on the $A_{3/2}$ helicity amplitude of the D_{13}. The S_{11}, on the other hand, is expected to dominate the resonance structure in the $\nu = 1/2$ channel, where the D_{13} plays a minor role. The separation of the two resonances in this channel would be possible due to the different angular dependence of s- and d-waves. The sensitivity of the unpolarized cross section, the helicity components, as well as the photon beam asymmetry to the $P_{11}(1440)$ resonance is relatively small.

Figure 34 shows unpolarized cross sections and the difference of the helicity components as a function of the pion polar angle for the reaction $\gamma p \to \pi^o p$ [190, 154] throughout the excitation range of the $D_{13}(1520)$. They are compared to the result of the MAID and SAID analyses obtained without using

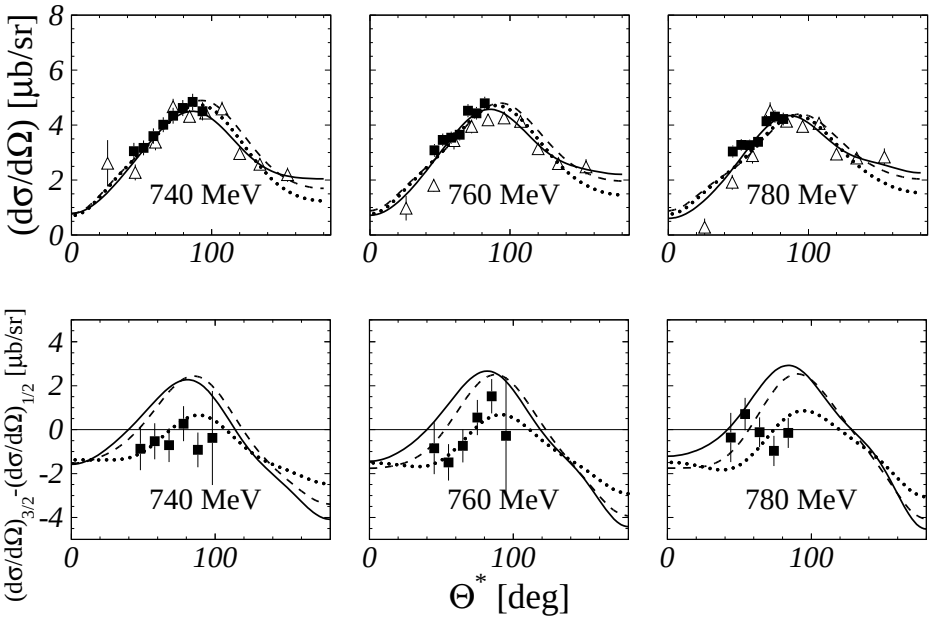

Figure 34: Unpolarized angular distributions (upper part) and difference of the helicity components (lower part) in the range of the $D_{13}(1520)$ resonance [154]. Full squares are from [154], open triangles from [190]. The solid curves correspond to the SAID analysis [57], the dashed curve to the MAID solution [67], and the dotted curves to a re-fit of the MAID solution to the data.

the helicity dependent data. Both analyses reproduce the unpolarized data. This is to be expected since the angular distributions from [190] were included in the fits. However, good agreement with the helicity difference is not achieved. Therefore, the MAID analysis was re-fitted including the polarization data [154]. The result is indicated by the dotted lines. The effect on the unpolarized cross section is small but the agreement for the helicity dependence is significantly improved. As discussed in [154], the modified MAID solution is also in much better agreement with the $n\pi^+$ photon asymmetry (Σ) data but still disagrees with the $p\pi^o$ Σ-measurement. The main difference in the amplitudes, extracted from the original and modified MAID fits, apart from background contributions, appears in the $E_{2-}^{1/2}$ and $M_{2-}^{1/2}$ components which are associated with the D_{13} excitation. In the modified fit, the strength of the first is reduced by a factor of (0.81±0.01) and the second is increased by a factor of (1.11±0.01). These partial amplitudes are directly related to the helicity couplings $A_{3/2}$ and $A_{1/2}$ of the D_{13} resonance, as long as background can be neglected. In [228], it can be found that

$$\begin{aligned} R_A = \frac{A_{3/2}}{A_{1/2}} &= \sqrt{3}\,\frac{E_{2-}+M_{2-}}{E_{2-}-3M_{2-}} = \sqrt{3}\,\frac{1+R_M}{R_M-3} \\ R_M = \frac{E_{2-}}{M_{2-}} &= \frac{\sqrt{3}+3R_A}{R_A-\sqrt{3}}\ . \end{aligned} \tag{44}$$

The change of the multipole amplitudes corresponds to a significant lowering of the magnitude of the ratio of the helicity couplings (see. table 3) from -9.8 (MAID1998) to -3.8 (MAID2002).

A multipole analysis (SAID) of the full data base has recently been reported by Arndt and collaborators [58]. The results for the multipoles involving the excitation of the S_{11}, P_{11}, and D_{13} on the proton are summarized in fig. 35. In the figure, the symbols correspond to the energy independent solutions,

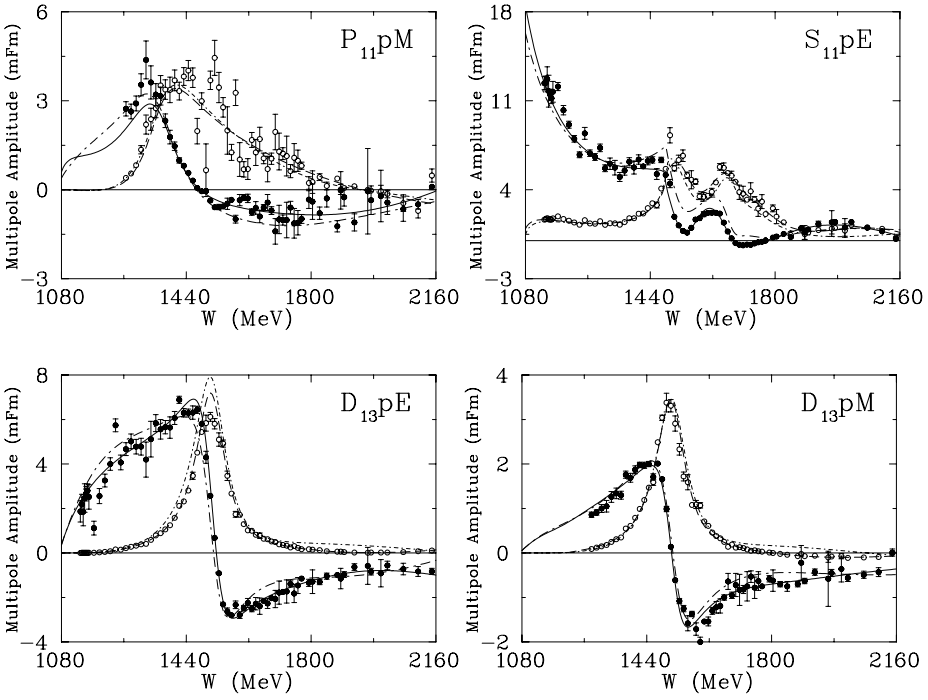

Figure 35: Partial wave amplitudes extracted from pion photoproduction in the SAID analysis [58]. Solid (dashed) curves: energy dependent real (imaginary) parts of the SM02 solution. Filled (open) circles: real (imaginary) parts of the single energy solutions. Long dash-dotted (short dash-dotted) lines correspond to the real (imaginary) parts of the SM95 solutions [57]. Notation: X_{2I2J} denotes orbital angular momentum, isospin and spin, 'p' denotes the reaction on the proton, and M,E magnetic or electric multipole, e.g. D_{13}pM corresponds to $M_{2-}^{1/2}$ on the proton.

i.e. to multipole fits done independently for each incident photon energy. The curves correspond to energy dependent solutions, parameterized in terms of the T-matrix for πN-scattering in the appropriate partial wave. The general observation is that in all cases the solutions show a structure very similar to the corresponding πN amplitudes (see fig. 31). The following remarks can be made to the individual resonances:

• $\mathbf{S_{11}(1535)}$: As has been discussed in the context of pion induced reactions, the structure corresponding to the lowest lying S_{11} resonance is obscured by the cusp arising from the opening of the η production threshold. The determination of the helicity couplings of the $S_{11}(1535)$ has thus always been less precise than for the other resonances. The results from different analyses were not in good agreement. In their most recent multipole analysis, Arndt et al. [58] find significant sensitivity of the $S_{11}pE$ ($E_{0+}^{1/2}$) multipole to details of the data base and of the parameterization. It is concluded that the coupling requires a more detailed treatment. The value ($A_{1/2}^p$ =(30±3)$10^{-3}\,\mathrm{GeV}^{-1/2}$) that is finally quoted is quite low even when compared to other analyses of pion data. It is much lower than results from analyses of η photoproduction data. We will discuss the S_{11} helicity couplings further in the context of η-photoproduction (see sec. 4.2).

• $\mathbf{P_{11}(1440)}$: The observables studied so far are marginally sensitive to the P_{11}. Consequently, the scattering/spread of the energy independent solutions is larger than for the other channels. Nevertheless, the helicity couplings extracted from the data are given with relatively small uncertainties. The results of different analyses are in fair agreement ($A_{1/2}^p$ = −67±2 [58], −63±5 [57], −71 [67]). A comparison with the predictions of quark models underlines that the Roper resonance does not at all fit into the conventional constituent quark picture of the nucleon. Close and Lee [223] predict $A_{1/2}^p$=+10, Capstick [101] a value of +4, and Bijker et al., in their algebraic nucleon model, [13] quote a range from 0 to +67. (values for $A_{1/2}$ in units of $10^{-3}\mathrm{GeV}^{-1/2}$). The measurement of the helicity coupling as function of the four-momentum transfer can provide important information about the structure of the resonance. This is demonstrated in fig. 36 where the predictions for the transverse and longitudinal couplings of

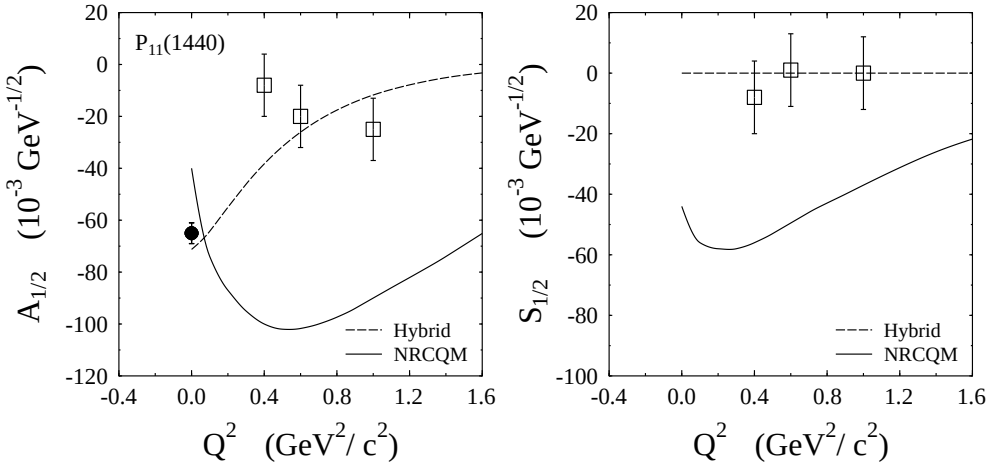

Figure 36: Transverse ($A_{1/2}$) and longitudinal ($S_{1/2}$) helicity coupling of the Roper resonance. Real photon point (filled circle): PDG [36]. Open squares: Gerhardt [229]. Full lines: q^3 quark model prediction (Barnes and Close) [230, 231], dashed lines: q^3G hybrid model (Li, Burkert and Li) [217].

a conventional q^3 quark model [230, 231] are compared to the prediction of a q^3G hybrid model [217]. The predictions are quite different but the data at finite four-momentum transfers [229] have large systematic uncertainties from incomplete data sets and theoretical assumptions in the analysis. From the above discussion, it is evident that it would be helpful to find observables more sensitive to the Roper resonance, so that the systematic uncertainties could be better controlled. Recently, Beck [232] has pointed out that the double polarization observable G (linearly polarized photons and longitudinally polarized protons) in the reaction $\vec{p}(\vec{\gamma}, \pi^o)p$ is ideally suited for this purpose (see fig. 37).

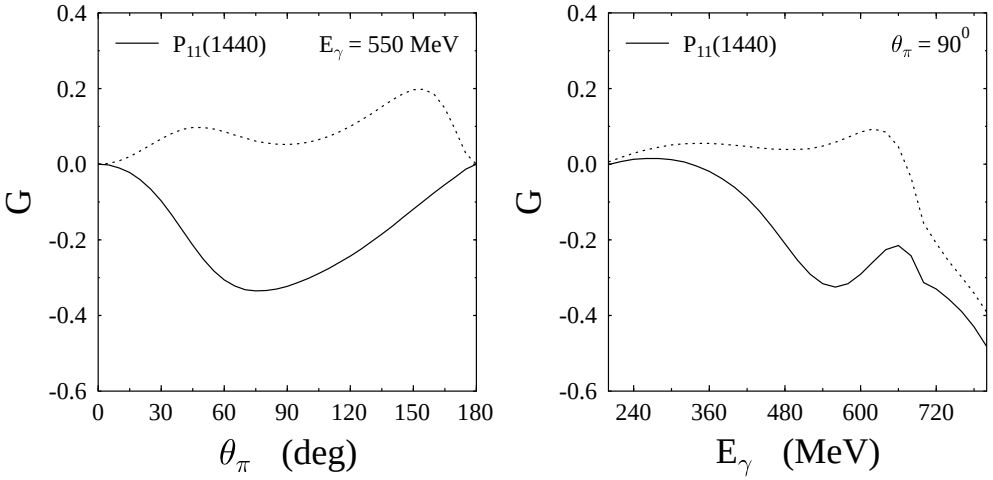

Figure 37: Sensitivity of the polarization observable G to the Roper resonance [232]. Solid lines: full MAID model, dashed lines: without Roper.

• **D_{13}(1520)**: The signal for the $D_{13}(1520)$ state is by far the clearest. The imaginary part of the amplitude displays an almost perfect shape of a Breit-Wigner resonance. Again, the properties of interest are the helicity couplings $A_{1/2}$, $A_{3/2}$, and their ratio. As discussed in connection with the Δ resonance (see sec. 3.1), the onset of perturbative QCD is characterized by helicity conservation. For very large Q^2, $A_{1/2} \gg A_{3/2}$ is expected. At the photon point, the behavior is dictated by the non-perturbative QCD effects which may result in a large violation of helicity conservation. In fact, in case of the D_{13}, the coupling for $Q^2 = 0$ is dominated by $A_{3/2}$. Therefore, the helicity couplings are very sensitive to the internal structure of the resonances and thus very well suited for model tests. However, stringent tests are only possible when the couplings can be determined precisely. Usually, the ratio of the couplings can be determined with smaller systematic uncertainties than the couplings themselves because resonance parameters like width and decay branching ratios cancel. The typical range of model predictions for $A^p_{3/2}/A^p_{1/2}$ is indicated in table 3. Most conventional quark models predict ratios between -5 and -10 but the algebraic model of Bijker et al. [13] predicts a smaller value of -2.5. Typical results

extracted from older data not including the new measurements of polarization observables corresponded to fairly large values of the ratio (SAID95: -8.4, MAID98: -9.8). On the other hand, values extracted from η-photoproduction are much smaller, between $-2.$ and -2.5 (see table 3). The coupling of the D_{13} to the η channel is weak, the decay branching ratio is smaller than 0.1 %. Meanwhile, the pion production is dominated by this resonance, and one might wonder whether the extraction of the coupling from the η channel is possible with reasonable precision, as compared to the pion channel. However, as discussed in the following section, the photon beam asymmetry Σ in η photoproduction is extremely sensitive to contributions of the D_{13}.

The question is whether a serious discrepancy between the results from pion and η photoproduction persists. Workman et al. have discussed this problem [228] and find that it is still possible to find a reasonable description of the pion data with $R_A = -2.5$ although fits to the (old) pion data base tend to produce large values of R_A. Inclusion of the new polarization observables for pion production into the fits has reduced the discrepancy. We have seen that inclusion of the helicity difference $\sigma_{3/2} - \sigma_{1/2}$ into the fit of the MAID model has lowered the ratio to only -3.8. The same trend is visible for the SAID analysis where inclusion of all polarization data has lowered the ratio to -5.6. The effect of the new data on the fit is clearly visible in fig. 35. The magnetic multipole is practically unchanged between the 1995 and 2002 SAID solution but the imaginary part of the electric multipole at the resonance position is reduced from about 8 to 6 mFm. According to eq. (44) this corresponds to a decrease of R_A. In fact, we could use the same procedure as in [154], ignore possible background contributions to the imaginary parts and calculate R_A from the values read-off from fig. 35 ($\mathrm{Im}(E_{2-}^{1/2}) = 6$ mFm, $\mathrm{Im}(M_{2-}^{1/2}) = 3.3$ mFm) via eq. (44). Then we obtain $R_A = -4.1$ which is even closer to the MAID analysis. The discrepancy between pion and η results is thus reduced from a factor of 4-5 to less than a factor of two. This is one of the examples which demonstrates the importance of new precise measurements of

Table 3: Photon couplings of the $D_{13}(1520)$ resonance. All values in units of $10^{-3}\mathrm{GeV}^{-1/2}$. PDG: Review of Particle Properties [36], GW: Breit-Wigner resonance fits to SAID multipole analysis [58], VPI: 1995 SAID analysis [57], MAID: unitary isobar model [67], MAID II: re-fit to helicity cross sections [154], ETA-I: analysis of η photoproduction with effective Lagrangian model [221], ETA-II: analysis of η-production observables with isobar model [222], ETA-MAID: isobar model for η photoproduction [68]. QM-I: non relativistic quark model (Koniuk,Isgur) [27]. QM-II: quark model with relativistic corrections (Close, Li) [223] (first number: calculation in c.m frame, in brackets: calculation in Breit-Frame) QM-III: relativized quark model (Capstick) [101]. $^{\star)}$: re-calculated from $A_{3/2}$, $A_{1/2}$. AM: algebraic model of hadron structure (Bijker, Iachello, Leviatan) [13].

Ref.	$A^p_{1/2}$	$A^p_{3/2}$	$A^p_{3/2}/A^p_{1/2}$	$A^n_{1/2}$	$A^n_{3/2}$
PDG (2002)	-24 ± 9	$+166\pm5$	-6.9 ± 2.6 $^{\star)}$	-59 ± 9	-139 ± 11
GW (2002)	-24 ± 2	$+135\pm2$	-5.6 ± 0.5 $^{\star)}$	-67 ± 4	-112 ± 3
VPI (1995)	-20 ± 7	$+167\pm5$	-8.4 ± 3.0 $^{\star)}$	-48 ± 8	-140 ± 10
MAID (1998)	-17	$+164$	-9.8 $^{\star)}$	-40	-135
MAID II (2002)	-37	$+141$	-3.8 $^{\star)}$		
ETA-I (1998)			$-2.5\pm0.2\pm0.4$		
ETA-II (1999)	-79 ± 9		-2.1 ± 0.2		
ETA-MAID (2002)	-52				
QM-I (1980)	-23	$+128$	-5.56 $^{\star)}$	-45	-122
QM-II (1990)	$-28(-30)$	$+143(+146)$	$-5.1(-4.9)$ $^{\star)}$	$-46(-49)$	$-143(-146)$
QM-III (1992)	-15	$+134$	-8.9 $^{\star)}$	-38	-114
AM (1994)	-43	$+108$	-2.5 $^{\star)}$	-27	-108

different observables. When resonance parameters like the helicity ratio are uncertain by factors of five, comparisons to model predictions are not useful. Often, it is the comparison of results from different channels that reveals systematic problems, thus underlining the importance of studying resonances in other than the pion decay channel alone. In the present case, it has to be seen whether the results from pion and η photoproduction will eventually converge.

Until now, we have discussed the second resonance region for the proton. Further information about isospin $I = 1/2$ $N^\star$ resonances is related to the isospin structure of their electromagnetic excitation. It involves the two independent amplitudes A^{IS} (isoscalar) and A^{IV} (isovector) which are related to the proton and neutron amplitudes (A^p, A^n) via eq. (10). The separation of the isospin components requires measurements on the neutron which can only be done on neutrons bound in the deuteron or other light nuclei. As discussed in sec. 3.4, additional systematic problems are introduced which are related to the model dependence of the extracted neutron cross section. The data base for the reactions off the neutron is thus much more sparse and less reliable than for the proton. This is reflected in the results of the multipole analyses. As an example, the D_{13} multipoles from SAID [58] on the neutron are shown in fig. 38. In particular in the case of the magnetic M_{2-} multipole, the situation is unsatisfactory, and a reliable determination of the coupling is not possible. The imaginary part at resonance position has changed by a factor of four between the 1996 and 2002 analyses. Also, the change of the neutron helicity couplings between the two analyses is far larger than the quoted uncertainties (see table 3).

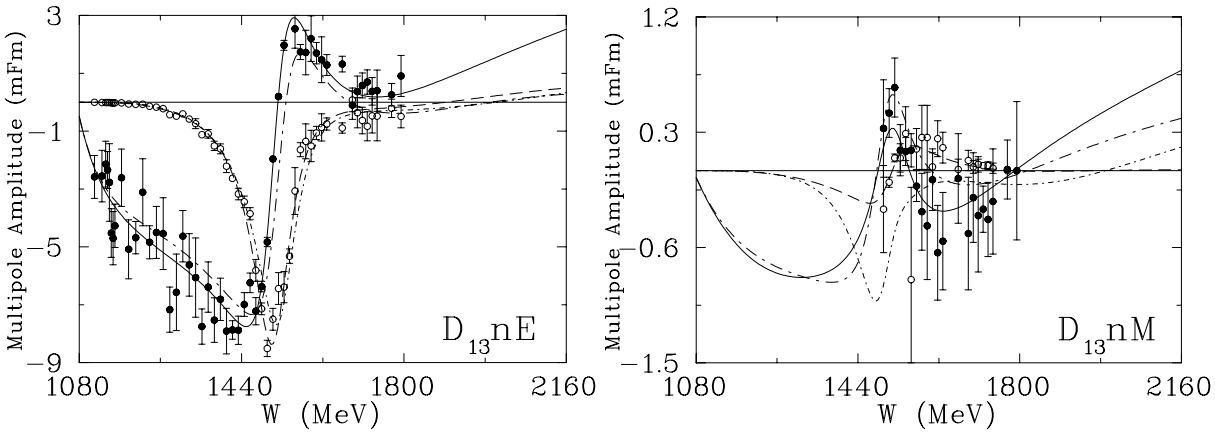

Figure 38: Partial wave amplitudes for the D_{13} excitation on the neutron from the SAID analysis [58]. Caption like fig. 35.

Most of the data from deuteron targets still stem from measurements with untagged photon beams. Often, only ratios of proton - neutron cross sections have been measured with at times insufficient separation of single and double pion production channels (see discussion in [190]). The need for better data is obvious. Recently, a new measurement of the breakup reaction $\gamma d \to \pi^o np$ was reported [190]. The total cross section and typical angular distributions throughout the second resonance region are compared in fig. 39 to the proton data and to predictions from the SAID and MAID analyses. The deuteron cross section has been modeled in a simple participant - spectator approximation where the sum of the proton and neutron cross sections predicted by MAID (respectively SAID) was folded with the deuteron Fermi motion calculated from the deuteron wave function [233]. The proton cross section is well reproduced by both models. This is not surprising since the data was included into the fits.
For the deuteron, the PWIA calculations based on the MAID and SAID predictions for the neutron cross section agree almost perfectly with the data for photon energies up to 550 MeV. The angular distributions of the deuteron data are close to two times the proton data in this energy range, indicating similar angular distributions for $p(\gamma, \pi^o)p$ and $n(\gamma, \pi^o)n$. However,the models significantly overestimate the data in the region of the D_{13}. In this range, the angular distributions for the proton and the deuteron

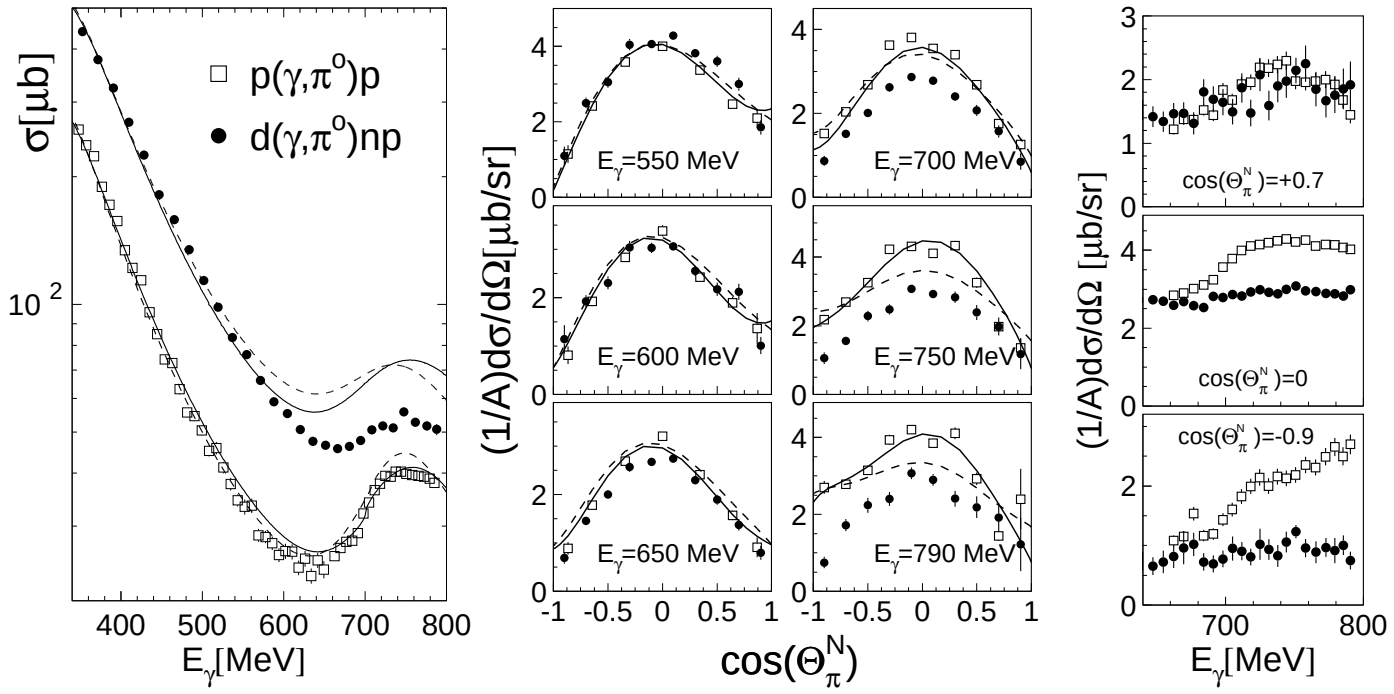

Figure 39: Quasifree π^o photoproduction off the deuteron (filled circles) compared to the elementary reaction on the proton (open squares). Left hand side: total cross sections. Solid lines: SAID results [57] for the proton cross section and Fermi smeared average of proton and neutron cross sections. Dashed lines: same for MAID results [67]. Center: angular distributions normalized to the mass number. Solid lines: SAID results for the proton, dashed lines: Fermi smeared average over SAID proton and neutron cross sections. Right hand side: differential cross section as function of the incident photon energy.

develop noticeable differences. This is most clearly seen in the energy dependence of the differential cross section for forward, central, and backward pion angles (fig. 39, right side). The cross section is still similar for forward angles, but behaves differently for backward angles. The question is again whether FSI effects are important as in the Δ range. The situation is different. Coherent contributions do not play any role at the higher incident photon energies. The momentum mismatch between participant and spectator nucleons is already so large that FSI effects should be much reduced. Furthermore, the agreement between the PWIA approximations and the data is excellent between 350 and 550 MeV incident photon energy. On the other hand, the comparison of the proton and deuteron cross sections at backward angles basically rules out that the effect could be entirely due to the $n(\gamma, \pi^o)n$ reaction. It is not possible to construct a cross section for the reaction on the neutron which together with the measured proton cross section can reproduce the inclusive deuteron data at backward angles in PWIA.

The interpretation of the suppression of the structure on the deuteron is complicated by the production threshold of the η meson at approximately 705 MeV. It is known [234] that the opening of the η-production threshold causes a unitarity cusp at backward angles resulting in a pronounced s-shape step in the cross section around the threshold at 705 MeV. This cusp structure is superimposed on the rise of the cross section towards the D_{13} resonance position.

In contrast to the Δ region, model predictions for the nuclear effects on the pion production cross sections are not available for this energy region. Experimentally, it would be very useful to have measurements where the recoil nucleons are detected in coincidence. In that way, one could first investigate if the behavior of the $p(\gamma, \pi^o)p$ reaction is different for free protons and protons bound in the deuteron. Overall, the investigation of the higher-lying resonances of the neutron is still in an early state. Even results for such prominent resonances like the $D_{13}(1520)$ should be received critically.

4.2 *η-Photoproduction and the $S_{11}(1535)$-Resonance*

The lowest-lying S_{11} resonance has two characteristic features which distinguish this state from other resonances in this excitation energy range. They are not easily explained in the framework of nucleon models: the strong coupling of the state to the $N\eta$ decay channel and the small slope of its electromagnetic transition form factor. The small decay branching ratios of the $D_{13}(1520)$ and $P_{11}(1440)$ resonances into $N\eta$ are not surprising since they involve higher partial waves close to threshold. However, the decay patterns of the first and second S_{11} resonances, both involving $l = 0$ transitions, are very different. The ratios of the hadronic decay matrix elements $\langle N\eta|\mathcal{H}_s|S_{11}\rangle$ and $\langle N\pi|\mathcal{H}_s|S_{11}\rangle$ follow simply from their partial widths Γ_η, Γ_π via:

$$\frac{\langle N\eta|\mathcal{H}_s|S_{11}\rangle}{\langle N\pi|\mathcal{H}_s|S_{11}\rangle} \;=\; \sqrt{\frac{\Gamma_\eta}{\Gamma_\pi}\frac{q_\pi^\star}{q_\eta^\star}}\,, \tag{45}$$

where $q_\eta^\star$ and $q_\pi^\star$ are the meson cm momenta at the resonance positions. Inserting the nominal resonance masses of 1535 MeV and 1650 MeV, and the partial widths taken from the multi-channel analysis of pion induced pion and η production from Vrana, Dytman, and Lee (b_η=51%, b_π=35% for the $S_{11}(1535)$ and b_η=6%, b_π=74% for the ß) yields:

$$\frac{\langle N\eta|\mathcal{H}_s|S_{11}(1535)\rangle}{\langle N\pi|\mathcal{H}_s|S_{11}(1535)\rangle} = 1.9 \qquad \frac{\langle N\eta|\mathcal{H}_s|ß\rangle}{\langle N\pi|\mathcal{H}_s|ß\rangle} = 0.35\,. \tag{46}$$

This means more than a factor of five difference for the two resonances. These decay patterns are very important for the understanding of the underlying spin-flavor structure of the two resonances. The only possibility to produce such a pattern in the constituent quark model is a fine tuning of the configuration mixing of the two S_{11} SU(6)⊗O(3) basis states. However, some authors argue (see e.g. [235]), that this mixing is probably not sufficient to explain the properties of the two states.

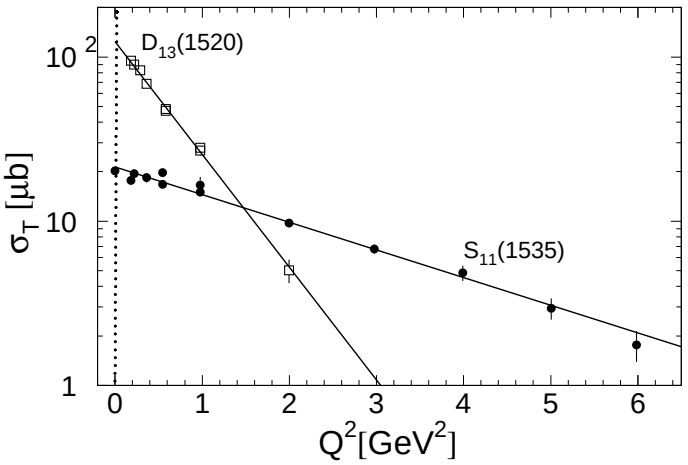

Figure 40: Q^2 dependence of the total transverse cross section for the excitation of the D_{13} and S_{11} resonances [241].

The other characteristic feature of the $S_{11}(1535)$ is the Q^2 dependence of its electromagnetic transition form factor. It was found in electron scattering experiments at Bonn and at DESY in the 1970's [236]-[241] that the decrease of the excitation strengths with four momentum transfer is much steeper for the D_{13} resonance than for the S_{11}. The effect is so large, that although the total cross section for real photons is larger for the D_{13} by roughly a factor of 6, the situation is almost reversed at Q^2=3 GeV^2. This behavior is shown in fig. 40 where the total transverse excitation cross sections are plotted versus the momentum transfer.

The separation of the contributions from the two resonances was achieved with simplifying assumptions. The η yield was attributed entirely to the S_{11}. The cross section difference between inclusive electron scattering and η production at the W corresponding to the D_{13} excitation was attributed completely to the D_{13}. Finally, it was assumed that at momentum transfers above 4 GeV^2 the inclusive cross section is dominated by the S_{11}. It is difficult to explain this large effect in quark models since both resonances belong to the same SU(6) multiplet. It is interesting to note that this behavior could be in

qualitative agreement with the helicity conservation predicted by QCD for large momentum transfers. At the photon point, the D_{13} is excited dominantly by the helicity 3/2 amplitude while the S_{11} can be only excited by the helicity 1/2 amplitude. Thus, more exclusive measurements allowing to extract the precise Q^2 dependence of the helicity couplings of the two resonances are highly interesting. Such results are now becoming available from JLab (see below).

The unusual decay pattern of the $S_{11}(1535)$ has been used by several groups as an argument for very particular structures of this state. One example is the chiral constituent quark model of Glozman and Riska [15, 16]. In this model, an interaction of the quarks via exchange of the pseudo-scalar octet mesons is introduced in addition to the harmonic confining potential. The interaction gives rise to a particular fine structure interaction coming from Goldstone boson exchange rather than from one-gluon exchange

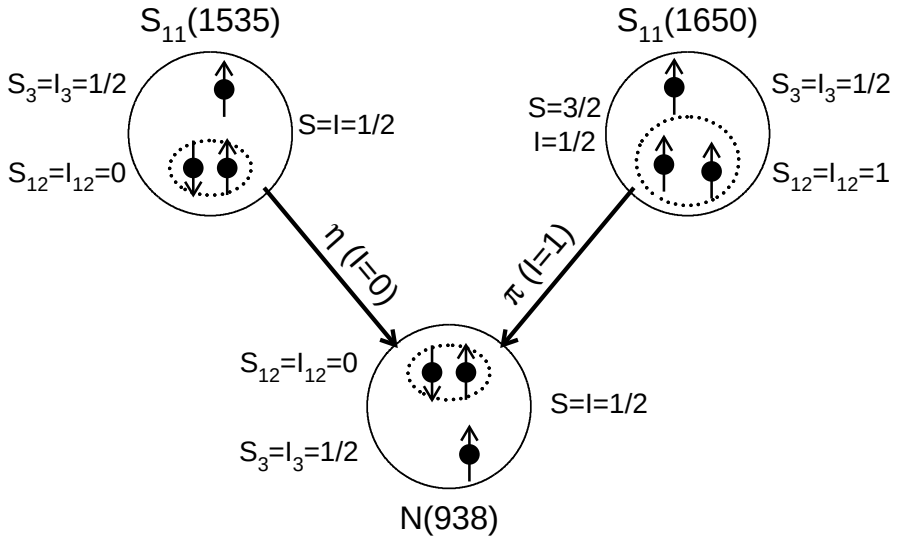

Figure 41: Quark - diquark clusterization and selection rules in the chiral quark model of Glozman and Riska. [15, 16]. S_{12} and I_{12} denote spin and isospin of the diquark, S_3, I_3 spin and isospin of the third quark and S, I the total spin and isospin of the states.

as in most other quark models. As a consequence of this interaction, the nucleon states develop a quark-diquark structure. In particular, a rather compact diquark with spin/isospin zero ($S_{12} = I_{12} = 0$) appears in the nucleon ground state and the $S_{11}(1535)$, while a less closely bound $S_{12} = I_{12} = 1$ diquark dominates the wave function of the ß. This leads to the decay selection rules depicted in fig. 41: the decay of the ß resonance via emission of the isoscalar η is forbidden since the transition involves an isospin flip of the diquark but the decay of the $S_{11}(1535)$ into $N\eta$ is not hindered. The remaining decay strengths of the ß into $N\eta$ is attributed to a small admixture of other components to the wave function.

The model discussed above still gives a conventional description of the S_{11} in the sense that it is treated as a three-quark configuration. Other models, in particular the chiral coupled channel calculations of η and kaon photoproduction by Kaiser and collaborators [210, 211], question this. The model starts from the chiral effective meson - baryon Lagrangian so that the only explicit degrees-of-freedom are the baryon and the octet mesons. Nucleon resonances are then dynamically generated. As a result a strong attraction is found in some of the channels, in particular in the $\bar{K}N$ isospin $I = 0$ channel and in the $K\Sigma$ isospin $I = 1/2$ channel, which gives rise to quasi-bound meson-nucleon states. These two quasi-bound states show many of the characteristic properties of the $\Lambda(1405)$ and the $S_{11}(1535)$ baryon states. The $K\Sigma$ state has a large decay branching ratio into $N\eta$, and the cross section for η photoproduction on the proton is well reproduced by this model (see below). This means that the S_{11} is treated as a dynamically generated quasi-bound $(q\bar{q})(qqq)$ state. If this interpretation were correct, the immediate question would be: where is the q^3 S_{11} state predicted by the constituent quark model? A further question arises from the Q^2 dependence of the form factor. As we will discuss below, models of the S_{11} as a q^3 configuration tend to predict steeper slopes than what is observed. The natural expectation is that a molecular-like quasi-bound $K\Sigma$ state should have an even stronger Q^2 dependence of the transition form factor. Li and Workman [235] have argued that the $K\Sigma$ state, if existent, should be strongly mixed with a three-quark configuration to account for the behavior of the form factor at large

Q^2. In this case, a third S_{11} resonance with a mass close to the two known states should exist. There was circumstantial evidence for a third S_{11} resonance close to 1700 MeV in the 1995 VPI analysis of pion elastic scattering [25]. However, such a state is not seen in the 2000 PIT-ANL analysis [26]. Recently, Saghai and Li [249] have claimed evidence for a third S_{11} state at 1729 MeV in η-photoproduction. We will see below that this result needs further confirmation.

4.2.1 *η-Photoproduction from the Proton*

The investigations of the second resonance region, in particular concerning the $S_{11}(1535)$, with η-photoproduction have intensified since the mid 1990's. Precise tagged beam experiments accompanied by new theory developments for the reaction models have been necessary. Even today, a full multipole analysis of the reaction is out of reach. One of the first comprehensive analyses of η photoproduction was performed by Hicks and collaborators [62] using an isobar analysis. The analysis parameterized the nucleon resonances in Breit-Wigner forms, and included a smooth, phenomenological background parameterization. This analysis pointed at the importance of the lowest lying S_{11}. However, even a refitting of the model 15 years later by Tabakin, Dytman and Rosenthal [242] did not reveal much more detail. The data base consisted of less than 160 scattered points for differential cross sections, mostly from bremsstrahlung experiments which were internally inconsistent.

First precise measurements of the threshold behavior of the η photoproduction from tagged beam experiments were reported from Bonn [243] and Mainz [205] in 1995. A measurement of electroproduction in Bonn [244] close to the photon point (Q^2=0.056 GeV^2) can be considered as well. The two experiments from Bonn reported total cross sections but not angular distributions. The results from the three experiments are summarized in figs. 42,43. The total cross sections are in good agreement in the overlap region. The Mainz experiment used the $\eta \to 2\gamma$ and $\eta \to 3\pi^o$ decays for the detection of the η meson simultaneously. The two channels have different instrumental detection efficiencies [205], and the agreement indicates small systematic uncertainties.

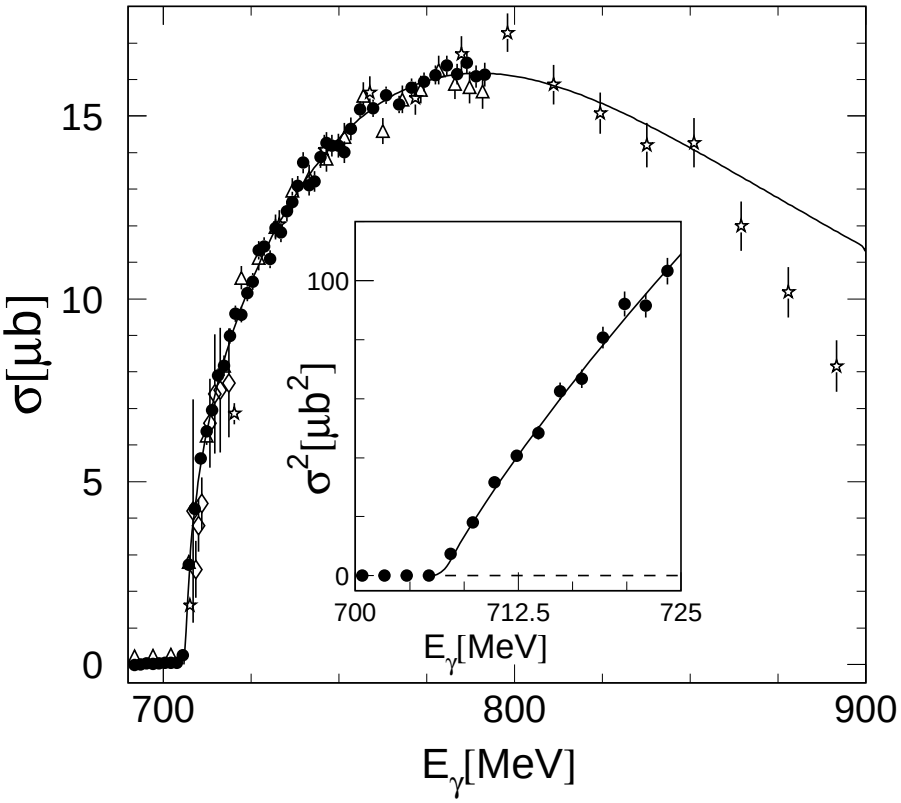

Figure 42: Total cross section for the reaction $p(\gamma,\eta)p$ in the threshold region. Open stars: electroproduction close to the photon point [244], filled circles, (open triangles): photoproduction Mainz, two-photon decay channel of the η ($3\pi^o$ decay channel) [205], open diamonds: photoproduction Bonn [243]. Insert: linear energy dependence of the squared cross section close to threshold. The curves are Breit-Wigner fits to the data (see text).

The typical s-wave behavior of the reaction is apparent from the experimental data. The expected

energy dependence at threshold is given by:

$$\sigma(E_\gamma) \propto (E_\gamma - E_{thr})^{(l+1/2)} \;\; l = 0, 1, 2, ... \;\; (s, p, d...) \; , \tag{47}$$

where E_{thr} ≈707 MeV is the threshold energy. Indeed, the square of the cross section is a linear function of the incident photon energy close to threshold, as shown in the insert of fig. 42. At the same time, the angular distributions are almost isotropic (see fig. 43). The fit of the total cross section, shown in the figure, was achieved with a single Breit-Wigner curve for the S_{11} resonance, neglecting other contributions:

$$\sigma(E_\gamma) \;\; = \;\; 4\pi \frac{q_\eta^\star}{k^\star} |E_{0+}|^2 \;\; = \;\; \frac{q_\eta^\star}{k^\star} \frac{C M_R^2 \Gamma_R^2}{(M_R^2 - W^2)^2 + M_R^2 \Gamma_R^2 x^2} \tag{48}$$

where the energy dependence of the total width, important due to the proximity of the η threshold, is parameterized by:

$$x = b_\eta \frac{q_\eta^\star}{q_{\eta R}^\star} + b_\pi \frac{q_\pi^\star}{q_{\pi R}^\star} + b_{\pi\pi} \tag{49}$$

where $k^\star$, $q_\eta^\star$, $q_\pi^\star$ are the photon, η and pion cm momenta, $q_{\eta R}^\star$, $q_{\pi R}^\star$ are the momenta at resonance position, M_R, Γ_R are position and width of the resonance, b_η, b_π, $b_{\pi\pi}$ are the branching ratios for the indicated decay channels and $W = \sqrt{s(E_\gamma)}$. Under the assumption of S_{11} dominance the electromagnetic helicity coupling follows from:

$$|A_{1/2}^p| = \left[\frac{M_R}{2m_p} \frac{\Gamma_R}{b_\eta} \sigma(M_R) \right]^{1/2} \tag{50}$$

As discussed below it is assumed that $b_\eta = b_\pi = 0.45$. The fit curve corresponds to the resonance parameters $M_R = 1544 \pm 2$ MeV, $\Gamma_R = 203 \pm 9$ MeV, and $A_{1/2}^p = (124 \pm 3) 10^{-3}$ GeV$^{-1/2}$ [246].

Contributions from the other resonances in the second resonance region can affect the angular distributions, fitted with the ansatz:

$$\frac{d\sigma}{d\Omega} = \frac{q^\star}{k^\star} [a + b \cos(\Theta^\star) + c \cos^2(\Theta^\star)] \tag{51}$$

where $\Theta^\star$ is the cm polar angle of the η-mesons. The a-, b-, c-coefficients can be related to a low energy multipole expansion of the differential cross sections under the following assumptions:

- The dominance of the $S_{11}(1535)$ allows to keep only terms proportional to the E_{0+} multipole.
- At low incident photon energies in the second resonance region only $l \leq 2$ multipoles must be accounted for.

In this case the expansion is given by:

$$\begin{aligned} a &= E_{0+}^2 - Re(E_{0+}^\star (E_{2-} - 3M_{2-})) \\ b &= 2Re(E_{0+}^\star (3E_{1+} + M_{1+} - M_{1-})) \\ c &= 3Re(E_{0+}^\star (E_{2-} - 3M_{2-})) \quad . \end{aligned} \tag{52}$$

The a coefficient comes mainly from the S_{11} contribution, the b coefficient from a possible interference of the S_{11} with the $P_{11}(1440)$ (M_{1-} multipole) and with Born terms and vector meson exchange (E_{1+}, M_{1+}), and the c coefficient from the interference of the S_{11} with the D_{13} (E_{2-}, M_{2-} multipoles). The results of the fits shown in fig. 43 reflect the dominance of the constant term. The b coefficient is small and consistent with zero. Thus, evidence for a contribution of the $P_{11}(1440)$ resonance was not found. The c coefficient is clearly negative which was taken as first evidence for a contribution of the D_{13} to η photoproduction [205] because background contributions in this multipole are expected to be negligible. Practically identical results were found later in the GRAAL experiment [248].

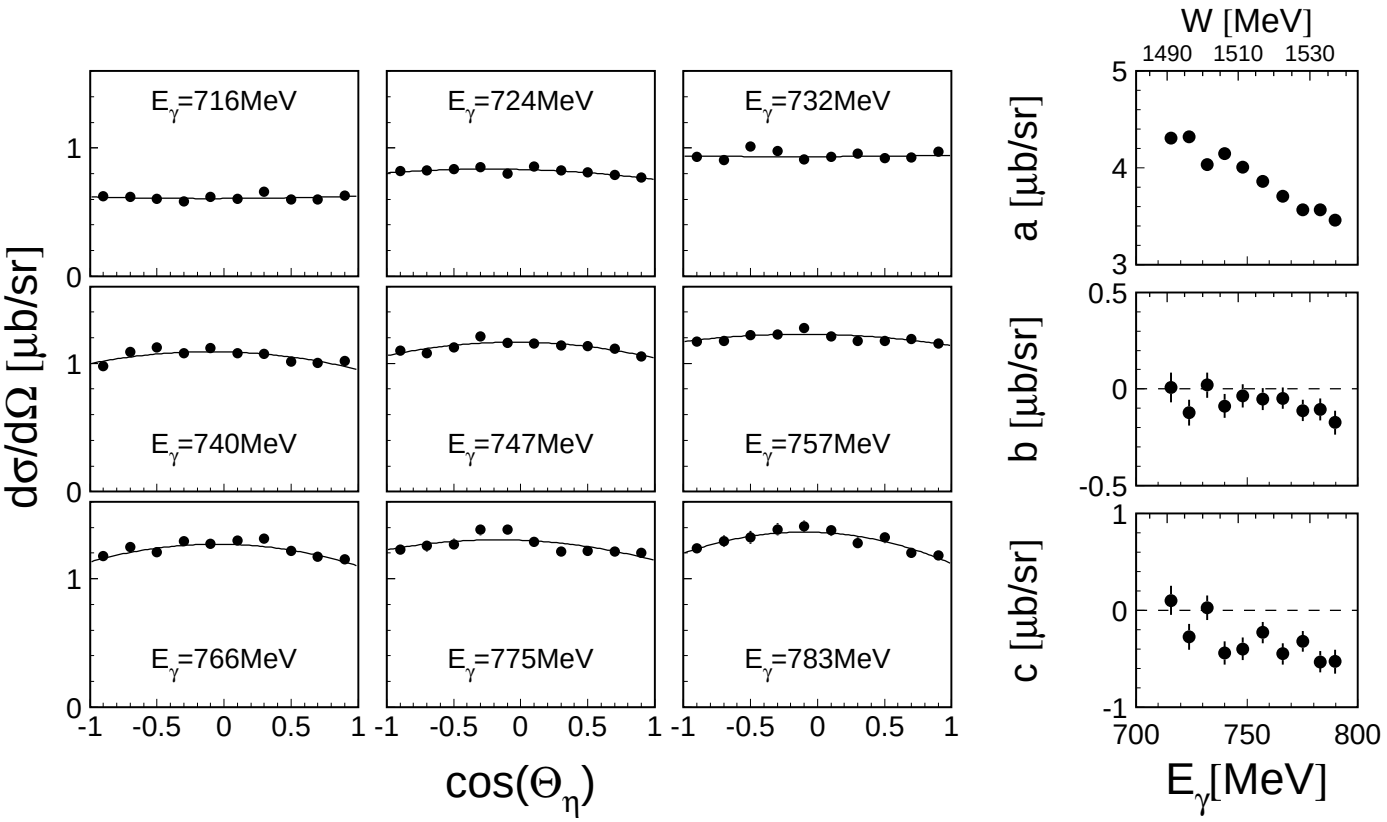

Figure 43: Angular distributions for $p(\gamma,\eta)p$ [205]. The curves are fits with eq. (51). The pictures on the right hand side show the energy dependence of the fit coefficients a,b,c.

The above analysis seems to account for the main features of the experimental results. Obviously, a more detailed analysis is wanted, taking into account possible background contributions. The analyses were pushed ahead by the RPI group (see e.g. [38]-[40]) and the Mainz group (see e.g. [43, 222, 68]). In both cases, the background contributions from Born terms and vector meson exchange are parameterized in an effective Lagrangian formalism. In fig. 44, results from model calculations are compared to experiment. Here, the quantity $[(\sigma k^\star)/(4\pi q_\eta^\star)]^{1/2}$ is plotted instead of the total cross section. In case of a background-free S_{11} excitation it equals $|E_{0+}|$. The first observation is that the energy dependence is not intuitive for an amplitude which is resonant at $\sqrt{(}s) \approx 1544$ MeV corresponding to $E_\gamma \approx 800$ MeV. The amplitude does not peak at this energy but instead rises towards the threshold. This behavior stems from the strong energy dependence of the resonance width (see eq. (49)) due to the phase space opening of the η-channel above threshold. It is apparent that all models can reproduce the data at the same level. This holds for the simple Breit-Wigner fit [205], the effective Lagrangian model [39, 246], the isobar model [68], and also for the coupled channel model with the dynamically generated $K\Sigma$ quasi-bound state [211]. A comparison of truncated versions of the models allows to estimate the background contributions. This was done in the same way for the ELA [246] and the ETA-MAID: the full model including all terms was fitted to the data. Then, different contributions were switched off without refitting any parameters. In case of the ELA, the contribution from the $S_{11}(1535)$ all by itself results in a smaller E_{0+} amplitude, roughly 4% at the resonance position. In case of the ETA-MAID, contributions from Born terms and vector meson exchange seem to cancel. Only the second S_{11} resonance makes an effect of roughly 8% at the resonance position.

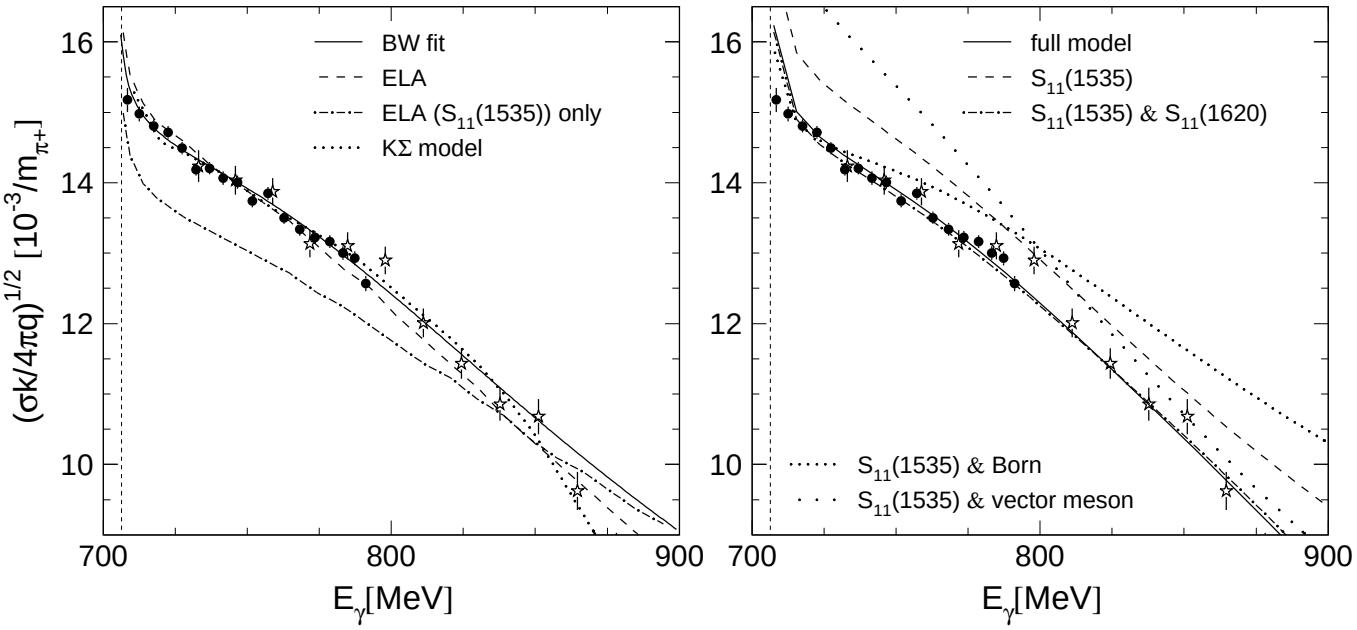

Figure 44: Comparison of the phase space reduced cross section (see text) to model calculations. Left hand side: Breit-Wigner fit [205], prediction from $K\Sigma$ quasi-bound state [211] and effective Lagrangian model (ELA) [39, 246]. For the effective Lagrangian model the result of the full model and the result of switching off all non-S_{11} contributions is shown. Right hand side: results from ETA-MAID [68]. Shown is the result of the full calculation (solid line), the contribution of the $S_{11}(1535)$ alone, the contribution of both S_{11} resonances, and the combination of $S_{11}(1535)$ with different background contributions. Data are from [205] (filled circles) and [244] (open stars).

Due to the small influence of non-$S_{11}(1535)$ contributions, one expects that the extraction of the electromagnetic coupling of the resonance from η photoproduction is less prone to systematic uncertainties than the extraction from pion data where the $S_{11}(1535)$ makes only a small contribution. A comparison of the values of $A^p_{1/2}$ from different analyses of η and pion photoproduction is given in table 4. The extracted parameters of the resonances are not independent of each other, and the helicity coupling depends on the hadronic widths which are not very well known. Therefore, we have included renormalized values of the helicity couplings assuming a total width of 150 MeV, branching ratios of $b_{N\eta}$ =0.5, $b_{N\pi}$ =0.4 and the proportionalities:

$$A^p_{1/2} \propto \sqrt{\Gamma / b_{Nm}} \qquad m = \eta, \pi. \tag{53}$$

As seen from the table, the total width of the resonance is not well constrained by the analyses of the photoproduction data. Values are ranging from 80 MeV to more than 200 MeV where the pion data seem to favor the smaller values. After renormalization of the width effects, the scatter of the helicity couplings is much reduced. Almost all the results extracted from η production fall into the range (90 - 107)10^{-3}GeV$^{-1/2}$ while the results from the pion data lie in the range (60 - 80)10^{-3}GeV$^{-1/2}$. The analysis of η photoproduction by Homma et al. [247] was based on a much inferior data base than the other analyses and is not used further. The remaining exceptions are the chiral quark model analysis of η photoproduction by Saghai and Li [249] and the most recent SAID analysis of pion photoproduction [58]. When these two analyses are not included, the average values of $A^p_{1/2}$ extracted from the two reactions are:

$$(A^p_{1/2})_{N\eta} = \quad 100 \times 10^{-3}\text{GeV}^{-1/2} \quad = 182.6 \times 10^{-3}\text{GeV}^{-1}\sqrt{\Gamma / b_{N\eta}} \tag{54}$$

$$(A^p_{1/2})_{N\pi} = \quad 78 \times 10^{-3}\text{GeV}^{-1/2} \quad = 127.4 \times 10^{-3}\text{GeV}^{-1}\sqrt{\Gamma / b_{N\pi}} \tag{55}$$

which would be equivalent for $b_{N\eta}/b_{N\pi} \approx 0.5$.

Table 4: Photon couplings of the $S_{11}(1535)$ resonance. $(A^p_{1/2})_{nor}$: normalized to $\Gamma = 150$ MeV, $b_{N\eta}$ =0.5, $b_{N\pi}$ =0.4, respectively. Method: $N\eta$: analysis of $\gamma p \to p\eta$, $N\pi$: analysis of $\gamma p \to N\pi$, QM: quark model predictions. Sauermann et al. (Sau96) [70] did a simultaneous analysis of η and π data. $b_{N\eta,N\pi}$: $b_{N\eta}$ if Method N_η, $b_{N\pi}$ if Method N_π. [1)] error includes uncertainty of partial widths. [2)] assumed to be 0.4 for the calculation of $(A^p_{1/2})_{nor}$ and ξ^p_π. [3)] not including Hom88 and Sag01. [3)] not including Arn02. See eqs. (56,57) for the definition of the electrostrong coupling ξ.

Ref.	Method	Γ MeV	$b_{N\eta,N\pi}$	$A^p_{1/2}$ $10^{-3}\text{GeV}^{-1/2}$	$(A^p_{1/2})_{nor}$ $10^{-3}\text{GeV}^{-1/2}$	ξ^p_η, ξ^p_π 10^{-4}MeV^{-1}
Hom88 [247]	$N\eta$	240	0.27	133^{+55}_{-39}	77^{+32}_{-23}	$1.7^{+0.7}_{-0.5}$
Kru95 [205, 206]	$N\eta$	203	0.45	125±25[1)]	102±3	2.22±0.07
Kno95 [43]	$N\eta$	166	0.5	107	102	2.25
Li95 [80]	$N\eta$	198	0.5	111	97	2.20
Ben96 [39]	$N\eta$	150	0.5	89±7	89±7	2.04±0.16
Sau95 [70]	$N\eta$, $(N\pi)$	162	0.55	102	103	2.35
Kru97 [246]	$N\eta$	212	0.45	120±20[1)]	96±9	2.11±0.20
Sag01 [249]	$N\eta$	162	0.55	64	65	1.44
Chi02 [68]	$N\eta$	191	0.5	118	105	2.34
Ren02 [248]	$N\eta$	150	0.55	102	107	2.38
Average [3)]		180			100±3	2.24±0.04
Met74 [61]	$N\pi$	100	0.34	63±13	71±15	0.9±0.2
Ara82 [52]	$N\pi$	173	0.38	80-83	73 - 75	0.94 - 0.97
Cra83 [53]	$N\pi$	136	? [2)]	65±16	68±17	0.9±0.2
Arn90 [55]	$N\pi$	124	0.38	78	84	1.1
Arn93 [56]	$N\pi$	84	0.42	61±3	84±4	1.10±0.05
Arn96 [57]	$N\pi$	103	0.31	60±15	64±16	0.83±0.21
Arn02 [58]	$N\pi$	106	0.4	30±3	36±4	0.47±0.05
Dre99 [67]	$N\pi$	80	0.4	67	92	1.2
Che02 [250]	$N\pi$	95	0.4	72±2	90±3	1.17±0.04
Average [4)]		112			78±4	1.02±0.05
Fey71 [9]	QM			157		
Met74 [61]	QM			166		
Kon80 [10]	QM			147		
Clo90 [223]	QM			150 - 160		
Cap92 [101]	QM			76		
Bij94 [13]	QM			126		

Table 5: Hadronic widths of the $S_{11}(1535)$ resonance from analyses of $\pi p \to \pi p$ and $\pi p \to \eta p$

Ref.	Γ MeV	b_π	b_η	$b_{\pi\pi}$	b_π/b_η
KSU92 [24]	151±21	0.51±0.05	0.43±0.06	0.06±0.03	1.19
Sau95 [70]	162	0.41	0.55	0.04	0.75
Bat95 [251]	155±16	0.34±9	0.63±7	0.03±0.03	0.54
Gre97 [252]	167.9±9.4	0.394±0.009	0.568±0.011		0.69
Pit-ANL00 [26]	112±19	0.35	0.51		0.69

The results for the branching ratios from recent analyses of pion induced reactions are summarized in table 5. The more recent results tend to smaller values of the ratio, but only one analysis comes close to 0.5 which indicates some discrepancy between the results for $A^p_{1/2}$ from pion and η photoproduction. It is particularly disturbing that the most recent VPI multipole analysis of pion photoproduction [58] (see tab. 4) gives such a small value for $A_{1/2}$ (30±3). On the other hand, the authors discuss that the results for the $S_{11}(1535)$ are very unstable and are only given for completeness. This analysis uses the best of the available data bases of pion photoproduction making it unlikely that earlier analyses of pion photoproduction could be more reliable. The problem is that the S_{11} contributes little to pion photoproduction and that the close-by threshold cusp obscures the signal.

In this sense, η photoproduction is better suited albeit currently lacking data for polarization observables in η photoproduction. Therefore, a complete multipole analysis is impossible, and the results are model dependent. The dependence seems to be small due to the dominance of the S_{11}. Interestingly, a coupled channel analysis of η *and* pion photoproduction of Sauermann et al. [70] could describe both data sets with a coupling close to the typical results obtained from the η data alone (see tab. 4). Independent of the above discussion, the following remarks can be made concerning the electromagnetic coupling at the photon point:

- Most quark models predict values above $125\times10^{-3}\text{GeV}^{-1/2}$, up to almost $170\times10^{-3}\text{GeV}^{-1/2}$. Even if we adopt the result from η photoproduction (eq. (54)) such large values require a total width in the range 250 - 400 MeV which is unrealistic. Therefore, only the relativized quark model of Capstick [101] predicts a value in the range of the experimental results. However, there could be a further twist. As we have already discussed for the Δ, quark models predict the 'bare' values of the couplings while the results extracted from data usually correspond to the 'dressed' vertices in the presence of re-scattering terms. Recently, Chen et al. [250] have analyzed pion scattering and pion photoproduction with a coupled channel dynamical model. They find not only a value of the 'dressed' $A_{1/2}$ which lies more in the range of the η results than typical results from other pion production analyses. They also find a much larger value of the 'bare' coupling. Rescaled to Γ=150 MeV, their result corresponds to $(145\pm4)\times10^{-3}\text{GeV}^{-1/2}$.

- In view of the unexplained discrepancy between the results from pion and η photoproduction, the value from η photoproduction (eq. (54)) should be used consistently as the photon point result for the analysis of the electromagnetic transition form factor as function of Q^2 since the results for $Q^2 > 0$ are all obtained from η electroproduction (see fig. 45).

Since most of the uncertainty in the electromagnetic coupling comes from the hadronic widths, Mukhopadhyay and coworkers [38, 253, 40] have suggested to use the electrostrong coupling ξ defined via:

$$\xi = \left(\frac{k^\star m_p b_\eta}{q^\star_\eta M_R \Gamma_R}\right)^{1/2} \times A_{1/2} \tag{56}$$

for precision tests of models. This quantity is proportional to the product of the electromagnetic and strong matrix elements:

$$\xi \propto \langle N\eta|\mathcal{H}_s|S_{11}\rangle\langle S_{11}|\mathcal{H}_{em}|\gamma N\rangle \tag{57}$$

and the extracted values (see tab. 4) indeed agree within a small band. Our best estimate of this parameter is $\xi = (2.24 \pm 0.05)10^{-4}$ MeV^{-1} which even agrees with the original result of Benmerrouche and Mukhopadhyay [38] (2.2±0.2) extracted from the sparse old data base. An analogous parameter can be defined for pion photoproduction, and the experimental results again range in a relatively narrow window (see tab. 4). It will be interesting to get predictions from quark models for these quantities.

The Q^2 dependence of the helicity coupling has recently been investigated in two experiments at JLab via η electroproduction. The measurement with the CLAS detector [254] covered the Q^2 range from 0.25 - 1.5 GeV^2, and the HMS experiment [255] measured two high Q^2 points at 2.4 and 3.6 GeV^2. The results are compared in fig. 45 with older measurements, the photon point value and quark model

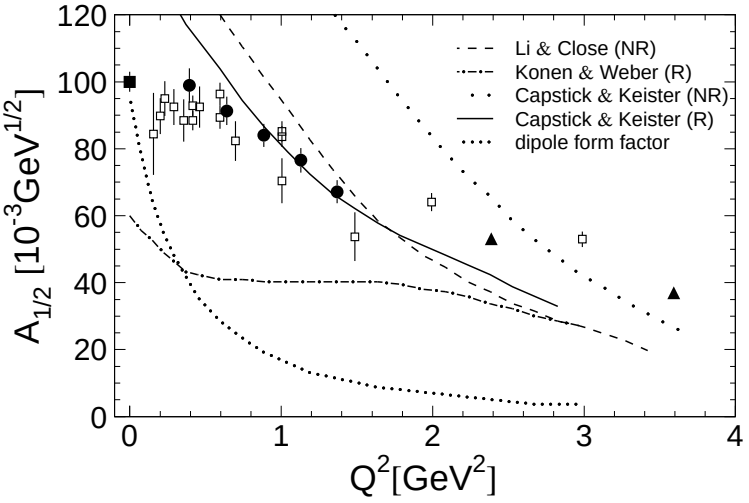

Figure 45: Q^2 dependence of the helicity coupling of the $S_{11}(1535)$ resonance. Filled circles: CLAS [254], filled triangles: HMS [255], filled square: photon point (see table 4), open squares: pre-1985 data [236]-[241]. All data renormalized to Γ_R=150 MeV, b_η=0.5. Quark model calculations: [223, 256, 257].

predictions. It should be noted that all data are renormalized to Γ_R =150 MeV and b_η=0.5. In this way, the absolute scale of $A_{1/2}$ can vary within the limits of the hadronic widths while the shape of the form factor is well determined. The new data confirm the small falloff with Q^2 which is presently not reproduced by the quark models. Unfortunately, a prediction of the form factor from the $K\Sigma$ quasi-bound state model of the S_{11} does not exists. Naively, it can be expected that the form factor for such a molecular-like system should fall off even steeper than the normal quark models.

The contribution of other resonances to η photoproduction in the threshold region is weak, but in case of the D_{13} it is now well established. The first indication came from the interference term in the angular distributions eq. (52). However, this is a small effect, as can be seen in fig. 46. Here, calculations in the effective Lagrangian approach [39] with and without contribution of the D_{13} are compared to the data. Polarization observables, in particular the photon beam asymmetry Σ, have a

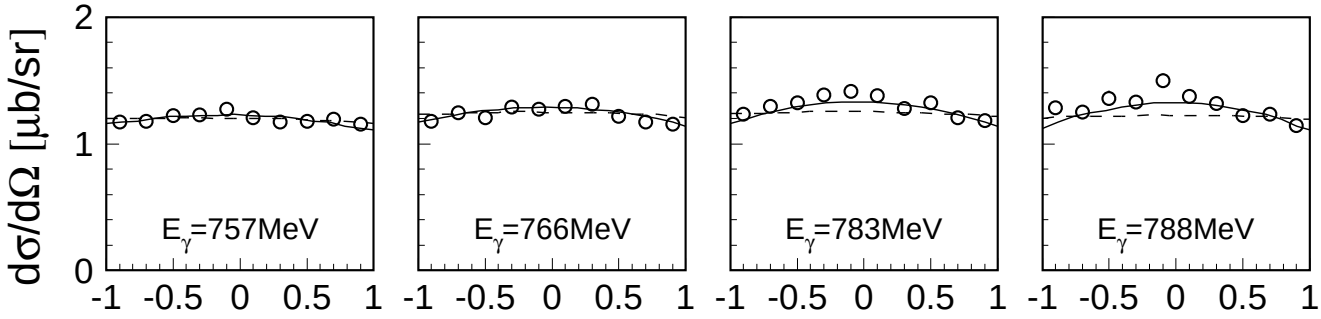

Figure 46: Angular distributions of $\gamma p \to p\eta$ [205] compared to model results of the effective Lagrangian approach [39]. Solid lines: full model, dashed lines: without D_{13} resonance.

higher sensitivity to the D_{13}. A measurement of the photon beam asymmetry from threshold up to 1 GeV was reported from the GRAAL experiment [258]. A measurement of the target asymmetry T from threshold to 1.15 GeV was done at the Bonn PHOENICS tagged photon facility [227]. Combined analyses of the differential cross sections and the polarization observables have been reported by several groups. Mukhopadhyay and Mathur [221] fitted the data with their ELA. A consistent description of all three observables with the exception of the target asymmetry in the threshold region was found. At low incident photon energies, the target asymmetry has a nodal structure. If enforced in the fit, it spoils the

agreement with the other observables and with the target asymmetry itself at higher incident photon energies. The ratio of the helicity couplings $A^p_{3/2}$ and $A^p_{1/2}$ is extracted from the fit with a relatively small uncertainty (see table 3) as well as the electrostrong couplings:

$$\begin{aligned} \xi_{3/2}(\mathrm{D}_{13}) &= (+0.165 \pm 0.015 \pm 0.035)10^{-4}\mathrm{MeV}^{-1} \\ \xi_{1/2}(\mathrm{D}_{13}) &= (-0.065 \pm 0.010 \pm 0.015)10^{-4}\mathrm{MeV}^{-1} \end{aligned} \tag{58}$$

which also avoid the uncertainty of the hadronic widths. The first error is statistical, the second reflects the systematic uncertainty from possible variations of other parameters. The much smaller values of the electrostrong coupling of the D_{13} as compared to the S_{11} are due to the small branching ratio of this resonance into $N\eta$. Using eq. (56) and PDG parameters for widths and helicity couplings of the resonance, the branching ratio $b_{N\eta}(D_{13})$ is estimated in the range 0.06% - 0.4%. However, this is a rough estimate, more precise values can be obtained when all parameters are consistently fitted to the data (see below).

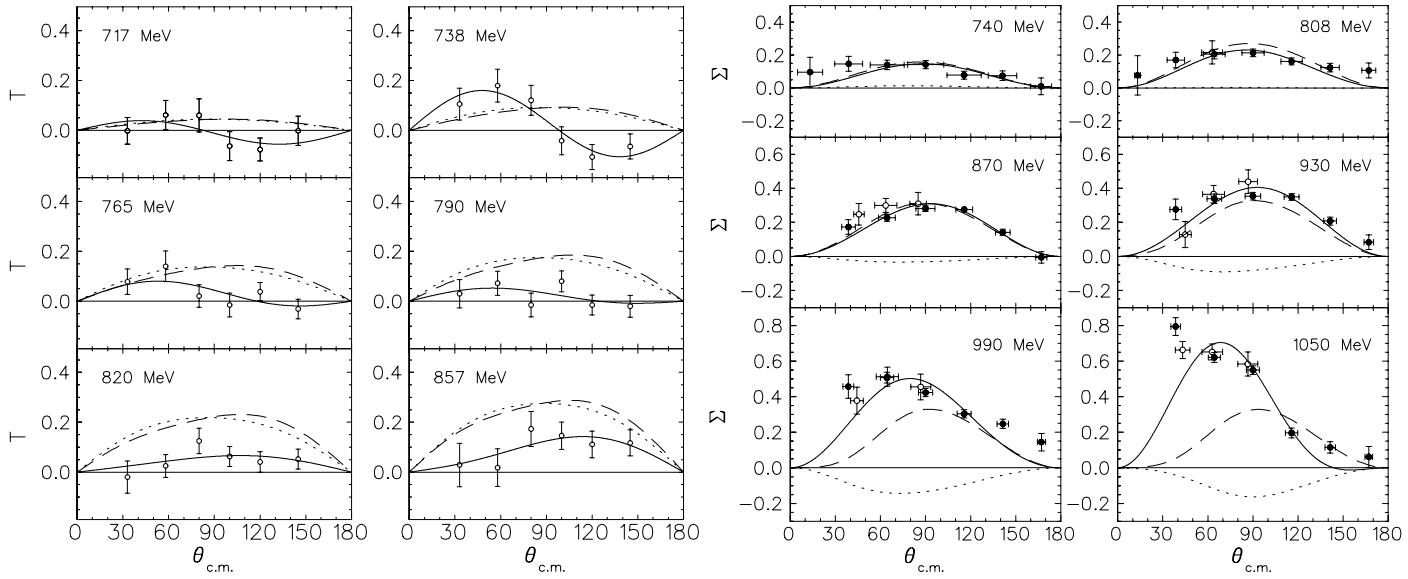

Figure 47: Fit of polarization observables [222]. Target asymmetry (left side) [227] and photon beam asymmetry (right side) [258]. The curves are from Tiator et al. [222]. Solid lines: fit to data (see text), dashed lines: isobar model from [43], dotted: isobar model without D_{13}.

Tiator et al. [222] have analyzed the data in two different ways. First they included the polarization observables into the fit of their isobar model of ref. [43]. The main results are:

- The fit simultaneously reproduces all three observables with two exceptions. In the same way as in the analysis of Mukhopadhyay and Mathur, the nodal structure of the target asymmetry in the vicinity of the threshold is not in agreement with the model (see fig. 47, left hand side). This effect is not yet understood (see discussion below). At the highest incident photon energies, the photon beam asymmetry does not agree with the data. This is taken as tentative evidence for the contribution of a higher lying resonance (see below).

- The effect of the D_{13} resonance, negligible in case of the differential cross sections, is prominent in the beam asymmetry and allows to establish the coupling of this resonance to the $N\eta$ channel beyond doubt. Figure 47 (right hand side) compares the model results with (dashed) and without (dotted) D_{13} resonance. In the D_{13} range the beam asymmetry would basically vanish without this resonance. The large positive values found in the experiment agree with the D_{13} contribution extracted from the small effect in the angular distributions.

The second analysis is a truncated multipole analysis. Differential cross sections, target, and beam asymmetry do not allow a fully model independent analysis. However, assuming $S_{11}(1535)$-dominance and neglecting partial waves with $l > 2$ allows to extend the multipole expansion for the differential cross section (eqs. (51),(52)) to the polarization observables via:

$$T = \sin(\Theta^\star)[d + e\cos(\Theta^\star)] \tag{59}$$
$$\Sigma = f\sin^2(\Theta^\star) \tag{60}$$

where:

$$d = \frac{3}{a+c/3}\mathrm{Im}[E_{0+}^\star(E_{1+} - M_{1+}] \tag{61}$$
$$e = \frac{3}{a+c/3}\mathrm{Im}[E_{0+}^\star(E_{2-} + M_{2-}]$$
$$f = \frac{3}{a+c/3}\mathrm{Re}[E_{0+}^\star(E_{2-} + M_{2-}] \; .$$

The magnitudes of the multipoles E_{0+}, E_{2-}, M_{2-}, $B_{2-} = E_{2-} + M_{2-}$, $A_{2-} = 1/2(3M_{2-} - E_{2-})$, and the phase between the s- and d-waves are then simple expressions of the fitted coefficients a,...,f [222]:

$$|E_{0+}| = \sqrt{a + c/3} \tag{62}$$
$$|E_{2-}| = \frac{1}{4}\sqrt{(a+c/3)(e^2+f^2)}\left|1 + \frac{c}{3f(a+c/3)}\right|$$
$$|M_{2-}| = \frac{1}{12}\sqrt{(a+c/3)(e^2+f^2)}\left|1 - \frac{c}{f(a+c/3)}\right|$$
$$|A_{2-}| = -\frac{c}{6f}\sqrt{\frac{e^2+f^2}{a+c/3}}$$
$$|B_{2-}| = \frac{1}{3}\sqrt{(e^2+f^2)(a+c/3)}$$

$$\tan(\Phi_{E_{0+}} - \Phi_{B_{2-}}) = \frac{e}{f} \tag{63}$$

where the definition of the helicity multipoles A_{2-}, B_{2-} is given in eq. (80), and $\Phi_{E_{0+}}$, $\Phi_{B_{2-}}$ are the phases of the respective multipoles.

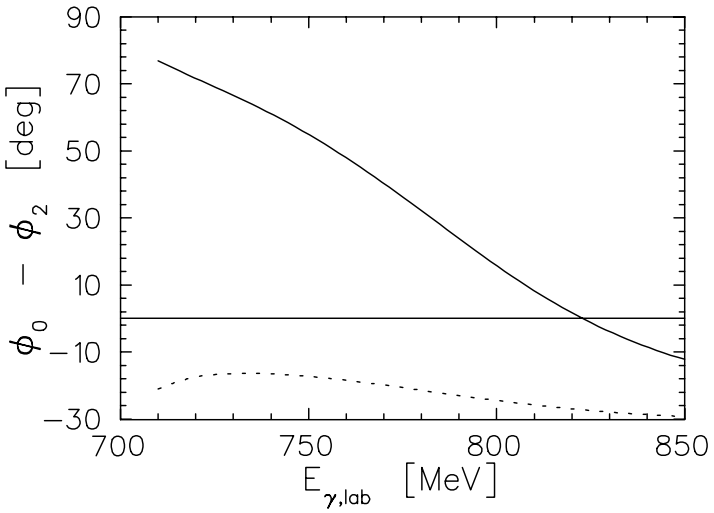

Figure 48: Phase difference between the B_{2-} helicity 3/2 multipole and the E_{0+} (see eq. (63)) [222]. Solid line: fit of multipole expansion, dotted: Breit-Wigner curves for $S_{11}(1535)$ and $D_{13}(1520)$.

The multipole expansion allows a simultaneous fit of the differential cross sections, beam, and target asymmetry up to incident photon energies of ≈900 MeV (see fig. 47). The low energy a, b, c coefficients agree with the result of the analysis of the differential cross section. This fit sheds light on the problems of the ELA and the isobar analyses with the low energy behavior of the target asymmetry. The multipole expansion can reproduce the node structure of the target asymmetry. However, a rather large, positive, and strongly energy dependent phase difference between the s- and d-waves arises (see fig. (48)) [222].

This is unexpected since the s-wave is dominated by the $S_{11}(1535)$ and the d-wave by the $D_{13}(1520)$. Both resonances have comparable widths, and the S_{11} lies only a little bit higher in energy than the D_{13}. Consequently, a Breit-Wigner shape of the two resonances results in a small negative phase difference. At least one of the two resonances would not have a Breit-Wigner shape. However, the shape of the D_{13} is well established and as discussed above, the total cross section of η production is dominated by the S_{11} and follows a Breit-Wigner curve. It is very desirable to measure the target asymmetry more precisely, since the unusual phase stems from the low energy behavior of this observable.

The analysis of the interference terms allows the determination of the decay branching ratio of the D_{13} into $N\eta$ and the ratio of the helicity couplings of the resonance. This is done in [222] where the first analysis fits $d\sigma/d\Omega$, Σ, and T with the model independent multipole analysis. In a second scenario, T is ignored, and the relative phase between D_{13} and S_{11} is taken from Breit-Wigner shapes. The results are summarized in table 6 and compared to other references.

Table 6: Properties of the $D_{13}(1520)$ extracted from η photoproduction. Tia99a and Tia99b [222] are the model independent analysis and the analysis assuming the Breit-Wigner phase. Muk98 is the ELA analysis of Mukhopadhyay and Mathur, and Chi02 the isobar model of Chiang et al. [68].

Ref.	b_η %	$A_{3/2}/A_{1/2}$	$\xi_{3/2}$ $10^{-4}\mathrm{MeV}^{-1}$	$\xi_{1/2}$ $10^{-4}\mathrm{MeV}^{-1}$
Tia99a [222]	0.08±0.01	−2.1±0.2	0.185±0.018	−0.087±0.013
Tia99b [222]	0.05±0.02	−2.1±0.2	0.134±0.018	−0.087±0.013
Muk98 [221]		−2.5±0.2±0.4	0.165±0.015±0.035	−0.065±0.010±0.015
Chi02 [68]	0.06	−3.2	0.155	−0.049

At incident photon energies above ≈900 MeV the beam asymmetry is no longer symmetric around 90^o and cannot be fitted with eq. (60). The shape requires an additional term in the photon asymmetry:

$$\Sigma = \sin^2(\Theta^\star)[f + g\,\cos(\Theta^\star)] \tag{64}$$

which stems from multipoles with $l \geq 3$ [222]. The fitted coefficient g rises strongly between 0.9 and 1.1 GeV. This higher partial wave is interpreted in [222] as a contribution of the $F_{15}(1680)$ resonance. A decay branching ratio of this resonance into $N\eta$ of $0.15^{+0.35}_{-0.10}\%$ is extracted.

In the meantime, the measurement of the angular distributions and the total cross section has been extended up to incident photon energies of 1.1 GeV (GRAAL [248]) respectively 2 GeV (CLAS [259]). The results for the total cross section are compared in fig. 49 (left hand side). The data sets are in excellent agreement up to incident photon energies of 1.0 GeV. However, between 1.0 and 1.1 GeV a systematic difference between the GRAAL and CLAS data is visible. This disagreement is important. The small bump in the GRAAL data between 1.0 and 1.1 GeV was interpreted in a quark model study of η photoproduction by Saghai and Li [249] as tentative evidence for a third S_{11} resonance with a mass of 1712 MeV and a width of 184 MeV. In this model, contributions from all known resonances in the relevant energy range are considered. It is argued that the fit is considerably improved around $E_\gamma = 1075$ MeV when a third S_{11} resonance is introduced. This state could correspond to the third

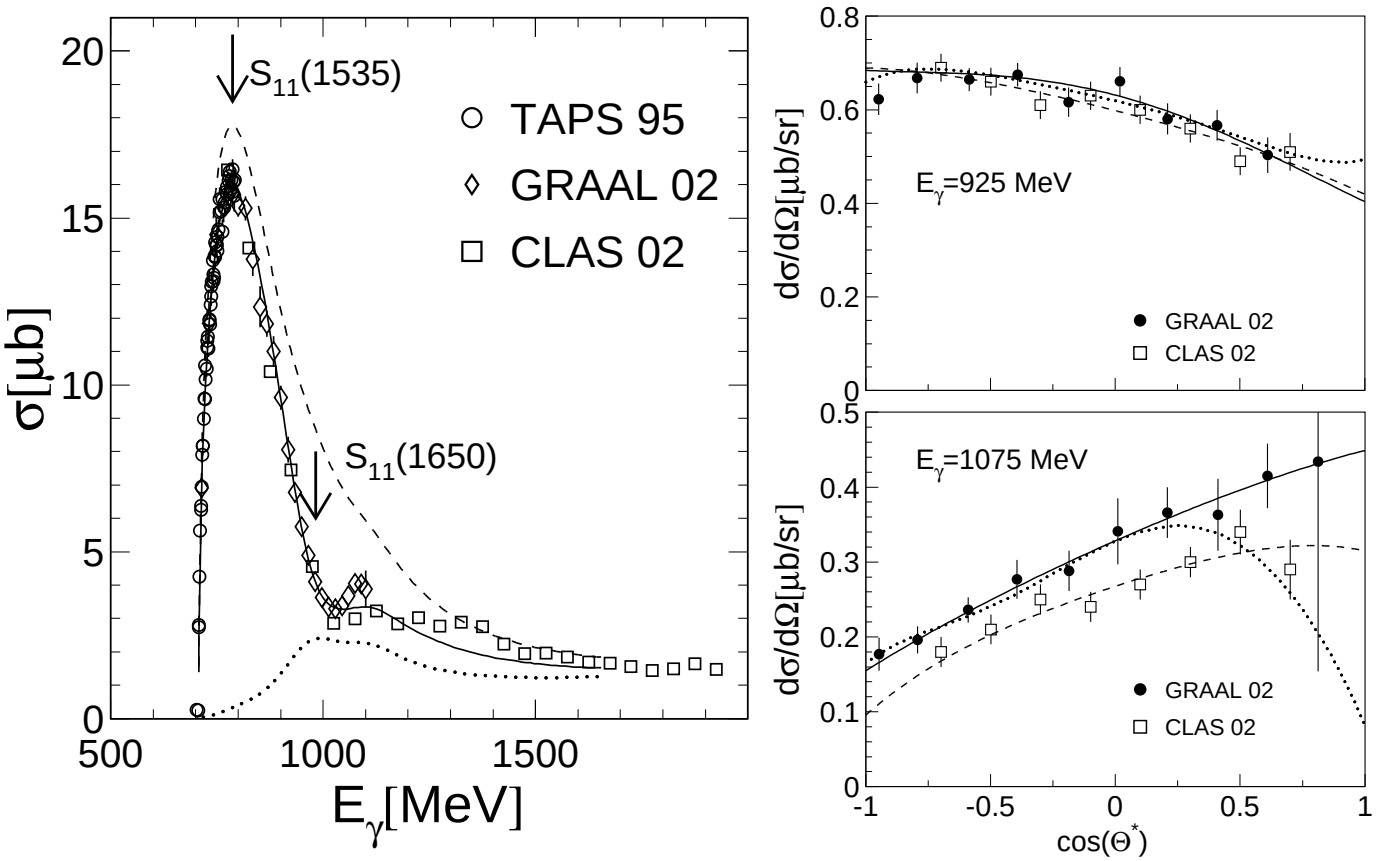

Figure 49: Left: Total cross section for $\gamma p \to p\eta$. Data are from TAPS [205] (circles), GRAAL [248] (diamonds) and CLAS [259] (squares). Curves: ETA-MAID model [68], solid: full model, dashed: without ß, dotted: without $S_{11}(1535)$. Arrows indicate positions of the two resonances. Right: Selected angular distributions. Data: GRAAL [248] (filled circles), CLAS [259] (open squares). Solid and dashed lines: fits to the data with cubic polynomials in cos(Θ). Dotted: ETA-MAID model [68].

S_{11} resonance predicted in [235]. Its inclusion into the fit also leads to significantly modified values for widths and electromagnetic couplings of the other two S_{11} states (see table 4). Figure 49 (right hand side) shows the angular distributions for E_γ=925 MeV and E_γ=1075 MeV for a more detailed comparison of the two measurements. The total cross section from both experiments agrees perfectly at the lower energy while disagreeing for the second energy. Also, the angular distributions agree within the statistical uncertainty for the lower photon energy, and polynomial fits to the data give identical results for the total cross section. However, the GRAAL data at 1075 MeV are systematically higher for all angles. Furthermore, large uncertainties arise from the extrapolation of the angular distribution to forward angles. In contrast to the lower photon energy, polynomial fits to the data differ strongly from the fit of the ETA-MAID model [68]. Further experimental effort should clarify the situation in this energy region. It is of particular importance to measure the angular distributions also for the extreme forward angles apart from a careful absolute normalization of the data.

At still higher incident photon energies the CLAS data [259] show a tendency for strong forward peaking of the angular distributions. This might be an indication for growing t-channel contributions. However, a detailed analysis of the reaction in this energy range is presently not available.

4.2.2 *η-Photoproduction from Light Nuclei*

As already discussed in the case of pion photoproduction, information about the isospin structure of the electromagnetic excitation can only be gained from measurements on nucleons bound in (light) nuclei. This introduces additional systematic uncertainties due to the nuclear effects. On the other hand, ratios of helicity couplings on the proton and neutron are free of the large systematic uncertainties of the hadronic widths of the resonances. In case of the isoscalar η mesons, it is possible to extract the isospin structure from a comparison of the cross section on the proton, the neutron and coherent production from the deuteron via:

$$\sigma_p \sim |A^{IS}_{1/2} + A^{IV}_{1/2}|^2, \quad \sigma_n \sim |A^{IS}_{1/2} - A^{IV}_{1/2}|^2, \quad \sigma_d \sim |A^{IS}_{1/2}|^2 \tag{65}$$

where $A^{IS}_{1/2}$ and $A^{IV}_{1/2}$ are the isoscalar and isovector parts of the helicity amplitude. In case of the neutron cross section, nuclear effects in the quasifree measurement must be considered. In case of the deuteron, the proportionality stands for a reaction model for coherent η photoproduction. The first attempts along these lines of investigating the isospin structure of the $S_{11}(1535)$ were undertaken in the late 1960's with bremsstrahlung. Bacci [260] and collaborators measured the breakup reaction and found that the inclusive cross section from the deuteron is roughly twice as large as for the proton at an incident photon energy of 850 MeV. The conclusion was, that $\sigma_n \approx \sigma_p$. According to eqs. (65)), either the isoscalar or the isovector part would dominate, and the other would vanish. In the same year, Anderson and Preprost [261] measured the coherent cross section from the $I = 0$ deuteron and found a rather large cross section which is only possible when the isoscalar part is large. Consequently, both experiments together seemed to indicate that $A^n_{1/2}/A^p_{1/2} \approx +1$ and thus the isovector part is *negligible*. This however, was in sharp contrast to the results from pion photoproduction and to model predictions which both favored ratios between -0.6 and -1, indicating that the isovector part is *dominant*. This problem was solved during the last few years with a series of precise measurements of breakup and coherent η photoproduction from the deuteron and from He-isotopes [262]-[268].

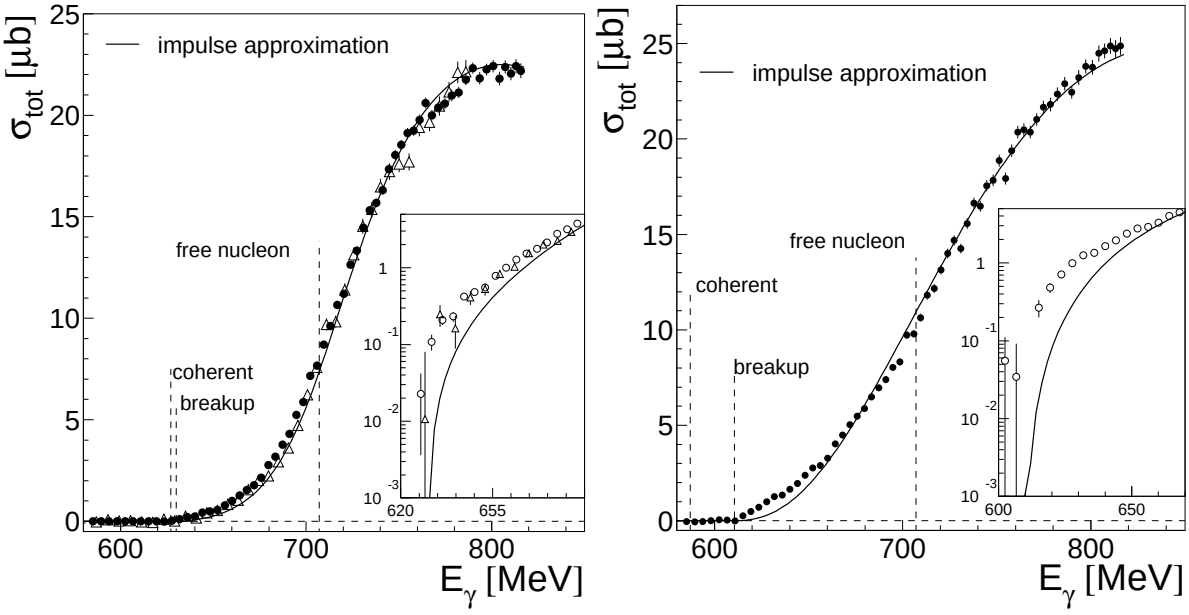

Figure 50: Inclusive η photoproduction cross section. Left hand side: from the deuteron. Circles: ref. [267], triangles: ref. [262]. Right hand side: from ^{4}He [264]. For both pictures the dashed lines indicate the coherent, the breakup, and the free nucleon production thresholds. The solid curves are the result of the impulse approximation model under the assumption of a constant σ_n/σ_p=2/3 ratio (see text). Inserts: threshold region.

The first group of experiments aimed at the extraction of the cross section ratio from the neutron and the proton via quasifree η-photoproduction from light nuclei. Different experimental concepts were exploited:

- Measurement of the inclusive $A(\gamma,\eta)X$ reaction. Comparison of the sum of the Fermi-smeared free proton cross section and a Fermi-smeared ansatz for the free neutron cross section to the inclusive nuclear cross section in PWIA. Variation of the ansatz for σ_n until agreement is achieved.
- Coincident measurement of η-mesons and recoil nucleons. Extraction of the ratio of σ_n/σ_p of the quasifree cross sections measured under identical conditions as a function of the incident photon energy E_γ.
- Coincident measurement of η-mesons and recoil nucleons and reconstruction of the effective $\sqrt{s^\star}$ and effective incident photon energy $E_\gamma^\star$ from the final state kinematics (E_η, E_R, $\vec{p}_\eta$, $\vec{p}_R$: energy and momentum of meson and recoil nucleon). Extraction of σ_n/σ_p as a function of $E_\gamma^\star$:

$$s^\star = (E_\eta + E_R)^2 - (\vec{p}_\eta + \vec{p}_R)^2 \tag{66}$$

$$E_\gamma^\star = (s^\star - m_R^2)/2m_R \ . \tag{67}$$

Two examples for the inclusive method are summarized in fig. 50. Shown is the total, inclusive cross section of the reactions $d(\gamma,\eta)X$ [262, 267] and ^{4}He$(\gamma,\eta)X$ [264]. The curves correspond to PWIA calculations. Here, the sum of the elementary cross sections off the proton and off the neutron were folded with the momentum distributions of the bound nucleons. For the free neutron cross section an ansatz was taken to be proportional to the free proton cross section. Agreement is obtained in both cases for $\sigma_n/\sigma_p \approx 2/3$. The influence of the different nuclear momentum distributions is severe. The total cross sections from ^{4}He and from the deuteron are almost equal at an incident photon energy of 800 MeV although twice the number of nucleons is involved in the He case. FSI effects are not included, and the effect stems from the nucleon momentum distributions. The good agreement of both data sets with impulse approximations using the same neutron - proton ratio is reassuring for the application of this method.

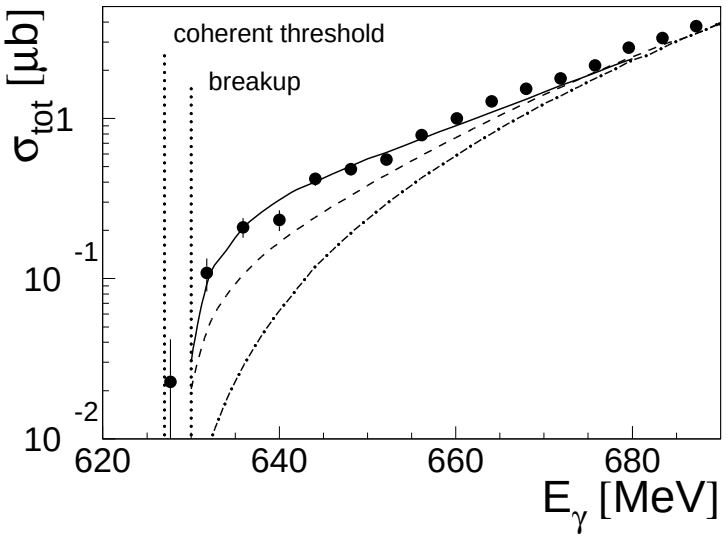

Figure 51: Threshold behavior of $d(\gamma,\eta)X$. Data from [267]. Model calculations from Sibirtsev et al. [271]. Dotted: PWIA, dashed: PWIA and NN FSI, full: PWIA and NN FSI and $N\eta$ FSI.

As shown in the inserts of fig. 50, and in more detail in fig. 51, the agreement with the PWIA calculations suffers in the vicinity of the absolute thresholds. The threshold behavior is further discussed in [266]. At least in case of the deuteron, where model calculations are available, it is understood via final state interaction effects which are large close to threshold. Fix and Arenhövel have studied these effects [269] and found that the data can only be reproduced with a three body (Faddeev-type) calculation of the $NN\eta$ system although the main contribution comes from NN FSI. Similarly, Sibirtsev et al. [270, 271] found a dominant contribution from NN FSI and some importance of the interference between NN and $N\eta$ FSI (see fig. 51). These effects are interesting in themselves for the study of the η-nucleon interaction. Here, it is only important, that they are negligible at incident

photon energies above the free nucleon threshold because the momentum mismatch between participant and spectator nucleon is always large at these energies. Then, the extraction of the neutron-proton cross section ratio is not spoiled .

The exclusive reaction with detection of the recoil nucleons was also investigated for deuteron and ^{4}He targets [263, 264, 267]. Typical results are summarized in fig. 52. The measured cross sections are

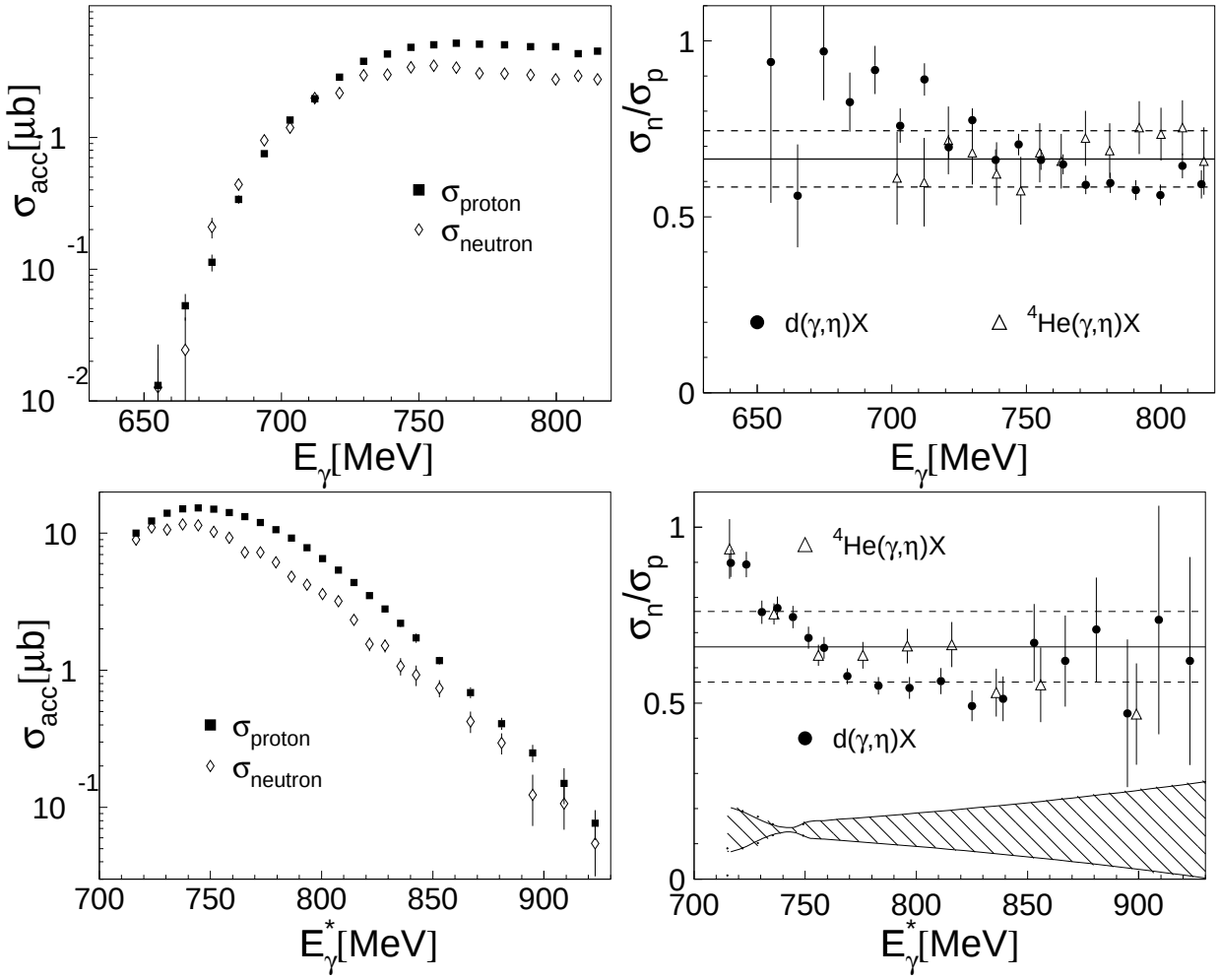

Figure 52: Exclusive η photoproduction off the deuteron [267] and ^{4}He [264]. Left hand side: measured cross section within the detector acceptance for the proton and the neutron from the deuteron target. Right hand side: neutron/proton cross section ratios σ_n/σ_p obtained for d and ^{4}He tagets. Upper parts: versus incident photon energy, bottom part: versus effective photon energy.

given within the detector acceptance [264, 267] since a small fraction of the phase space of the recoil nucleons was not covered in the experiments. Meanwhile, this should not significantly influence the ratios (see discussion in [267]). The ratios are shown as a function of the incident photon energy and as function of the effective photon energy. The latter is defined (see eqs. (66,67)) as the laboratory energy of a photon which produces the same $\sqrt{s}$ on a *nucleon at rest* as was reconstructed from the reaction kinematics for the incident nucleon with Fermi motion. This representation avoids the averaging over the Fermi momenta. It is thus better suited for the comparison to model predictions, and extends to higher effective photon energies for reactions with Fermi momenta anti-parallel to the incident photon. However, it is subject to an additional systematic uncertainty, shown as a shaded band in the lower right hand corner of the figure, which arises from the relative detector energy calibration for protons and neutrons. The results obtained from the exclusive measurements are in agreement with a neutron/proton ratio close to 2/3. The rise of the ratios close to the thresholds is due to the FSI effects discussed above.

The results from the different exclusive measurements are compared in fig. 53 to the predictions from the $K\Sigma$ model of the $S_{11}(1535)$ [210, 211] and to the results of the ETA-MAID model [68]. The $K\Sigma$ model is not favored by the data which are in good agreement with the ETA-MAID model. The

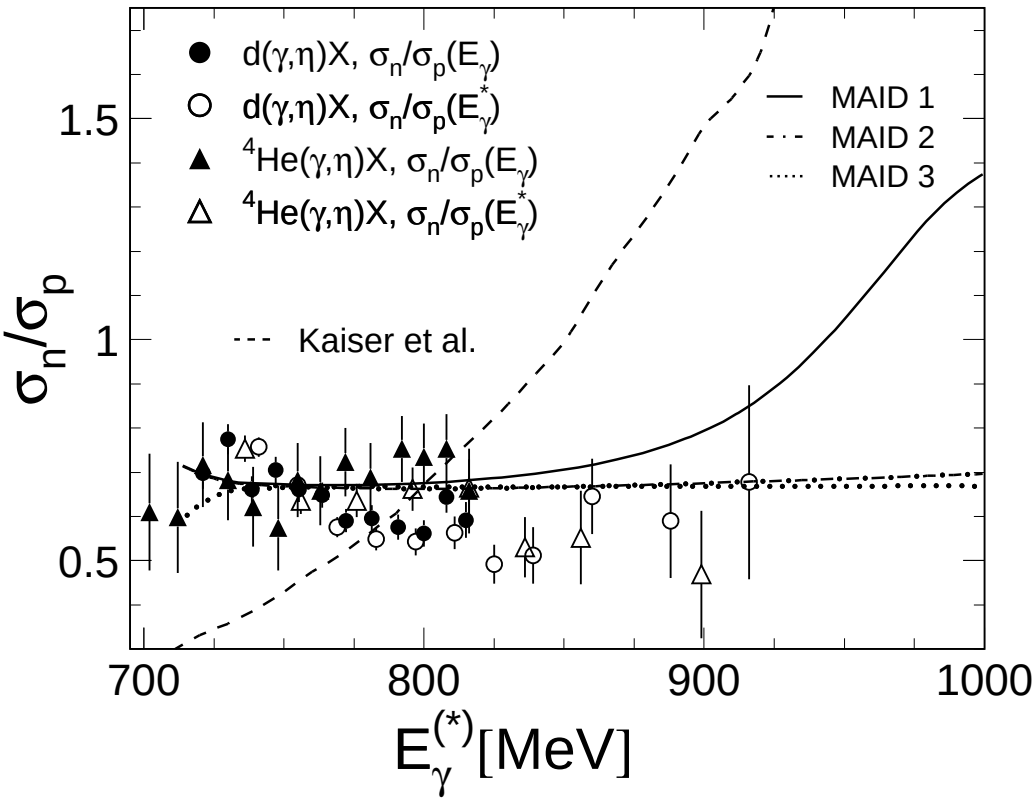

Figure 53: Ratio of exclusive neutron - proton cross sections for the deuteron and for ^{4}He [267, 264]. Dashed curve: prediction from the $K\Sigma$ model of the $S_{11}(1535)$ (Kaiser et al. [210, 211]). The curves labelled MAID are the predictions from the MAID model [68] for the full model (MAID 1), the $S_{11}(1535)$-resonance, Born terms and vector meson exchange (MAID 2), and for the $S_{11}(1535)$ alone (MAID 3).

MAID predictions in the range used for the extraction of the ratio of the helicity couplings of the $S_{11}(1535)$ ($E_\gamma \approx 750$ - 800 MeV) are practically identical for the full model and for truncations of the model up to the extreme case where only the $S_{11}(1535)$ is considered. This is further evidence that the helicity ratio extracted from the data is not influenced by background contributions. At higher photon energies a strong rise of the ratio is predicted which comes from the contribution of higher lying resonances. The presently available data do not extend to sufficiently high energies for a test of these predictions. Measurements on the deuteron at higher incident photon energies are necessary for the search for contributions from other resonances to the $N\eta$ channel.

The results for the neutron/proton cross section ratio in the S_{11} range from the different experiments are summarized in table 7 along with the ratios of the helicity couplings resulting under the assumption that background contributions are negligible. The uncertainty of the ratio of the couplings has much smaller uncertainties than the couplings themselves since the poorly known hadronic widths cancel. The results from all experiments are in good agreement. The systematic effects (which dominate the uncertainties) come from different sources (different targets, different extraction methods). It is therefore reasonable to average over the results which yields a precise result for the comparison to quark model predictions. In addition, the table includes two results for the analysis of the data from [205, 262] in the framework of models which explicitly included background terms. One of them lies a little above and one a little below the other results. In contrast, the results from multipole analyses of pion photoproduction are more scattered due to the small contribution of the S_{11} to this channel. The result indicates that either the isoscalar or the isovector part is dominant. Which one it is depends on the relative sign of the couplings. The results from pion photoproduction agree on a negative sign, corresponding to a dominant isovector part.

Table 7: Cross section ratio of $n(\gamma,\eta)n$ and $p(\gamma,\eta)p$ and the corresponding helicity ratios. Muk95: effective Lagrangian analysis of proton and neutron cross sections, Sau95: coupled channel analysis. [1)] the result from Bac69 [260] (bremsstrahlung beam, no invariant mass analysis for η, Fermi motion neglected) is not included.

Ref.	target	method	σ_n/σ_p	$\lvert A^n_{1/2}\rvert/\lvert A^P_{1/2}\rvert$
Bac69 [260]	^{2}H	η detected	$\approx$1	$\approx$1
Kru95 [205]	^{2}H	η detected	0.66±0.07	0.81±0.04
Hof97 [263]	^{2}H	recoil nucleons	0.68±0.06	0.83±0.04
Hej99 [264]	^{4}He	η detected	0.67±0.07	0.82±0.04
Hej99 [264]	^{4}He	η and recoil nucleons	0.68±0.09	0.83±0.05
Wei02 [267]	^{2}H	η detected	0.67±0.07	0.82±0.04
Wei02 [267]	^{2}H	η and recoil nucleons	0.66±0.10	0.81±0.06
		average[1])	0.67±0.03	0.82±0.02
Muk95 [272]		ELA, data from [205, 262]		0.84±0.15
Sau95 [70]		CC, data from [205, 262]		0.80
Met74 [61]		pion production		0.8
Ara82 [52]		pion production		0.9
Cra83 [53]		pion production		1.5
Arn90 [55]		pion production		0.74
Arn93 [56]		pion production		0.75
Arn94 [57]		pion production		0.33
Arn02 [58]		pion production		0.53

A possibility to access the relative sign in η photoproduction is the interference term of the S_{11} with the D_{13} in the angular distributions (coefficient c in eq. (52)). Relying on the dominance of the S_{11} and Breit-Wigner shapes of the resonances, the angular distributions on the proton ($N = p$) and the neutron ($N = n$) can be approximated in the form [267]:

$$\left(\frac{d\sigma}{d\Omega}\right)_N \propto (A^N_{1/2}(S_{11}))^2 + \mathcal{G}(E_\gamma) A^N_{1/2}(S_{11}) A^N_{1/2}(D_{13})(3cos^2(\Theta) - 1) \ , \tag{68}$$

where the function $\mathcal{G}$ is identical for proton and neutron and can be determined from the angular distributions of $p(\gamma,\eta)p$. Inserting $A^p_{1/2}(D_{13})$=(−24±2) and $A^n_{1/2}(D_{13})$=(−67±3) [58] and folding with the deuteron Fermi momenta results in the curves compared to the data in fig. 54. Obviously, the negative sign for $A^n_{1/2}$ is favored.

Consequently, only the measurement of coherent η photoproduction off the deuteron by Anderson and Preprost [261] favored a dominant isoscalar contribution. In the meantime, this result has been ruled out. The reported cross sections at $\Theta^\star_\eta \approx 90^o$ ranged from 40 nb/sr to 27 nb/sr in the energy range from 665 to 705 MeV, but in [262], an upper limit (without detection of actual signal) of 10 nb/sr was found. The results from two recent measurements are summarized in fig. 55. The measurements with the PHOENICS and AMADEUS detectors in Bonn [263] detected the recoil deuterons. The measurement with the TAPS detector in MAINZ [265] detected deuterons and η-mesons in coincidence. The results at 90^o are much smaller than reported earlier in [261], in case of the TAPS measurement more than an order of magnitude, so that they support a dominant isovector part of the amplitude. However, there is one last twist. When the signs of the helicity amplitudes and the ratio of their magnitudes are known, the isoscalar contribution to the amplitude can be calculated from eqs. (65): $A^{IS}_{1/2}/A^p_{1/2}$=(0.09±0.01). However, models for the coherent process using this ratio (see fig. 55) under predict the coherent cross

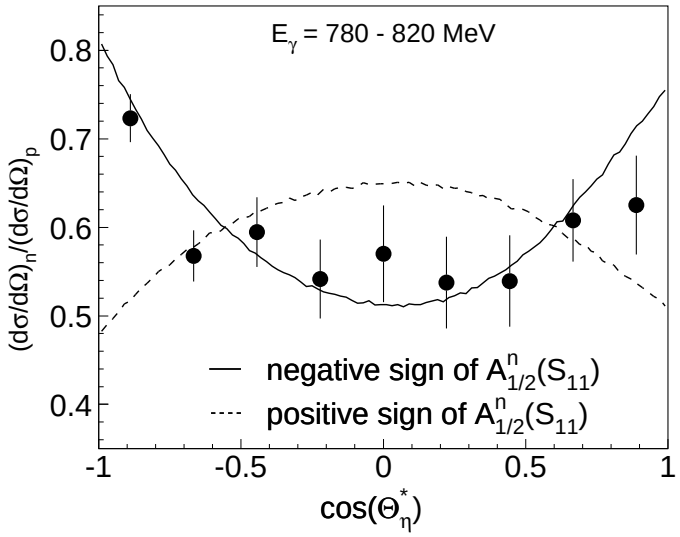

Figure 54: Ratio of the differential neutron/proton cross sections in the range of the $S_{11}(1535)$ compared to predictions (eq. (68)) with negative and positive relative sign of the S_{11} couplings [267].

section, which is better described with $A^{IS}_{1/2}/A^p_{1/2}$ ≈0.25. Recently, Ritz and Arenhövel [273, 274] have argued that there is an unexpected large complex phase between $A^p_{1/2}$ and $A^n_{1/2}$ due to re-scattering contributions. In their model they find:

$$\begin{aligned} A^p_{1/2} &= (+120.9 - \mathrm{i}\,66.1) \times 10^{-3}\mathrm{GeV}^{-1/2} \\ A^n_{1/2} &= (-114.0 - \mathrm{i}\,1.7) \times 10^{-3}\mathrm{GeV}^{-1/2} \end{aligned} \tag{69}$$

which allows to reproduce the coherent cross section (see fig. 55) and the ratio of the couplings determined from the breakup reactions ($|A^n_{1/2}|^2/|A^p_{1/2}|^2$=0.68). However, the magnitude of the coupling $A^p_{1/2}$ ($138\times10^{-3}\mathrm{GeV}^{-1/2}$) is quite large compared to other results.

A further check of the isospin structure can be obtained from coherent η photoproduction off He-isotopes which have different quantum numbers. The photoexcitation of the S_{11} resonance involves the E_{0+} spin-flip amplitude. According to the above discussion, the excitation is dominantly isovector. Consequently, the coherent reaction should be almost forbidden for the $I = J = 0$ ^{4}He nucleus but comparatively large for the $I = J = 1/2$ ^{3}He nucleus. In agreement with this expectation, an investigation of $^4\mathrm{He}(\gamma,\eta)^4\mathrm{He}$ did not find a signal but only upper limits for the reaction [264]. Meanwhile, total cross sections up to 250 nb at photon energies between 650 - 720 MeV were found for ^{3}He [268].

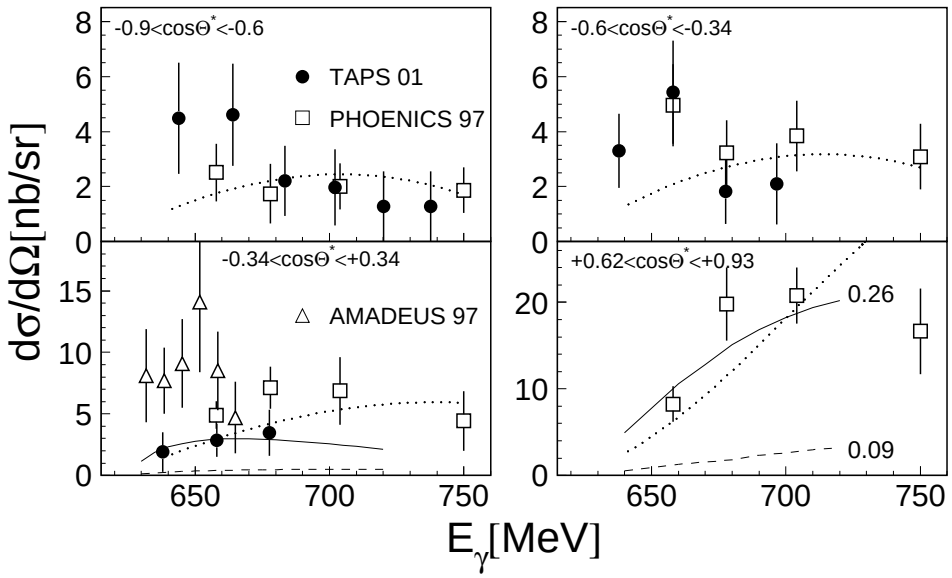

Figure 55: Coherent η photoproduction off the deuteron. The data are from TAPS [265] (full circles), PHOENICS [263] (open squares), and AMADEUS [263] (open triangles). Calculations by Fix and Arenhövel [269] for various values of $|A^s_{1/2}|/|A^p_{1/2}|$ (solid: 0.26, dashed: 0.09), and Ritz and Arenhövel [274] (dotted) are compared to the data.

4.3 *Double Pion-Photoproduction*

The production of pion pairs is important for the study of the second resonance region of the nucleon. We have already discussed (see fig. 29) that almost 50% of the total photoabsorption cross section at incident photon energies of ≈800 MeV can be attributed to double pion production. This is responsible for the bump structure in the total cross section of figs. 29,56. The much discussed suppression of the peak for photoproduction on nuclei will not be understood without a thorough investigation of double pion production. Furthermore, double pion production gives access to interesting decay properties of the resonances. Three different resonance decay processes can contribute in the double pion channel

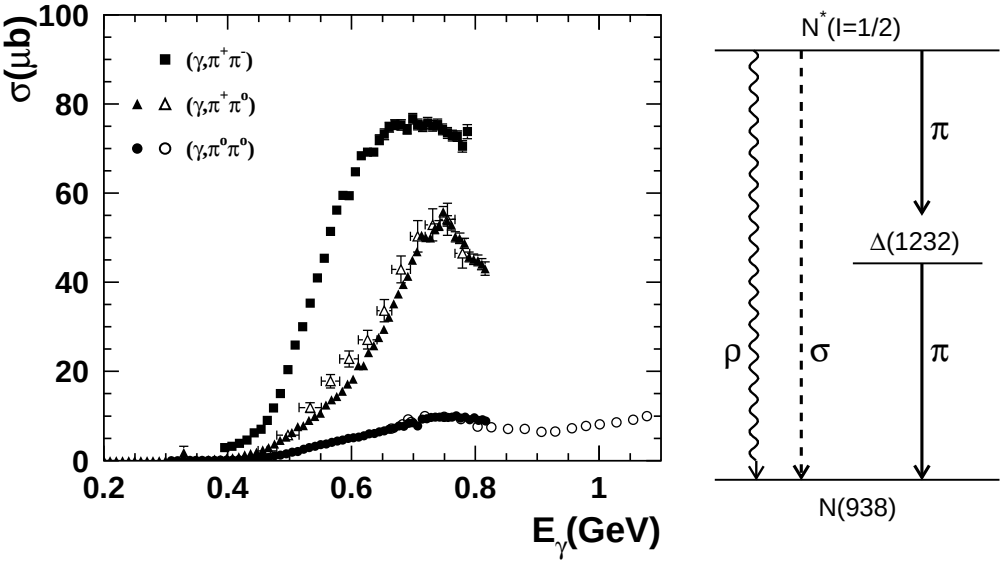

Figure 56: Left hand side: Total cross section of the three isospin channels of double pion production on the proton. Data are from [281, 287, 173, 289]. Right hand side: possible resonance contributions to double pion production in the second resonance region.

(see fig. 56, right hand side): the decays via emission of the ρ and σ mesons to the nucleon ground state with subsequent decays of the mesons into pion pairs and the cascade decay of the resonances via the intermediate Δ resonance. The sequential decays allow the study of resonance - resonance transitions. The decay via the ρ meson is suppressed since its nominal mass (m_ρ) ≈771 MeV corresponds to a kinematical production threshold on the free nucleon of 1086 MeV, well above the second resonance region. However, the large width of ≈150 MeV allows contributions from its low energy tail. The existence of the scalar-isoscalar σ meson is still under dispute (PDG: $f_0(600)$ with m = 400 - 1200 MeV, Γ = 600 - 1000 MeV). In the present context, it is not important whether we call such a broad state a meson or understand it as a correlated pion pair in the scalar-isoscalar state. What we have discussed so far corresponds to resonance decays to the nucleon ground state. In analogy to nuclear physics, we expect valuable structure information from transitions between higher lying states. In addition, like in single meson production, non-resonant background contributions complicate the picture and require detailed reaction models for the extraction of the resonance contributions.

Until very recently, data for double pion production reactions came mostly from bubble chamber experiments. Therefore, $\gamma p \to p\pi^+\pi^-$ had been the only isospin channel measured with reasonable precision. Total cross sections and invariant mass distributions of the $\pi^+\pi^-$-, $p\pi^+$-, and $p\pi^-$-pairs are available in the literature [275]-[280]. New interest arose during the last few years when the isospin channels with neutral particles became accessible. In a series of experiments with the DAPHNE [207] and TAPS [175, 176] detectors at the Mainz accelerator all isospin channels [281]-[287] except $\gamma n \to n\pi^+\pi^-$ were measured up to the second resonance region. The two detectors are complementary in the sense that DAPHNE has advantages for reactions with many charged particles in the final state while TAPS is optimized for the 2γ decay of neutral pions. At higher incident photon energies the $2\pi^o$ final state became available at GRAAL in Grenoble [289] and the $\pi^+\pi^-$ final state at SAPHIR in Bonn [288].

The $\gamma p \to p\pi^+\pi^-$ reaction was analyzed in an early attempt to extract the dominant production mechanisms by Lüke and Söding [290]. The total cross section is small between threshold at ≈310 MeV and ≈400 MeV. It then rises from ≈400 MeV to a maximum at ≈650 MeV (see fig. 57). This rise reflects the $\gamma p \to \pi\Delta$ threshold smeared by the width of the Δ-resonance. It is accompanied by a strong peak at the mass of the Δ in the invariant mass distribution of the $p\pi^+$-pair which is absent in the $p\pi^-$-invariant mass. An important contribution is assigned to the $\gamma p \to \Delta^{++}\pi^-$ channel while the $\gamma p \to \Delta^o\pi^+$ channel is negligible. The $\Delta\pi$ intermediate state could be populated by the decay of a resonance. However, a more detailed analysis [290] showed that the reaction is dominated by the Δ-Kroll-Ruderman term and the pion pole term (see fig. 57, diagrams upper right corner).

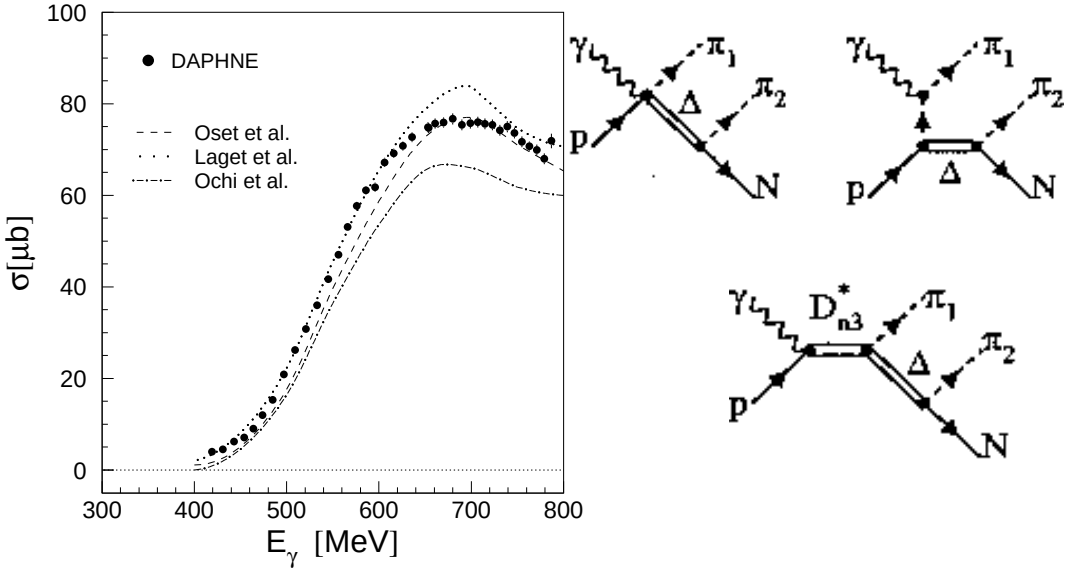

Figure 57: Left hand side: Total cross section for the reaction $\gamma p \to p\pi^+\pi^-$. Data are from [281]. Dashed, dotted, and dash-dotted curves: calculations from [291]-[293]. Right hand side: important contributions to the reaction (many more diagrams give small contributions, see e.g. [291]).

More recent analyses of this reaction [291]-[293], taking into account the new precise data from the DAPHNE-detector [281], have solidified this picture. Although the level of agreement between predictions and data is somewhat different (see fig. 57), all models find the reaction dominated by the Δ-Kroll-Ruderman term. However, even though the direct contribution from higher resonances is negligible, it was pointed out by Oset and coworkers [291] that the peak-like structure between 600 and 800 MeV is due to an interference of the Δ-Kroll-Ruderman term with the sequential decay of the $D_{13}(1520)$-resonance via $\gamma p \to D_{13} \to \Delta\pi$ (diagram lower right corner in fig. 57). This allows the extraction of the coupling constant of the D_{13}-decay into $\Delta\pi$ [294]. At higher photon energies (up to 2 GeV) total cross sections and invariant mass distributions were obtained with the SAPHIR-detector at ELSA [288]. The invariant mass distributions show clear signals for $\Delta \to N\pi$ and $\rho \to \pi^+\pi^-$ contributions.

The final state with two neutral pions is particularly well suited for the study of resonance decays. Most background terms are excluded since the photon does not couple to the neutral pion and the ρ-meson does not decay into a pair of neutral pions. Surprisingly, the two models from refs. [291, 292] made very different predictions. One of them [291] predicted that the sequential decay of the $D_{13}(1520)$ resonance via $D_{13} \to \pi\Delta \to \pi\pi N$, the other [292], that the decay of the $P_{11}(1440)$ resonance via a correlated pair of pions in a relative s-wave ($P_{11} \to \sigma N$) is the dominant process (see diagrams in fig. 58, right hand side). The total cross section was measured in several experiments with the DAPHNE [281] and TAPS [282, 285, 173] detectors in Mainz and at higher incident photon energies at GRAAL [289]. The total cross section agrees better [281, 89] with the result from the Oset model [291] in spite of a systematic discrepancy between the DAPHNE and TAPS data. The question was finally solved by the invariant mass distributions measured with TAPS (see fig. 60). While the $\pi^o\pi^o$-mass distribution is explained by phase space, the $p\pi^o$-distribution shows a peak at the mass of the $\Delta(1232)$. This favors the sequential D_{13} decay over the correlated P_{11} decay which predicted a strong shift of the $\pi^o\pi^o$ invariant

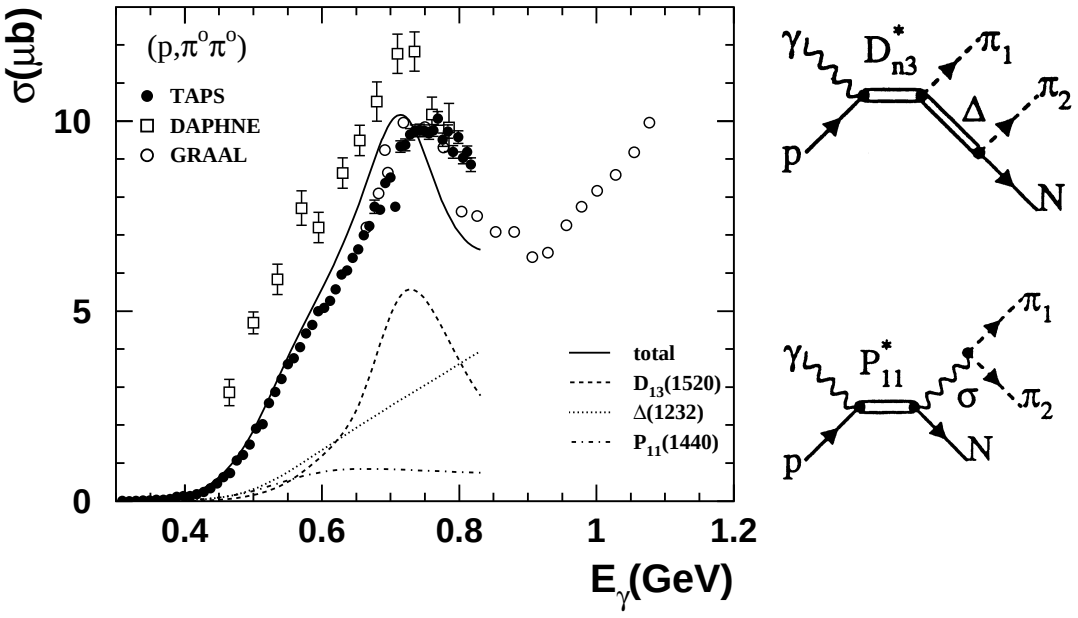

Figure 58: Total cross section for $\gamma p \to p\pi^o\pi^o$. Data are from references [281, 173, 289]. Curves are from the Oset model [291]. Right hand side: dominant reaction mechanisms predicted by different models (see text).

mass towards small values. The contribution of the partial channels to the total cross section in the Oset model is shown in fig. 58. The resonance-like contribution from the sequential decay of the D_{13} is dominant.

It came as a surprise when the first measurement of the $\gamma p \to n\pi^+\pi^o$ reaction [281] produced a total cross section that was strongly underestimated by all model predictions. Typical results from the models [291, 292] predicted a behavior of the total cross section corresponding to the dashed curve in fig. 59. A measurement of the reaction [287] with the TAPS detector confirmed the experimental result. The same problem was found for the $\gamma n \to p\pi^-\pi^o$ reaction which was measured in quasifree kinematics from a deuteron target [283] (see fig. 62). An important piece was obviously missing in the models which predicted that the dominant contribution comes from the Δ-Kroll-Rudermann term and the pion pole term, as is the case in the double charged channel.

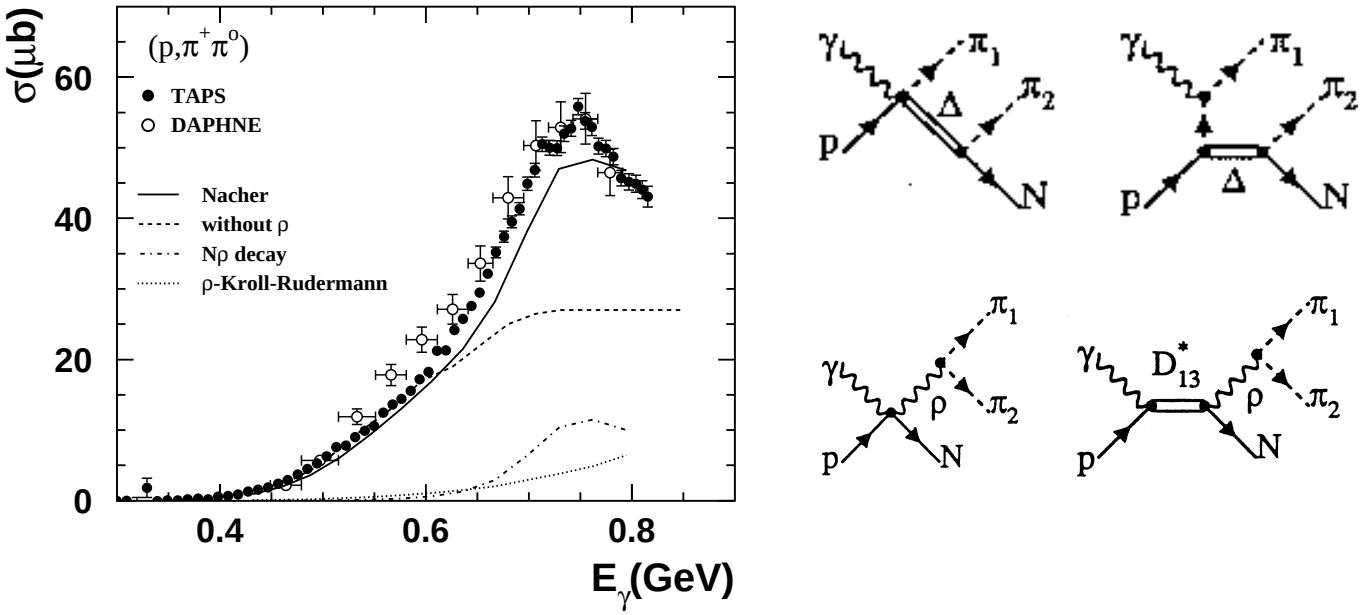

Figure 59: Left: Total cross section of $\gamma p \to n\pi^o\pi^+$. Data from: [281, 287]. Curves from: [295]. Right: upper part: leading diagrams, lower part: contribution of the ρ-meson.

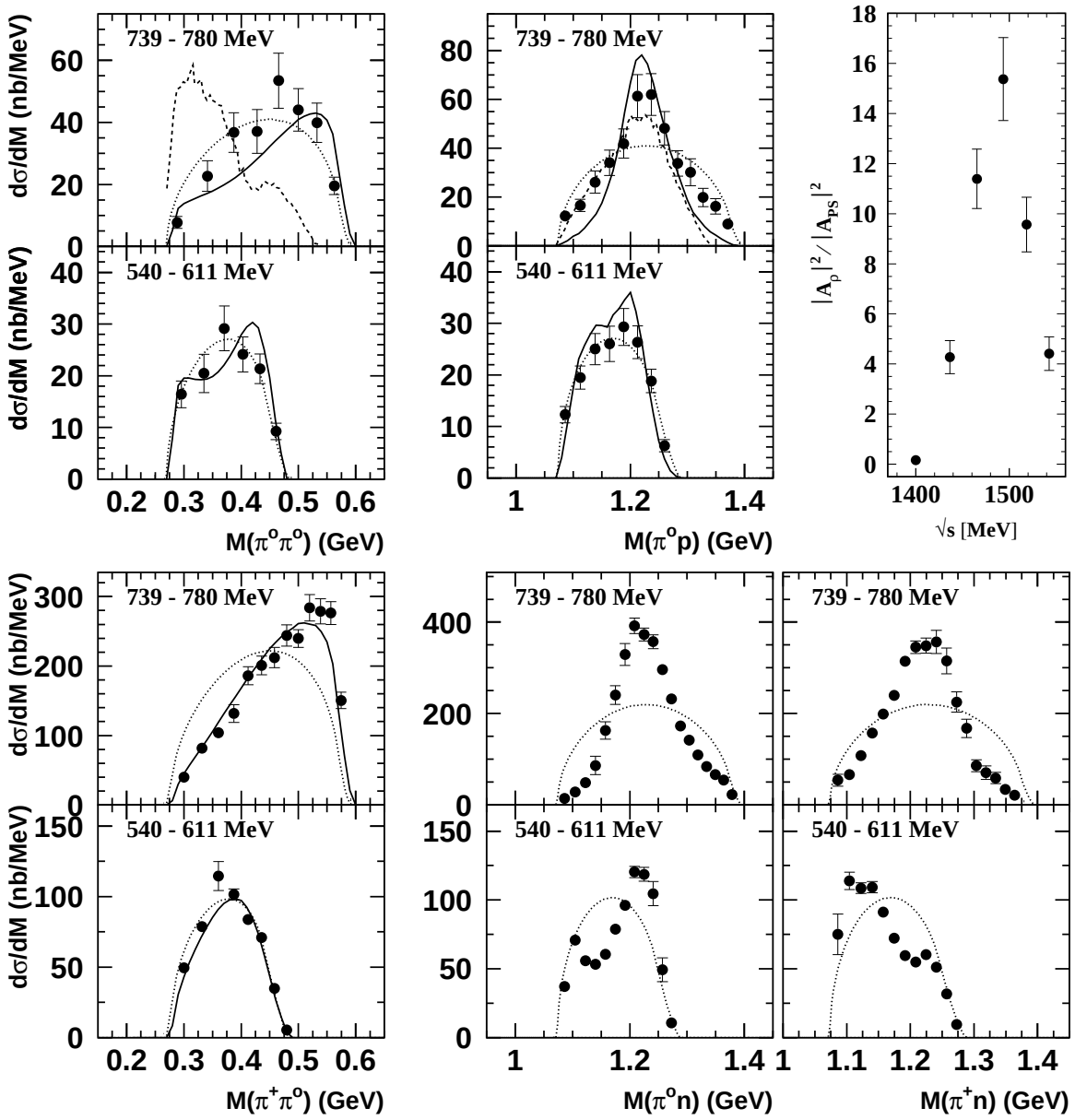

Figure 60: Invariant mass distributions for the reactions $\gamma p \to p\pi^o\pi^o$ and $\gamma p \to n\pi^+\pi^o$. Upper part (left and middle): double π^o production, data from [115]. Dotted curves: phase space, dashed: model with dominant $P_{11} \to N\sigma$ contribution [292], solid: model with dominant $D_{11} \to \Delta\pi$ decay [291]. Lower part: $n\pi^+\pi^o$ final state, data from [287]. Dotted curves: phase space, full: model including ρ mesons [295]. Upper right corner: fitted amplitude ratio for ρ production and phase space for $n\pi^+\pi^o$ [287].

Ochi et al. [293] suggested a strong contribution of off-shell ρ-meson decays even at low incident photon energies. This proposal was attractive since ρ-mesons would mainly contribute to the $\pi^+\pi^o$ and $\pi^-\pi^o$ channels. The $\rho^o \to \pi^o\pi^o$ decay is forbidden, and the contribution to $\pi^+\pi^-$ is suppressed since the neutral ρ is not produced via the Kroll-Rudermann term. Indeed, the model predicted a substantially larger cross section for the mixed charge channels. In other aspects it used more simplifications than other models and described the other charge states less well. However, this suggestion motivated a careful study of the invariant mass distributions of the pion - pion and pion - nucleon pairs from this reactions. Zabrodin et al. [284] measured the distributions from the $\gamma n \to p\pi^-\pi^o$ reaction and found a deviation of the pion - pion invariant mass from phase space, showing an enhancement at large invariant masses. The analysis was complicated by effects of the bound neutron. Subsequently, invariant mass distributions of the $\gamma p \to n\pi^+\pi^o$ reaction were obtained by Langgärtner et al. [287]. Typical examples

are compared in fig. 60 to the double π^o channel. The comparison is particularly instructive since the double π^o channel does not have a contribution from the ρ.

The $\pi^o n$ invariant mass peaks already at low incident photon energies at the Δ mass. This signal does not appear in the $\pi^+ n$ invariant mass at low photon energies. This behavior is expected if, as predicted in the models, the process is dominated at low photon energies by the Δ-KR- and Δ-pion-pole terms. Since the photon does not couple to the neutral pion, the charged pion is produced at the first vertex and the neutral pion stems from the subsequent $\Delta^o \to N\pi^o$ decay, giving rise to the $\pi^o n$ invariant mass correlation. At higher incident photon energies, sequential decays of $N^\star$ resonances may contribute. It can be seen from the relevant Clebsch-Gordan coefficients that for the $D_{13} \to \Delta\pi \to N\pi\pi$ reaction both sequences of the charged and neutral pion are equally probable, so that the Δ-signal may also appear in the $\pi^+ n$ invariant mass. The double π^o channel has the Δ signal only at higher incident photon energies from the sequential D_{13} decay, since the KR-term is forbidden.

The $\pi^o\pi^o$ invariant mass is similar to phase space behavior, but at the higher incident photon energies the $\pi^o\pi^+$ invariant mass is clearly shifted to large masses as expected for a contribution of the ρ^+ meson. The $\pi^o\pi^+$-data were fitted with a simple model assuming only phase space and ρ-decay contributions [287] via:

$$\frac{d\sigma}{dm} \propto |a(\sqrt{s}) + b(\sqrt{s}) p_\pi(m_{\pi\pi}) D_\rho(m_{\pi\pi})|^2 ps_{\sqrt{s}\to\pi\pi N} \tag{70}$$

where p_π is the momentum of the π in the ρ rest frame, $ps_{\sqrt{s}\to\pi\pi N}$ is the three body phase space factor, and D_ρ represents the ρ-meson propagator.

The constants a and b were fitted to the data. The ratio of the matrix elements for ρ-meson decays and phase space components was calculated via:

$$\frac{|A_\rho|^2}{|A_{ps}|^2} = \frac{\int |b(\sqrt{s}) p_\pi(m_{\pi\pi}) D_\rho(m_{\pi\pi})|^2 dm_{\pi\pi}}{\int |a(\sqrt{s})|^2 dm_{\pi\pi}} \,. \tag{71}$$

The result of the ratio of the matrix elements is shown in fig. 60 (upper right corner). This is the ratio of the matrix elements without phase space factors. The relative contribution of the ρ-decay matrix element peaks near the position of the D_{13} resonance hinting at a significant $D_{13} \to N\rho$ contribution to $\pi^o\pi^+$-photoproduction. Such a contribution would be interesting in view of the unexplained suppression of the second resonance bump in the total photoabsorption on nuclei. Since in this region the D_{13} resonance has the largest coupling to the initial photon - nucleon state, it has been argued that an in-medium broadening of this resonance is a likely cause for the observations. The broadening could arise from a coupling of the resonance to the $N\rho$ final state since it is predicted [296] that the ρ-meson itself is broadened appreciably in the nuclear medium. The extraction of a possible $D_{13} \to N\rho$ contribution requires a detailed model for the reaction $\gamma p \to n\pi^o\pi^+$ taking into account interference effects between all contributions. In view of the new experimental results, the Oset group has updated the model [295], now including ρ contributions correctly. The new calculation is compared to the total cross section and the invariant mass distributions demonstrating that the inclusion of the ρ is essential.

The invariant mass distributions have clarified the relative importance of the different reaction mechanisms involving resonance decays (sequential decay with an intermediate $\Delta\pi$ state, emission of ρ meson). However, they cannot assign these reactions to a specific resonance. For example, the large importance of the D_{13} and the negligible contribution of the S_{11} in the models results from the photon couplings and decay widths which are input parameters to the calculations. However, recently the GDH collaboration has measured the helicity dependence of the cross section for the $n\pi^o\pi^+$ final state [155]. The result (see fig. 61) shows that most of the resonance structure occurs in the helicity ν=3/2 channel. The ν=1/2 channel, where a contribution from the S_{11} would show up, has a flatter energy dependence and contributes less than 30% to the total cross section. The model predictions of Nacher et al. [297]

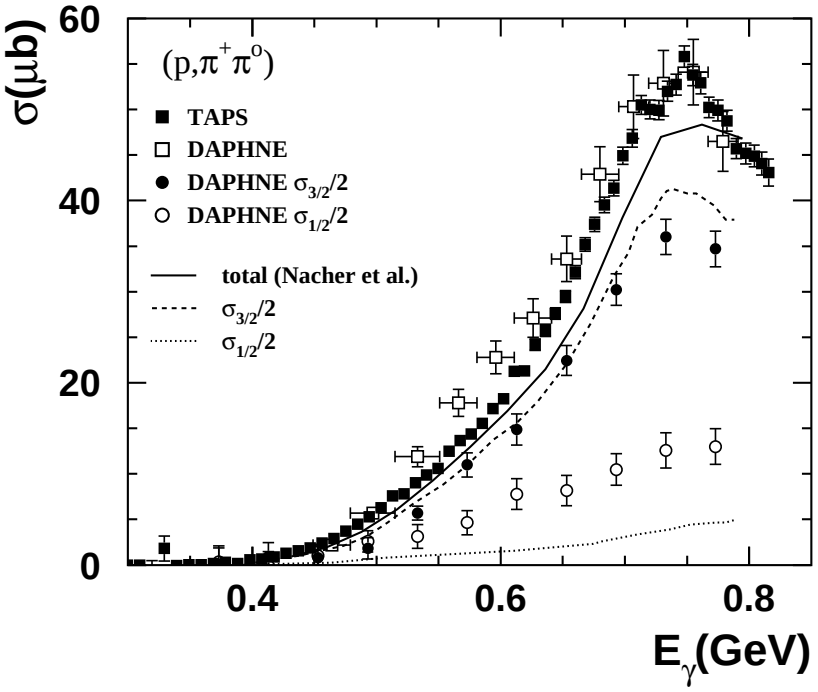

Figure 61: Helicity dependence of the $\gamma p \to n\pi^o\pi^+$ reaction. Shown are the total cross section and the $\sigma_{3/2}$ and $\sigma_{1/2}$ partial cross sections. Data from are from [283, 287, 155]. Curves (model predictions) are from Nacher et al. [295, 297].

agree qualitatively with the distribution of the strength on helicity 3/2 and 1/2 while underestimating the ν=1/2 contribution.

The isospin channels involving neutron targets have been studied in quasifree kinematics on the deuteron (see fig. 62) [282]-[286]. A comparison of the yields for the $p\pi^+\pi^-$ final state from the free proton and quasifree proton bound in the deuteron [283] demonstrates that nuclear effects are negligible except for Fermi smearing. The total cross sections for the $p(\gamma,\pi^+\pi^o)n$ [281, 287] and $n(\gamma,\pi^-\pi^o)p$ reactions are almost equal, and the cross section of $d(\gamma,\pi^0\pi^o)np$ is almost twice as large as for $p(\gamma,\pi^o\pi^o)p$. For double π^o production, the cross sections for protons and neutrons must be similar. Altogether, a large isospin dependence is not found which is important for the interpretation of the nuclear data.

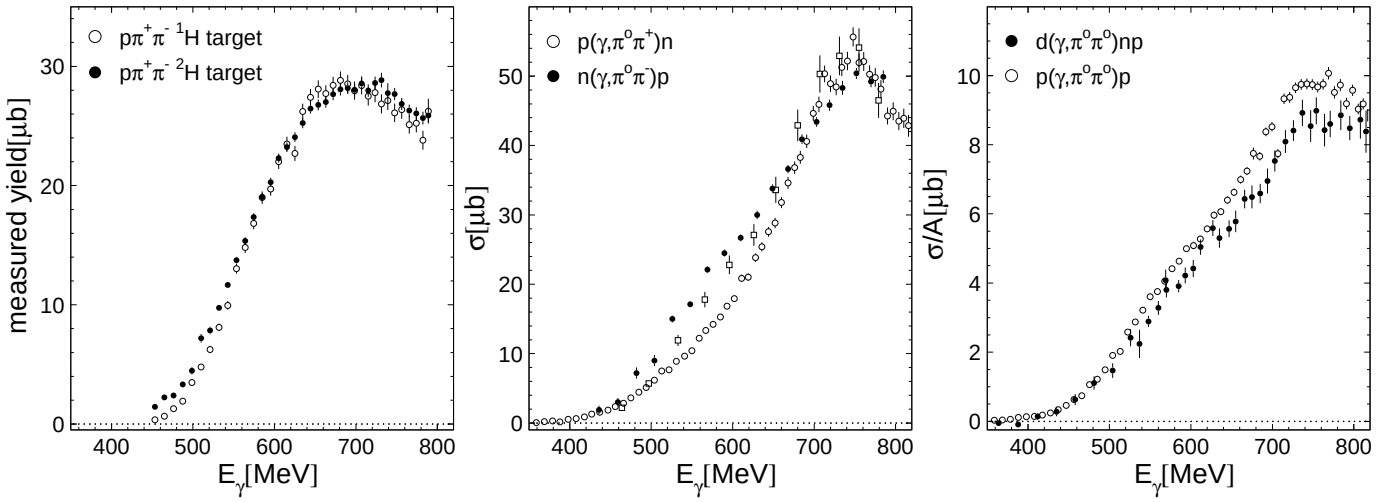

Figure 62: Double pion production from the neutron. Left: comparison of $p\pi^+\pi^-$ from proton and deuteron target (only the yield within the acceptance of the DAPHNE detector) [283]. Middle: comparison of $n\pi^o\pi^+$ [281, 287] with $p\pi^o\pi^-$ [283]. Right: comparison of $2\pi^o$ from the proton and deuteron.

5 Conclusion and Perspectives

The use of meson photoproduction reactions for the investigation of baryon resonances aims at a better understanding of non-perturbative QCD and has developed rapidly over the last decade. In this review, we have concentrated on the lowest-lying states of the nucleon which have been studied in much detail. The experimental precision that has been achieved recently has been possible due to the impressive progress in accelerator and detector technology. Among these are the measurement of the $E2$ admixture in the excitation of the Δ resonance and the investigation of the magnetic moment of the Δ. The detailed investigation of η photoproduction resulted not only in precise coupling constants for the $S_{11}(1535)$ resonance but also allowed to extract a decay branching ratio of the $D_{13}(1520)$ as small as 0.06%. Finally, the understanding of the reaction mechanisms for double pion production saw significant progress due to precise measurements of the different isospin channels.

What can we expect next? The next generation of experiments concentrating on the low-lying resonances will see a further advance in sensitivity. The advance will mainly be due to the use of 4π detection systems like the combinations of the TAPS detector with the Crystal Barrel in Bonn or with the Crystal Ball in Mainz. The combination of 4π detectors with linearly and circularly polarized photon beams as well as polarized targets will provide access to a wealth of new observables comprising a powerful tool for the extraction of specific resonance properties. The measurement of the magnetic moment of the Δ and also of the $S_{11}(1535)$ will certainly profit. Up to now, model independent multipole analyses have only been possible for pion photoproduction. Within the foreseeable future, η photoproduction should reach the same stage as more and more polarization observables are determined.

We have only briefly touched upon the problem of 'missing' resonances. The search for the many predicted but yet unobserved nucleon states will gain increasing importance as the modern facilities can operate in the necessary energy range. As schematically shown in fig. 63, the region of interest

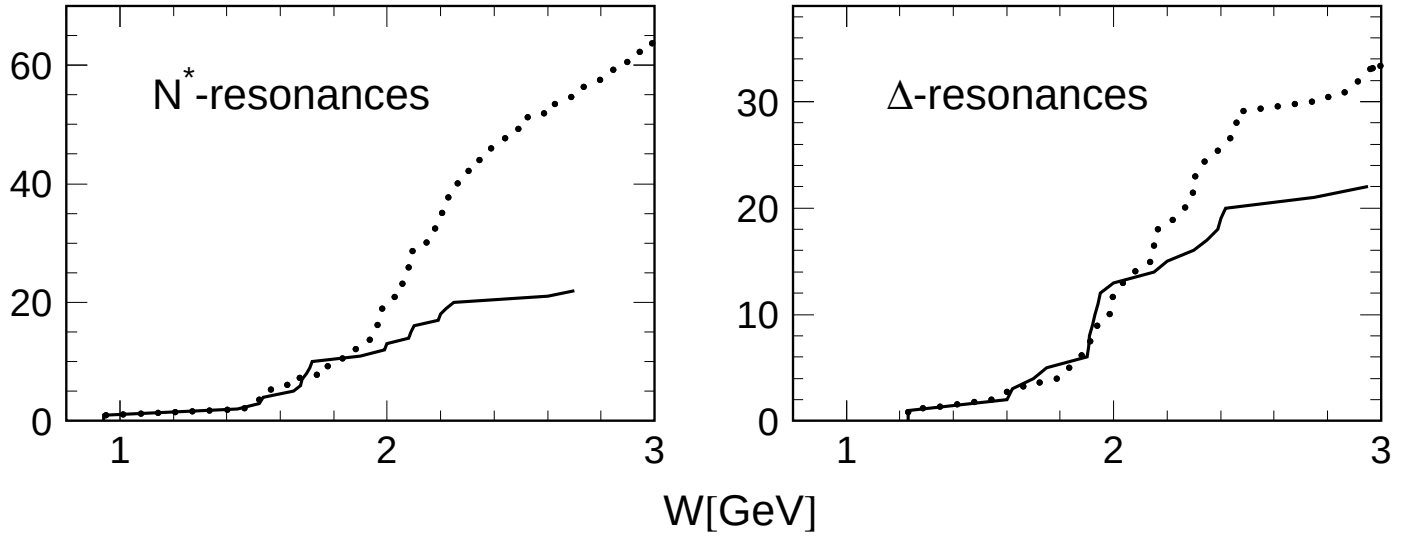

Figure 63: Comparison of predicted [28] and observed [36] numbers of nucleon resonances.

starts at resonance masses of 2 GeV corresponding to photon energies of roughly 1.7 GeV which are available at CLAS and at ELSA. It is in this energy regime that the discrepancy between the number of observed states and the number of predicted states sets in. What is the best strategy to identify new states? We have discussed in detail that the extraction of resonance contributions is problematic even in the second resonance region. The problems at higher energies are expected to be yet more severe in spite of the availability of high precision experiments. The development of reaction models, allowing the well-defined extraction of resonance contributions, will prove to be a challenge. However, it seems neither necessary nor feasible to provide a 'complete' experimental level scheme of the nucleon. It would

already add to the success of the quark model if some of those resonances could be identified which are predicted to have large decay branching ratios into channels other than $N\pi$.

One strategy is to concentrate on the threshold regions of heavier mesons. Close to threshold, only few partial waves contribute, reducing the necessary complexity of the models. There has already been an attempt to exploit the η' threshold region [298]. The cross section for $\gamma p \to p\eta'$ rises rapidly from threshold at E_γ=1.45 GeV to a maximum at ≈1.8 GeV (see fig. 64, left hand side). This might indicate a situation similar to η photoproduction at threshold. However, the angular distributions close to

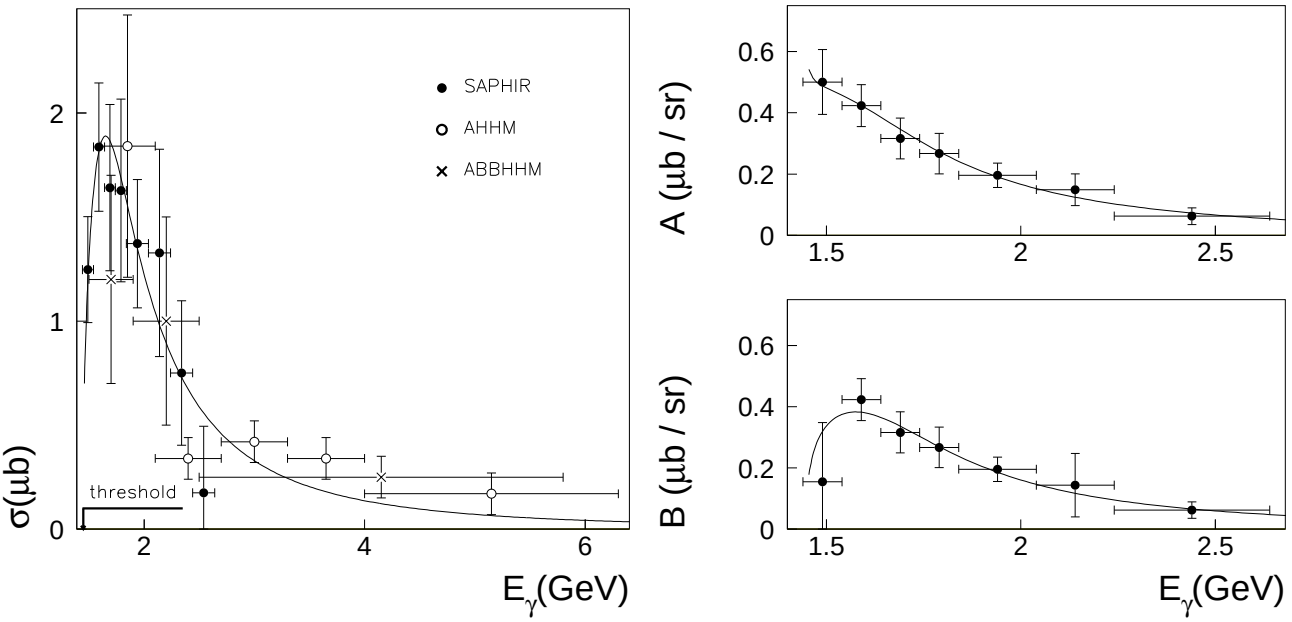

Figure 64: The reaction $p(\gamma, \eta')p$ at threshold [298]. Left hand side: total cross section. Data are from SAPHIR [298] (filled circles) and older data from [275, 302]. The curve is a fit to the data. Right hand side: fitted coefficients a, b of the angular distributions. Curves are fits with Breit-Wigner resonances.

threshold are not isotropic but show a strong forward - backward asymmetry. This is shown at the right hand side of fig. 64 where the coefficients a, b of fits of the angular distribution with the ansatz eq. (51) are plotted versus the incident photon energy (the coefficient c is consistent with zero within the statistical accuracy). In contrast to η-photoproduction, the $b \times \cos(\Theta)$-term is comparable to the constant term a. The simplest interpretation given in [298] in terms of resonance contributions is an interference between an S_{11} and a P_{11} resonance. A fit of the data with Breit-Wigner parameterizations of the two resonances is shown in the figure. Parameters of these resonances are quoted in [298]. However, the data have limited statistical accuracy and the systematic uncertainty, in particular of the absolute normalization, is substantial (other analyses of the SAPHIR data gave a peak cross section around $0.5\mu b$ [299]). More precise measurements of the angular distributions and of polarization observables will be soon available.

Similar studies are underway for the ω and the Φ meson. In the first case, evidence for a strong contribution of the $P_{11}(1720)$ resonance was found [300], while in the second case resonance contributions could not be identified [301].

Also, there are recent advances in photoproduction of non-strange nucleon resonances in reactions with open strangeness. The final states $K\Lambda$ and $K\Sigma$ have been studied at SAPHIR in Bonn [303, 306, 307]. Further results are expected from CLAS at JLab, from LEPS at SPring8, and from the Crystal Barrel and TAPS at ELSA. Due to isospin selection, $K\Lambda$ can only couple to $I = 1/2$ $N^\star$ resonances while $N^\star$ and Δ resonances can decay into $K\Sigma$. In the quark model, such decays have been investigated by Capstick and Roberts [309]. They predict that both channels have at least the potential to confirm weakly established resonances around excitation energies of 2 GeV. The data from SAPHIR

are compared in fig. 65 to calculations by Bennhold and Mart [305, 308] in the framework of an isobar model. In both cases, the reactions are dominated by resonance contributions. The total cross section for the $K\Lambda$ channel exhibits a structure around resonance masses of 1.9 GeV, which was not obvious in older data with inferior statistical quality. This structure is not reproduced by the model when only well established nucleon resonances are included (dashed line in fig. 65, left hand side). Much better agreement is achieved when a further D_{13} resonance is included (solid line). A D_{13} resonance with the necessary properties (relative strong coupling to the $K\Lambda$ channel and to the photon) is predicted by the quark model [309] at an excitation energy of 1960 MeV. Furthermore, there is circumstantial experimental evidence for such a state from pion induced $K\Lambda$ production [310, 311]. Nevertheless, more data, in particular polarization observables, will be necessary to establish the contribution of this state.

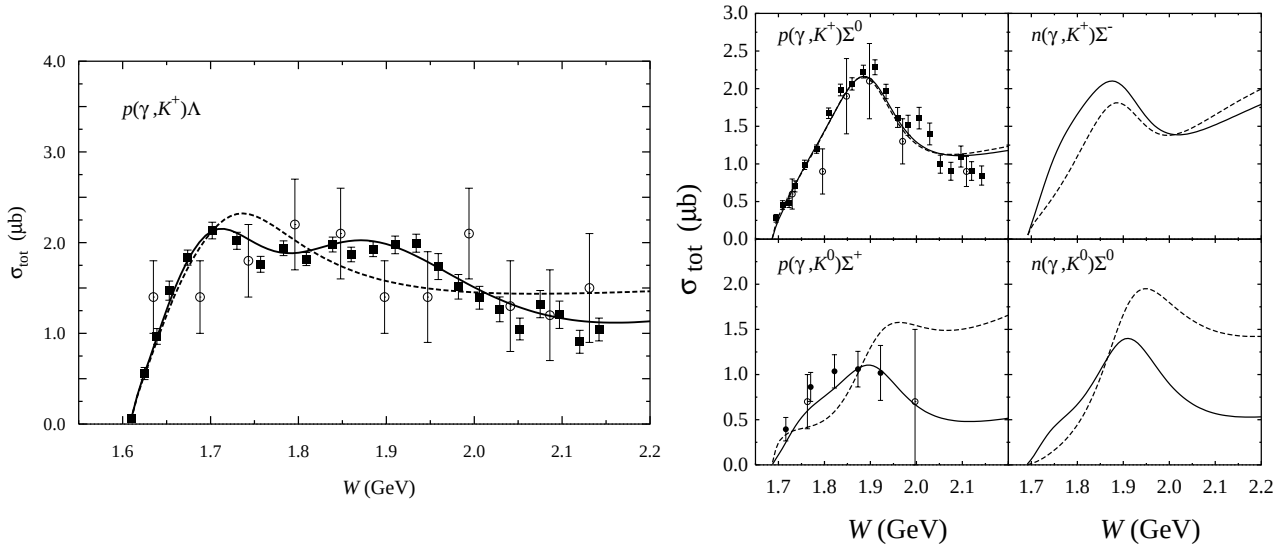

Figure 65: Final states with open strangeness [305, 308]. Left hand side: Total cross section for $p(\gamma, K^+)\Lambda$. Data: SAPHIR [303] (solid squares), ABBHHM collaboration [304] (open squares). Model fits: Mart et al.[305], full and dashed lines: with and without $D_{13}(1960)$ resonance. Right hand side: Total cross section for $K\Sigma$ photoproduction. Data: SAPHIR [303, 306] (solid symbols), ABBHHM [304] (open symbols). Model fits: Mart [308], full and dashed lines: with and without $P_{13}(1720)$ resonance.

In case of the $K\Sigma$ channel, cross section data with reasonable statistical quality is presently only available for the $K^+\Sigma^o$ final state (see fig. 65, right hand side). An interpretation in terms of resonance contributions with only one of the four possible isospin channels is certainly ambiguous. As an example fig. 65 shows two model fits of the reaction [308] which do include (solid lines), or do not include (dashed lines) a contribution of the $P_{13}(1720)$ four-star resonance. The fit quality for the $K^+\Sigma^o$ final state is almost the same while large differences are predicted for the other channels. The available data for the $K^o\Sigma^+$ channel seem to favor a coupling of this resonance to the $K\Sigma$ channel, but are not yet sufficiently precise to warrant a final conclusion. An investigation of the threshold behavior of this channel could shed new light on the structure of the low-lying S_{11} resonances. We have discussed the peculiar decay pattern of the $S_{11}(1535)$ as compared to the $S_{11}(1650)$ in the context of η-photoproduction. Kaiser et al. [210, 211] suggested a $K\Sigma$ quasibound state as possible explanation for the properties of the $S_{11}(1535)$. Li and Workman [235] have argued that such a configuration must be strongly mixed with a three-quark state in order to explain properties like the Q^2 dependence of the helicity amplitude. If this mixing occurs, a third S_{11} resonance should exist close to the other two. Due to its structure it should couple strongly to the $K\Sigma$ channel. The final states with neutral kaons would be most sensitive to a resonant s-wave behavior at threshold since, as discussed for pion photoproduction, the leading Born terms are suppressed. Attempts to study these reactions are under way at ELSA and SPring8.

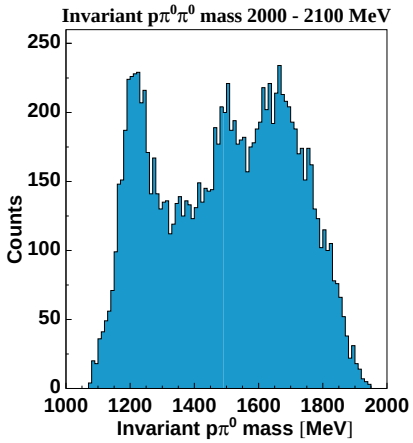

Figure 66: Invariant mass distribution of the $p\pi^o$ pairs observed in double π^o production from initial states in the range $\sqrt{s} \approx 2000$ -2100 MeV [313].

As a further outlook, we present recent data for the decay of higher lying resonances via intermediate states resulting in multiple meson reactions. We have discussed such a case for the double π^o decay of the $D_{13}(1520)$ resonance. Preliminary data from the CB-ELSA collaboration [313] extend the double π^o data to much higher energies. Figure 66 shows the invariant mass spectrum for the proton - π^o pairs at incident photon energies corresponding to excited nucleon states from 2.0 - 2.1 GeV. The Δ peak is clearly visible, and there is a peak corresponding to the second resonance region at $\sqrt{s} \approx 1.5$ GeV. Again, background terms are suppressed for neutral pions. This could be the first evidence for cascade decays of higher lying resonances via Δ and possibly $D_{13}(1520)$ intermediate states.

Furthermore, first results are available for the $\gamma p \to \pi^o \eta$ reaction. Invariant mass distributions of the $p\pi^o$ and $\pi^o\eta$ pairs for two ranges of incident photon energies are summarized in fig. 67. At the low incident energies, only the Δ peak is seen in $m_{p\pi^o}$ and $m_{\eta\pi^o}$ shows a distribution similar to phase space. But at higher energies $m_{p\pi^o}$

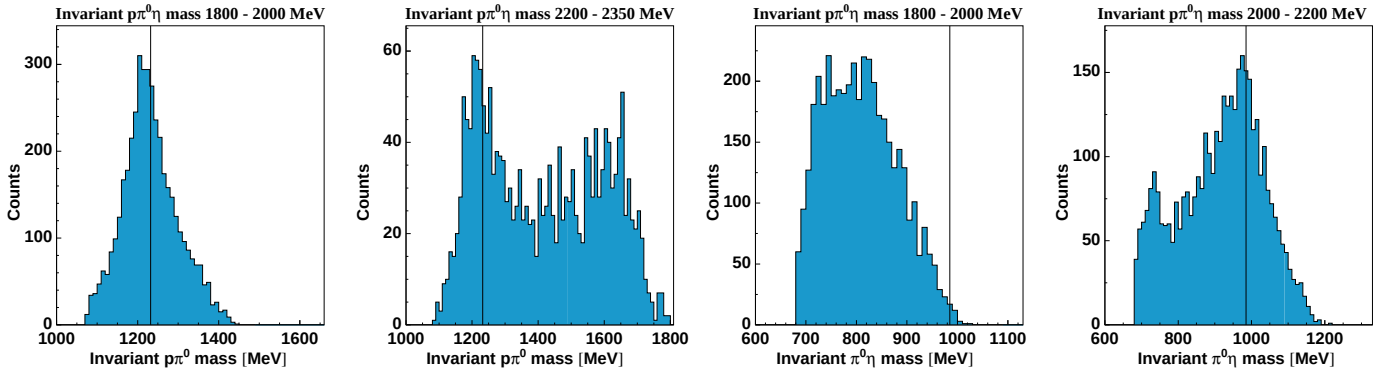

Figure 67: Invariant mass distributions of the $p\pi^o$ and $\eta\pi^o$ pairs observed in the reaction $\gamma p \to p\eta\pi^o$ for two different ranges of initial states [313].

develops a peak in the second resonance region and $m_{\eta\pi^o}$ shows a clear signal from the $a_o(980)$ meson. The cascade decays involving the $I = 0$ η meson are particularly useful for the study of resonances since the isospin of the initial state is fixed when the isospin of the final state is known ($\Delta \to \eta\Delta \to N\eta\pi^o$ or $N^\star \to \eta N^\star \to N\eta\pi^o$). Predictions for $\Delta \to \Delta\eta$ decays in the quark model are given by Capstick and Roberts [312].

In summary, the progress achieved in the field of meson photoproduction over the last decade has been substantial and contributes significantly to our understanding of hadron structure. But we have also seen that the extraction of resonance properties from the data is more complicated than the analog problem in nuclear physics. In the future this problem will be attacked from two directions: more complete experiments, in particular the measurement of polarization observables, will deliver better constraints for the analyses, and further improvements of the reaction models will decrease the model related uncertainties. Meanwhile, questions concerning the in-medium properties of hadrons, which have been intensely discussed in the context of heavy ion induced reactions, move into focus. Photon induced reactions do not suffer from initial state interactions, so that they can induce reactions throughout the entire nuclear volume (although final state interactions of the produced hadrons must be considered). Several photon facilities are presently developing programs in this field.

Acknowledgments

We thank L. Tiator for the careful reading of part of the manuscript, many inspiring discussions and instructive suggestions. We gratefully acknowledge stimulating discussions with H. Arenhövel and I. Strakovsky. Part of the figures were kindly provided by H.J. Arends, H. Arenhövel, I. Aznauryan, R. Beck, C. Bennhold, J. Ernst, M. Kotulla, T. Mart, V. Muccifora, L. Tiator, I. Strakovsky, and M. Vanderhaeghen.

6 Appendix

6.1 Properties of Light Unflavored Mesons

Table 8: Properties of non-strange light pseudo-scalar and vector mesons [36]. Only the most important decays are listed. E_{thr} is the threshold energy for photoproduction from the proton. In case of the ρ the threshold energy for the nominal mass is given, but due to the large width, production at much lower energies is possible.

	I^G	J^{PC}	**mass** [MeV]	$\mathbf{E}_{thr}$ [MeV]	**width** Γ [MeV]	**life time** (sec)	**decays** (%)	
$\pi^{\pm}$	1^-	0^-	139.57	149.95	2.5×10^{-14}	2.6×10^{-8}	$\mu^{\pm}\nu_{\mu}$	100.0
π^o	1^-	0^{-+}	134.98	144.69	7.8×10^{-6}	8.4×10^{-17}	$\gamma\gamma$	98.8
							γe^+e^-	1.2
η	0^+	0^{-+}	547.30	706.9	1.18×10^{-3}	5.6×10^{-19}	$\gamma\gamma$	38.8
							$\pi^o\pi^o\pi^o$	31.9
							$\pi^+\pi^-\pi^o$	23.6
							$\pi^+\pi^-\gamma$	4.9
η'	0^+	0^{-+}	957.78	1446.7	0.2	3.3×10^{-21}	$\pi^+\pi^-\eta$	43.7
							$\rho^o\gamma$	30.2
							$\pi^o\pi^o\eta$	20.8
ρ	1^+	1^{--}	770.0	(1086.)	150.2	4.4×10^{-24}	$\pi\pi$ (not $\rho^o\to\pi^o\pi^o$)	$\approx$100
ω	0^-	1^{--}	781.94	1108.	8.44	7.8×10^{-23}	$\pi+\pi-\pi^o$	88.8
							$\pi^o\gamma$	8.5
							$\pi^+\pi-$	2.21
ϕ	0^-	1^{--}	1019.413	1573.	4.458	1.5×10^{-22}	K^+K^-	49.1
							$K^o_LK^o_S$	34.1
							$\rho\pi+\pi^+\pi^-\pi^o$	15.5

6.2 Helicity Amplitudes

In the reaction $\gamma N\to Nm_{PS}$, where m_{PS} is any pseudo-scalar meson, the helicities involved can have the values $\lambda_\gamma=\pm1$ for the real photon and $\nu_i=\pm1/2$, $\nu_f=\pm1/2$ for the initial and final state nucleons. Therefore, 8 matrix elements $H_{\nu_f,\mu=\nu_i-\lambda_\gamma}=\langle\nu_f|T|\lambda_\gamma\nu_i\rangle$ are possible. They are reduced by parity conservation to the four independent helicity amplitudes H_1 - H_4:

$$H_1=H_{+1/2,+3/2}=+H_{-1/2,-3/2}\qquad H_2=H_{+1/2,+1/2}=-H_{-1/2,-1/2} \tag{72}$$

$$H_3=H_{-1/2,+3/2}=-H_{+1/2,-3/2}\qquad H_4=H_{+1/2,-1/2}=+H_{-1/2,+1/2}. \tag{73}$$

The relation between CGLN- and helicity amplitudes is given by [51]):

$$
\begin{aligned}
H_1(\Theta,\Phi) &= \frac{-1}{\sqrt{2}} e^{i\Phi} sin(\Theta^\star) cos\left(\frac{\Theta^\star}{2}\right)(F_3+F_4) \\
H_2(\Theta,\Phi) &= \sqrt{2} cos\left(\frac{\Theta^\star}{2}\right)\left[(F_2-F_1)+\frac{1}{2}(1-cos(\Theta^\star))(F_3-F_4)\right] \\
H_3(\Theta,\Phi) &= \frac{1}{\sqrt{2}} e^{2i\Phi} sin(\Theta^\star) sin\left(\frac{\Theta^\star}{2}\right)(F_3-F_4) \\
H_4(\Theta,\Phi) &= \sqrt{2} e^{i\Phi} sin\left(\frac{\Theta^\star}{2}\right)\left[(F_1+F_2)+\frac{1}{2}(1+cos(\Theta^\star))(F_3+F_4)\right]
\end{aligned}
\tag{74}
$$

The expression of the physical observables in terms of the helicity amplitudes is particularly simple [51]:

$$
\begin{aligned}
\frac{d\sigma}{d\Omega} &= \frac{1}{2}\frac{q^\star}{k^\star}(H_1^2+H_2^2+H_3^2+H_4^2) && (75)\\
\Sigma &= \frac{q^\star}{k^\star}\, Re(H_4^\star H_1 - H_3^\star H_2)/\frac{d\sigma}{d\Omega} && (76)\\
R &= -\frac{q^\star}{k^\star}\, Im((H_3^\star H_1 + H_4^\star H_2)/\frac{d\sigma}{d\Omega} && (77)\\
T &= \frac{q^\star}{k^\star}\, Im((H_2^\star H_1 + H_4^\star H_3)/\frac{d\sigma}{d\Omega} && (78)
\end{aligned}
$$

where $q^\star$, $k^\star$ are the cm momenta of meson and photon, and Σ, R and T are photon beam asymmetry, recoil polarization and target asymmetry.
Sometimes 'transversity' amplitudes are used instead of the helicity amplitudes (see e.g. [42]). The only difference is, that in this case the axis of spin quantization is the transverse, rather than the particle's momentum direction. This means that the axis of quantization is chosen perpendicular to the scattering plane. A certain advantage of this representation is that the differential cross section and the single polarization observables can be expressed as linear combinations of the squares of the amplitudes rather than as bilinear functions of the amplitudes.

6.3 Multipole Expansions

The partial wave expansion of the helicity amplitudes is given by [51]:

$$
\begin{aligned}
H_1(\Theta^\star,\Phi) = &\ \tfrac{1}{\sqrt{2}} e^{i\Phi} sin(\Theta^\star) cos(\tfrac{\Theta^\star}{2}) && \sum_{l=0}^{\infty}[B_{l+}-B_{(l+1)-}]P_l''(cos(\Theta^\star)) - P_{l+1}''(cos(\Theta^\star))] \\
H_2(\Theta^\star,\Phi) = &\ \sqrt{2} cos(\tfrac{\Theta^\star}{2}) && \sum_{l=0}^{\infty}[A_{l+}-A_{(l+1)-}]P_l'(cos(\Theta^\star)) - P_{l+1}'(cos(\Theta^\star))] \\
H_3(\Theta^\star,\Phi) = &\ \tfrac{1}{\sqrt{2}} e^{2i\Phi} sin(\Theta^\star) sin(\tfrac{\Theta^\star}{2}) && \sum_{l=0}^{\infty}[B_{l+}-B_{(l+1)-}]P_l''(cos(\Theta^\star)) + P_{l+1}''(cos(\Theta^\star))] \\
H_4(\Theta^\star,\Phi) = &\ \sqrt{2} e^{i\Phi} sin(\tfrac{\Theta^\star}{2}) && \sum_{l=0}^{\infty}[A_{l+}+A_{(l+1)-}]P_l'(cos(\Theta^\star)) + P_{l+1}'(cos(\Theta^\star))]
\end{aligned}
\tag{79}
$$

where the helicity elements $A_{l\pm}$, $B_{l\pm}$ correspond to transitions with nucleon - meson relative orbital angular momentum l, final state total angular momentum $J = l \pm 1/2$ and γN initial state helicity $1/2$ for $A_{l\pm}$ and $3/2$ for $B_{l\pm}$.
Examples for the lowest order multipoles of the CGLN-amplitudes with the relevant quantum numbers and angular distributions are summarized in table 9.

Table 9: Lowest order multipole ampl. for the photoproduction of pseudo-scalar mesons (x=$cos(\Theta^\star)$).

photon M-pole	initial state (L^P_γ, J^P_N)	interm. state $J^P_{N^\star}$	final state (J^P_N, L^P_η)	multi-pole	$(k^\star/q^\star)d\sigma/d\Omega$
E1	$(1^-,\frac{1}{2}^+)$	$\frac{1}{2}^-$	$(\frac{1}{2}^+,0^-)$	E_{o+}	$\|E_{o+}\|^2$
		$\frac{3}{2}^-$	$(\frac{1}{2}^+,2^-)$	E_{2-}	$\frac{1}{2}\|E_{2-}\|^2(5-3x^2)$
M1	$(1^+,\frac{1}{2}^+)$	$\frac{1}{2}^+$	$(\frac{1}{2}^+,1^+)$	M_{1-}	$\|M_{1-}\|^2$
		$\frac{3}{2}^+$	$(\frac{1}{2}^+,1^+)$	M_{1+}	$\frac{1}{2}\|M_{1+}\|^2(5-3x^2)$
E2	$(2^+,\frac{1}{2}^+)$	$\frac{3}{2}^+$	$(\frac{1}{2}^+,1^+)$	E_{1+}	$\frac{9}{2}\|E_{1+}\|^2(1+x^2)$
		$\frac{5}{2}^+$	$(\frac{1}{2}^+,3^+)$	E_{3-}	$\frac{9}{2}\|E_{3-}\|^2(1+6x^2-5x^4)$
M2	$(2^-,\frac{1}{2}^+)$	$\frac{3}{2}^-$	$(\frac{1}{2}^+,2^-)$	M_{2-}	$\frac{9}{2}\|M_{2-}\|^2(1+x^2)$
		$\frac{5}{2}^-$	$(\frac{1}{2}^+,2^-)$	M_{2+}	$\frac{9}{2}\|M_{2+}\|^2(1+6x^2-5x^4)$

The helicity elements are related to the multipole amplitudes via:

$$A_{l+} = \frac{1}{2}[(l+2)E_{l+} + lM_{l+}] \qquad A_{(l+1)-} = \frac{1}{2}[-lE_{(l+1)-} + (l+2)M_{(l+1)-}] \tag{80}$$

$$B_{l+} = E_{l+} - M_{l+} \qquad B_{(l+1)-} = E_{(l+1)-} + M_{(l+1)-} \ . \tag{81}$$

An advantage of this parameterization is the close connection between the helicity elements and the electromagnetic resonance couplings:

$$\begin{aligned} A_{1/2} &= \sqrt{2\pi\alpha/k^\star}\langle N^\star, J_z = +\frac{1}{2}|J_{em}|N, S_z = -\frac{1}{2}\rangle \\ A_{3/2} &= \sqrt{2\pi\alpha/k^\star}\langle N^\star, J_z = +\frac{3}{2}|J_{em}|N, S_z = +\frac{1}{2}\rangle \end{aligned} \tag{82}$$

which for a Breit-Wigner form of the resonances is given by [36]:

$$\begin{aligned} A_{1/2} &= \mp(1/C_{Nm})\sqrt{(2J+1)\pi\frac{q^\star}{k^\star}\frac{M_R}{m_N}\frac{\Gamma_R^2}{\Gamma_m}}\ Im[A_{l\pm}(W=M_R)] \\ A_{3/2} &= \pm(1/C_{Nm})\sqrt{(2J+1)\pi\frac{q^\star}{k^\star}\frac{M_R}{m_N}\frac{\Gamma_R^2}{\Gamma_m}}\ \sqrt{(2J-1)(2J+3)/16}\ Im[B_{l\pm}(W=M_R)] \end{aligned} \tag{83}$$

where m_N is the nucleon mass, M_R, Γ_R are resonance position and width, respectively, Γ_m is the partial width for the used decay channel, and J the momentum of the resonance. For pion photoproduction

C_{Nm} is the Clebsch-Gordan coefficient for the decay of the resonance ($I = 1/2$ $N^\star$ or $I = 3/2$ Δ) into the relevant Nπ charge state (note that due to the phase convention eq. (84) an additional minus sign appears for π^+ mesons). C_{Nm} equals -1 for η-photoproduction.

6.4 Isospin Amplitudes

In the notation $|I, I_3\rangle$ the isospin part of the wave-functions for the nucleon and the pion (or any other isovector meson) is written as:

$$|p\rangle = |\frac{1}{2}, +\frac{1}{2}\rangle \quad |n\rangle = |\frac{1}{2}, -\frac{1}{2}\rangle \tag{84}$$

$$|\pi^+\rangle = -|1, +1\rangle \quad |\pi^o\rangle = |1, 0\rangle \quad |\pi^-\rangle = |1, -1\rangle \ . \tag{85}$$

The nucleon - pion states are then given by:

$$\begin{aligned}
|\pi^+ p\rangle &= -|\frac{3}{2}, +\frac{3}{2}\rangle \\
|\pi^o p\rangle &= \sqrt{\frac{2}{3}}|\frac{3}{2}, +\frac{1}{2}\rangle - \sqrt{\frac{1}{3}}|\frac{1}{2}, +\frac{1}{2}\rangle \\
|\pi^- p\rangle &= \sqrt{\frac{1}{3}}|\frac{3}{2}, -\frac{1}{2}\rangle - \sqrt{\frac{2}{3}}|\frac{1}{2}, -\frac{1}{2}\rangle \\
|\pi^+ n\rangle &= -\sqrt{\frac{1}{3}}|\frac{3}{2}, +\frac{1}{2}\rangle - \sqrt{\frac{2}{3}}|\frac{1}{2}, +\frac{1}{2}\rangle \\
|\pi^o n\rangle &= \sqrt{\frac{2}{3}}|\frac{3}{2}, -\frac{1}{2}\rangle + \sqrt{\frac{1}{3}}|\frac{1}{2}, -\frac{1}{2}\rangle \\
|\pi^- n\rangle &= |\frac{3}{2}, -\frac{3}{2}\rangle
\end{aligned} \tag{86}$$

where the first and last state cannot occur in photoproduction reactions. The isospin amplitudes of eq. (10) follow from this wave-functions and the definitions in eq. (9).
Different sets of the isospin amplitudes are used in the literature. Alternative sets of amplitudes are:

$$\begin{aligned}
A(\gamma p \to \pi^+ n) &= \sqrt{2}\,(A^0 + A^-) & A(\gamma p \to \pi^o p) &= (A^+ + A^0) \\
A(\gamma n \to \pi^- p) &= \sqrt{2}\,(A^0 - A^-) & A(\gamma n \to \pi^o n) &= (A^+ - A^0)\ ,
\end{aligned} \tag{87}$$

with:

$$A^{IS} = -3\sqrt{3}A^0, \qquad A^{IV} = \sqrt{\frac{1}{3}}(A^+ + 2A^-), \qquad A^{V3} = \sqrt{\frac{2}{3}}(A^+ - A^-)\ , \tag{88}$$

and:

$$\begin{aligned}
A(\gamma p \to \pi^+ n) &= \sqrt{2}\,(A^{(0)} + \frac{1}{3}A^{(\frac{1}{2})} - \frac{1}{3}A^{(\frac{3}{2})}) \\
A(\gamma p \to \pi^o p) &= A^{(0)} + \frac{1}{3}A^{(\frac{1}{2})} + \frac{2}{3}A^{(\frac{3}{2})} \\
A(\gamma n \to \pi^- p) &= \sqrt{2}\,(A^{(0)} - \frac{1}{3}A^{(\frac{1}{2})} + \frac{1}{3}A^{(\frac{3}{2})}) \\
A(\gamma n \to \pi^o n) &= -A^{(0)} + \frac{1}{3}A^{(\frac{1}{2})} + \frac{2}{3}A^{(\frac{3}{2})}\ ,
\end{aligned} \tag{89}$$

with:

$$A^{(0)} = A^0, \qquad A^{(\frac{1}{2})} = A^+ + 2A^-, \qquad A^{(\frac{3}{2})} = A^+ - A^-\ , \tag{90}$$

where sometimes the following abbreviations are used:

$${}_pA^{1/2} = A^{(0)} + \frac{1}{3}A^{(\frac{1}{2})} \qquad {}_nA^{1/2} = A^{(0)} - \frac{1}{3}A^{(\frac{1}{2})}\ . \tag{91}$$

References

[1] F.X. Lee, D. B. Leinweber, L. Zhou, J. Zanotti, S. Choe, *Nucl. Phys.* B (Proc. Suppl.) 106 (2002) 248

[2] F.X. Lee and D.B. Leinweber, *Nucl. Phys.* B (Proc. Suppl.) 73 (1999) 258

[3] S. Sasaki, *Nucl. Phys.* B (Proc. Suppl.) 83 (2000) 206

[4] D.G. Richards, *Nucl. Phys.* B (Proc. Suppl.) 94 (2001) 269

[5] M. Gell-Mann, *Phys. Lett.* 8 (1964) 214

[6] O.W. Greenberg, *Phys. Rev. Lett.* 13 (1964) 598

[7] R.H. Dalitz, *Proceedings of the XII Int. Conf. on High Energy Physics Berkeley, Calif.* (1966)

[8] L.A. Copley, G. Karl, and E. Obryk, *Nucl. Phys.* B 13 (1969) 303

[9] R.P. Feynman, M. Kislinger, and F. Ravndal, *Phys. Rev.* D 3 (1971) 2706

[10] R. Koniuk and N. Isgur, *Phys. Rev.* D 21 (1980) 1868

[11] S. Capstick and W. Roberts, *Prog. Part. Nucl. Phys.* 45 (2000) S241

[12] M. Anselmino et al., *Rev. Mod. Phys.* 65 (1993) 1199

[13] R. Bijker, F. Iachello, A. Leviatan, *Ann. Phys.* 236 (1994) 69

[14] R. Bijker, F. Iachello, and A. Leviatan, *Phys. Rev.* D 55 (1997) 2862

[15] L.Ya. Glozman and D.O. Riska, *Phys. Rep.* 268 (1996) 263

[16] L.Ya. Glozman and D.O. Riska, *Phys. Lett.* B 366 (1996) 305

[17] N. Bianchi et al., *Phys. Rev.* C 54 (1996) 1688

[18] P. Moskal, M. Wolke, A. Khoukaz, W. Oelert, *Prog. Part. Nucl. Phys.* 49 (2002) 1

[19] R.E. Cutkosky et al., *Phys. Rev.* D 20 (1979) 2804; 2839

[20] R.L. Kelly and R.E. Cutkosky, *Phys. Rev.* D 20 (1979) 2782

[21] G. Höhler et al., *Handbook of Pion-Nucleon Scattering, Physics Data No.* 12 (1979) 1

[22] R. Koch and E. Pietarinen, *Nucl. Phys.* A 336 (1980) 331

[23] R. Koch, *Z. Phys.* C 29 (1985) 597; *Nucl. Phys.* A 448 (1986) 707

[24] D.M. Manley, E.M. Saleski, *Phys. Rev.* D 45 (1992) 4002

[25] R.A. Arndt, I.I. Strakovsky, R.L. Workman, M.M. Pavan, *Phys. Rev.* C 52 (1995) 2120

[26] T.P. Vrana, S.A. Dytman, T.-S.H. Lee, *Phys. Rep.* 328 (2000) 182

[27] R. Koniuk and N. Isgur, *Phys. Rev. Lett.* 44 (1980) 845

[28] S. Capstick and W. Roberts, *Phys. Rev.* D 49 (1994) 4570

[29] Th. Frommhold et al., *Phys. Lett.* B 295 (1992) 28

[30] N. Bianchi et al., *Phys. Lett.* B 299 (1993) 219

[31] N. Bianchi et al., *Phys. Lett.* B 325 (1994) 333

[32] M. Röbig-Landau et al., *Phys. Lett.* B 373 (1996) 45

[33] B. Krusche et al., *Phys. Rev. Lett.* 86 (2001) 4764

[34] D.M. Manley and C. Bennhold, *Proceedings NSTAR2002 Workshop, Pittsburgh, USA 9. -12. October 2002, World Scientific, in press* (2003)

[35] C. Bennhold, *Proceedings NSTAR2002 Workshop, Pittsburgh, USA 9. -12. October 2002, World Scientific, in press* (2003)

[36] D.E. Groom et al. (The Review of Particle Physics), *Eur. Phys. J.* C 15 (2000) 1

[37] D. Drechsel and L. Tiator, *J. Phys.* G 18 (1992) 449

[38] M. Benmerrouche and N.C. Mukhopadhyay, *Phys. Rev. Lett.* 67 (1991) 1070
[39] M. Benmerrouche and N.C. Mukhopadhyay, *Phys. Rev.* D 51 (1995) 3237
[40] M. Benmerrouche, N.C. Mukhopadhyay, J.F. Zhang, *Phys. Rev. Lett.* 77 (1996) 4716
[41] G.F. Chew, M.L. Goldberger, F.E. Low, and Y. Nambu, *Phys. Rev.* 106 (1957) 1345
[42] I.S. Barker, A. Donnachie, J.K. Storrow, *Nucl. Phys.* B 95 (1975) 347
[43] G. Knöchlein, D. Drechsel, L. Tiator, *Z. Phys.* A 352 (1995) 327
[44] G. Keaton and R. Workman, *Phys. Rev.* C 53 (1996) 1434; *Phys. Rev.* C 54 (1996) 1437
[45] W.T. Chiang and F. Tabakin, *Phys. Rev.* C 55 (1997) 2054
[46] C. Bennhold, *private communication.*
[47] M. Pichowsky, C. Svakli, F. Tabakin, *Phys. Rev.* C 53 (1996) 593
[48] C. Svakli, F. Tabakin, S.N. Yang, *Phys. Rev.* C 53 (1996) 1132
[49] W.M. Kloet, F. Tabakin, *Phys. Rev.* C 61 (2000) 015501
[50] K.M. Watson *Phys. Rev.* 85 (1952) 852
[51] R.L. Walker, *Phys. Rev.* 182 (1969) 1729
[52] I. Arai and H. Fujii, *Nucl. Phys.* B 194 (1982) 251
[53] R.L. Crawford and W.T. Morton, *Nucl. Phys.* B 211 (1983) 1
[54] O. Hanstein, D. Drechsel, L. Tiator, *Nucl. Phys.* A 632 (1998) 561
[55] R.A. Arndt, R.L. Workman, Z.J. Li, L.D. Roper, *Phys. Rev.* C 42 (1990) 1853; 1864
[56] Z.J. Li, R.A. Arndt, L.D. Roper, R.L. Workman, *Phys. Rev.* C 47 (1993) 2759
[57] R.A. Arndt, I.I Strakovsky, R.L. Workman, *Phys. Rev.* C 53 (1996) 430
[58] R.A. Arndt, W.J. Briscoe, I.I. Strakovsky, R.L. Workman, *Phys. Rev.* C 66 (2002) 055213
[59] R.A. Arndt, I.I. Starkovsky, R.L. Workman, *Int. J. Mod. Phys.* A 18 (2003) 449
[60] SAID homepage: http://gwdac.phys.gwu.edu
[61] W.J. Metcalf and R.L. Walker, *Nucl. Phys.* B 76 (1974) 253
[62] H.R. Hicks, S.R. Deans, D.T. Jocabs, P.W. Lyons, D.L. Montgomery, *Phys. Rev.* D 7 (1973) 2614
[63] R.M. Davidson, N.C. Mukhopadhyay and R.S. Wittmann, *Phys. Rev.* D 43 (1991) 71
[64] M.G. Olsson and E.T. Osypowski, *Nucl. Phys.* B 87 (1975) 399 ; *Phys. Rev.* D 17 (1978) 174
[65] H. Garcilazo and E. Moya de Guerra, *Nucl. Phys.* A 562 (1993) 521
[66] I. Blomqvist and J.M. Laget, *Nucl. Phys.* A 280 (1977) 405
[67] D. Drechsel, O. Hanstein, S.S. Kamalow, L. Tiator, *Nucl. Phys.* A 645 (1999) 145 ,
[68] W.-T. Chiang, S.N. Yang, L. Tiator, D. Drechsel, *Nucl. Phys.* A 700 (2002) 429
[69] MAID homepage: *http://www.kph.uni-mainz.de/MAID/maid.html*
[70] C. Sauermann, B.L. Friman, W. Nörenberg, *Phys. Lett.* B 341 (1995) 261 ;
C. Sauermann, *PhD thesis, TH Darmstadt (1996), unpublished* (1996)
[71] H. Tanabe and K. Otha, *Phys. Rev.* C 31 (1985) 1876
[72] S.N. Yang *J. Phys.* G 11 (1985) L205
[73] S. Nozawa, B. Blankleider and T.-S. H. Lee, *Nucl. Phys.* A 513 (1990) 459
[74] S. Sato and T.-S. H. Lee, *Phys. Rev.* C 54 (1996) 2660
[75] C. Bennhold et al., *Proceedings NSTAR2001 Workshop, Mainz 7. -10. March 2001, World Scientific 2001, ISBN 981-02-4760-5, Edts. D. Drechsel, L. Tiator,* (2001) 109
[76] T. Feuster and U. Mosel, *Phys. Rev.* C 58 (1998) 457

[77] T. Feuster and U. Mosel, *Phys. Rev.* C 59 (1999) 460
[78] G. Penner and U. Mosel, *Phys. Rev.* C 66 (2002) 055211; 055212
[79] D.M. Manley, *Few-Body Systems Suppl.* 11 (1999) 104
[80] Zhenping Li, *Phys. Rev.* D 52 (1995) 4961
[81] Zhenping Li, *Phys. Rev.* C 52 (1995) 1648
[82] Zhenping Li, Hongxing Ye, and Minghui Lu, *Phys. Rev.* C 56 (1997) 1099
[83] Qiang Zhao, Zhenping Li, and C. Bennhold, *Phys. Rev.* C 58 (1998) 2393; *Phys. Lett.* B 436 (1998) 42
[84] Q. Zhao, J.S. Al-Khalili, Z.P. Li, R.L. Workman, *Phys. Rev.* C 65 (2002) 065204
[85] A. Manohar and H. Georgi, *Nucl. Phys.* B 234 (1984) 189
[86] BRAG homepage: *http://cnr2.kent.edu/∼manley/BRAG.html*
[87] R.A. Arndt et al., *Proceedings NSTAR2001 Workshop, Mainz 7. -10. March 2001, World Scientific 2001, ISBN 981-02-4760-5, Edts. D. Drechsel, L. Tiator,* (2001) 467
[88] M. Fuchs et al., *Phys. Lett.* B 368 (1996) 20
[89] F. Härter, *PhD thesis, University of Mainz (1996) KPH15/96* (1996)
[90] K. Büchler et al., *Nucl. Phys.* A 570 (1994) 580
[91] I.G. Aznauryan, *Phys. Rev.* C 67 (2003) 015209
[92] A. De Rujula, H. Georgi, and S.L. Glashaw, *Phys. Rev.* D 12 (1975) 147
[93] S.S. Gersteyn and G.V. Dzhikiya, *Sov. J. Nucl. Phys.* 34 (1981) 870
[94] N. Isgur, G. Karl, and R. Koniuk, *Phys. Rev.* D 25 (1982) 2394
[95] D. Drechsel and M.M. Giannini, *Phys. Lett.* B 143 (1984) 329
[96] A.J. Buchmann, E. Hernandez, and A. Faessler, *Phys. Rev.* C 55 (1997) 448
[97] A.J. Buchmann, *Z. Naturforsch.* 52 a (1997) 877
[98] A. Faessler, *Prog. Part. Nucl. Phys.* 44 (2000) 197
[99] A.J. Buchmann , E.M. Henley, *Phys. Rev.* D 65 (2002) 073017
[100] S. Capstick and G. Karl, *Phys. Rev.* D 41 (1990) 2767
[101] S. Capstick, *Phys. Rev.* D 46 (1992) 2864
[102] G. Kälbermann, and J.M. Eisenberg, *Phys. Rev.* D 28 (1983) 71
[103] K. Bermuth, D. Drechsel, L. Tiator, and J.B. Seaborn, *Phys. Rev.* D 37 (1988) 89
[104] A. Wirzba and W. Weise, *Phys. Lett.* B 188 (1987) 6
[105] D. B. Leinbweber, T. Draper, R.M. Woloshyn, *Phys. Rev.* D 48 (1993) 2230
[106] R. Beck et al., *Phys. Rev. Lett.* 78 (1997) 606
[107] R. Beck et al., *Phys. Rev.* C 61 (2000) 035204
[108] G. Blanpied et al., *Phys. Rev. Lett.* 79 (1997) 4337
[109] A.M. Sandorfi et al., *Nucl. Phys.* A 629 (1998) 171c
[110] K.M. Watson, *Phys. Rev.* 95 (1954) 228
[111] C.E. Thorn et al., *Nucl. Instr. and Meth.* A 285 (1989) 447
[112] I. Anthony et al., *Nucl. Instr. and Meth.* A 301 (1991) 230
[113] D. Lohmann et al., *Nucl. Instr. and Meth.* A 343 (1994) 494
[114] G. Galler et al., *Phys. Lett.* B 503 (2001) 245
[115] S. Wolf et al., *Eur. Phys. J.* A 12 (2001) 231

[116] G. Blanpied et al., *Phys. Rev.* C 64 (2001) 025203
[117] H. Genzel, *Z. Phys.* 268 (1974) 37
[118] H. Genzel et al., *Z. Phys.* 268 (1974) 43
[119] G. Fischer, J. Stumpfig, G. Knop, G.V. Holtey, *Z. Phys.* 253 (1972) 38
[120] R.M. Davidson, N.C. Mukhopadhyay, *Phys. Rev. Lett.* 79 (1997) 4509
[121] R.L. Workman, *Phys. Rev. Lett.* 79 (1997) 4511
[122] R. Beck, H.P. Krahn *Phys. Rev. Lett.* 79 (1997) 4510, 4512
[123] G. Blanpied et al., *Phys. Rev. Lett.* 69 (1992) 1880
[124] A.A. Belyaev et al., *Nucl. Phys.* B 213 (1983) 201
[125] V.A. Getman et al., *Nucl. Phys.* B 188 (1981) 397
[126] A.A. Belyaev et al., *Sov. J. Nucl. Phys.* 40 (1984) 83
[127] A.A. Belyaev et al., *Sov. J. Nucl. Phys.* 43 (1986) 947
[128] H. Dutz et al., *Nucl. Phys.* A 601 (1996) 319
[129] D. Menze, W. Pfeil, R. Wilcke, *Compilation of Pion Photoproduction Data, Univ. Bonn, Publisher: H. Behrens, G. Ebel, Zentralstelle für Atomkernenergie-Dokumentation* 7-1 (1977)
[130] V. Rossi et al., *Nuovo Cimento* A 13 (1973) 59
[131] A. Bagheri et al., *Phys. Rev.* C 38 (1988) 875
[132] R.L. Workman, *Proceedings of the 8th Int. Conf. on the Structure of Baryons Bonn, Germany 1982, Edts. D.W. Menze, B. Ch. Metsch, World Scientific, ISBN 981-02-3865-7* (1999) 717; *nucl-th/9810013*
[133] L. Tiator, D. Drechsel, O. Hanstein, S.S. Kamalov, and S.N. Yang, *Nucl. Phys.* A 689 (2001) 205c
[134] S.S. Kamalov and S.N. Yang, *Phys. Rev. Lett.* 83 (1999) 4494
[135] T. Sato and T.-S. H. Lee, *Phys. Rev.* C 63 (2001) 055201
[136] P. Bartsch et al., *Phys. Rev. Lett.* 88 (2002) 142001
[137] S.J. Brodsky, G.P. Lepage, and S.A.A. Zaidi, *Phys. Rev.* D 23 (1981) 1152
[138] C.E. Carlson and J.L. Poor, *Phys. Rev.* D 38 (1988) 2758
[139] C.E. Carlson and N.C. Mukhopadhyay, *Phys. Rev. Lett.* 81 (1998) 2646
[140] C. Mertz et al., *Phys. Rev. Lett.* 86 (2001) 2963
[141] F. Kalleicher et al., *Z. Phys.* A 359 (1997) 201
[142] R.W. Gothe, *Prog. Part. Nucl. Phys.* 44 (2000) 185
[143] V.V. Frolov et al., *Phys. Rev. Lett.* 82 (1999) 45
[144] K. Joo et al. (The CLAS Collaboration), *Phys. Rev. Lett.* 88 (2002) 122001
[145] T. Pospischil et al., *Phys. Rev. Lett.* 86 (2001) 2959
[146] C. Papanicolas, *Proceedings NSTAR2001 Workshop, Mainz 7. -10. March 2001, World Scientific 2001, ISBN 981-02-4760-5, Edts. D. Drechsel, L. Tiator,* (2001) 11
[147] G.A. Warren et al., *Phys. Rev.* C 58 (1998) 3722
[148] S.B. Gerasimov, *Sov. J. Nucl. Phys.* 2 (1966) 430
[149] S.D. Drell, A.C. Hearn, *Phys. Rev. Lett.* 16 (1966) 908
[150] C. Bradtke et al., *Nucl. Instr. and Meth.* A 436 (1999) 430
[151] S. Goertz, W. Meyer, G. Reicherz, *Prog. Part. Nucl. Phys.* 49 (2002) 403
[152] J. Ahrens et al., *Phys. Rev. Lett.* 84 (2000) 5950
[153] J. Ahrens et al., *Phys. Rev. Lett.* 87 (2001) 022003

[154] J. Ahrens et al., *Phys. Rev. Lett.* 88 (2002) 232002
[155] J. Ahrens et al., *Phys. Lett.* B 551 (2003) 49
[156] O. Stern und R. Frisch, *Z. Phys.* 85 (1933) 4
[157] F. Schlumpf, *Phys. Rev.* D 48 (1993) 4478
[158] S.T. Hong and D.P. Min, *nucl-th/9909004* (1999)
[159] H.C. Kim, M. Praszalowicz, and K. Goeke, *Phys. Rev.* D 57 (1998) 2859
[160] M.N. Butler, M.J. Savage, and R.P. Springer, *Phys. Rev.* D 49 (1994) 3459
[161] F.X. Lee, *Phys. Rev.* D 57 (1998) 1801
[162] T.M. Aliev, A. Özpineci, M. Savci, *Nucl. Phys.* A 678 (2000) 443
[163] D.B. Leinweber, T. Draper, and R.M. Woloshyn, *Phys. Rev.* D 46 (1992) 3067
[164] M. Arman et al., *Phys. Rev. Lett.* 29 (1972) 962
[165] B.M.K. Nefkens et al., *Phys. Rev.* D 18 (1978) 3911
[166] A. Bosshard et al., *Phys. Rev.* D 44 (1991) 1962
[167] G.L. Castro, A. Mariano, *Nucl. Phys.* A 697 (2002) 440
[168] D.H. Lin, M.K. Liou, *Phys. Rev.* C 43 (1991) R930
[169] D.H. Lin, M.K. Liou, Z.M. Ding, *Phys. Rev.* C 44 (1991) 1819
[170] R. Wittman, *Phys. Rev.* C 37 (1988) 2075
[171] L. Heller, S. Kumano, J.C. Martinez, E.J. Moniz, *Phys. Rev.* C 35 (1987) 718
[172] L. Kontratyuk and L. Ponomarev, *Sov. J. Nucl. Phys.* 7 (1968) 82
[173] M. Kotulla, *PhD thesis, University of Giessen (2001), unpublished* (2001)
[174] M. Kotulla et al., *Phys. Rev. Lett.* 89 (2002) 272001
[175] R. Novotny, *IEEE Trans. Nucl. Sci.* 38 (1991) 379
[176] A.R. Gabler et al., *Nucl. Instr. and Meth.* A 346 (1994) 168
[177] A.I. Machavariani et al., *Nucl. Phys.* A 646 (1999) 231 ; erratum: 686 (2001) 601
[178] D. Drechsel, M. Vanderhaeghen, M.M. Giannini, *Phys. Lett.* B 484 (2000) 236
[179] D. Drechsel, M. Vanderhaeghen, *Phys. Rev.* C 64 (2001) 065202
[180] W.-T. Chiang, S.N. Yang, M. Vanderhaeghen, D. Drechsel, *nucl-th/0211061* (2002)
[181] P. Benz et al., *Nucl. Phys.* B 65 (1973) 158
[182] G. Chiefari, E. Drago, M. Napolitano, and C. Sciacca, *Lett. Nuovo Cimento* 13 (1975) 129
[183] M. Asai et al., *Phys. Rev.* C 42 (1990) 837
[184] R.W. Clifft et al., *Phys. Rev. Lett.* 33 (1974) 1500
[185] G. von Holtey, G. Knop, H. Stein, J. Stümpfig, and H. Wahlen, *Z. Phys.* 259 (1973) 51
[186] E. Hilger, H.J. Roegler, L.M. Simons, and M. Tonutti, *Nucl. Phys.* B 93 (1975) 7
[187] B. Bouquet et al., *Phys. Lett.* B 41 (1972) 536
[188] B. Bouquet et al., *Nucl. Phys.* B 79 (1974) 45
[189] J.C. Bergstrom et al., *Phys. Rev.* C 57 (1998) 3203
[190] B. Krusche et al., *Eur. Phys. J.* A 6 (1999) 309
[191] U. Siodlaczek et al., *Eur. Phys. J.* A 10 (2001) 365
[192] S.S. Kamalov, L. Tiator, C. Bennhold, *Phys. Rev.* C 55 (1997) 98
[193] J.M. Laget, *Phys. Rep.* 69 (1981) 1 , and priv. com.
[194] P. Wilhelm and H. Arenhövel, *Nucl. Phys.* A 593 (1995) 435 ; *Nucl. Phys.* A 609 (1996) 469

[195] R. Schmidt, H. Arenhövel, and P. Wilhelm, *Z. Phys.* A 355 (1996) 421 , and priv. com.
[196] F. Blaazer, B.L.G. Bakker, H.J. Boersma, *Nucl. Phys.* A 590 (1995) 750
[197] F. Rambo et al., *Nucl. Phys.* A 660 (1999) 69
[198] D. Drechsel et al., *Nucl. Phys.* A 660 (1999) 423
[199] B. Krusche et al., *Phys. Lett.* B 526 (2002) 287
[200] T.A. Armstrong et al., *Nucl. Phys.* B 41 (1972) 445
[201] M. MacCormick et al., *Phys. Rev.* C 53 (1996) 41
[202] V.M. Kolybasov, V.G. Ksenzov, *Sov. J. Nucl. Phys.* 22 (1975) 372
[203] M.I. Levchuk, M. Schumacher, F. Wissmann, *nucl-th/0011041* (2000)
[204] E.M. Darwish, H. Arenhövel, M. Schwamb, *Eur. Phys. J.* A 16 (2003) 111
[205] B. Krusche et al., *Phys. Rev. Lett.* 74 (1995) 3736
[206] B. Krusche et al., *Phys. Rev. Lett.* 75 (1995) 3023
[207] G. Audit et al., *Nucl. Instr. and Meth.* A 301 (1991) 473
[208] G. Höhler, A. Schulte, *πN Newslett.* 7 (1992) 94
[209] G. Höhler, *πN Newslett.* 9 (1993) 1
[210] N. Kaiser, P.B. Siegel, W. Weise, *Phys. Lett.* B 362 (1995) 23
[211] N. Kaiser, T. Waas, W. Weise, *Nucl. Phys.* A 612 (1997) 297
[212] B. Metsch, *Baryon Excitations, Lectures of the COSY Workshop held at the Forschungszentrum Jülich, 2 to 3 May 2000, Edts. T. Barnes and H.P. Morsch, ISBN 3-89336-273-8* (2000) 73
[213] U. Löring, K. Kretzschmar, B.C. Metsch, H.R. Petry, *Eur. Phys. J.* A 10 (2001) 309
[214] U. Löring, B.C. Metsch, H.R. Petry, *Eur. Phys. J.* A 10 (2001) 395
[215] U. Löring, B.C. Metsch, H.R. Petry, *Eur. Phys. J.* A 10 (2001) 447
[216] B. Schwesinger, *Nucl. Phys.* A 537 (1992) 253
[217] Zhenping Li, Volker Burkert, Zhujun Li, *Phys. Rev.* D 46 (1992) 70
[218] O. Krehl, C. Hannhart, S. Krewald, J. Speth, *Phys. Rev.* C 62 (2000) 025207
[219] H.P. Morsch, P. Zupranski, *Phys. Rev.* C 61 (2000) 024002
[220] *Baryon Excitations, Lectures of the COSY Workshop held at the Forschungszentrum Jülich, 2 to 3 May 2000, Edts. T. Barnes and H.P. Morsch, ISBN 3-89336-273-8* (2000)
[221] N.C. Mukhopadhyay and N. Mathur, *Phys. Lett.* B 444 (1998) 7
[222] L. Tiator, D. Drechsel, G. Knöchlein, C. Bennhold, *Phys. Rev.* C 60 (1999) 035210
[223] F.E. Close, Z. Li, *Phys. Rev.* D 42 (1990) 2194
[224] J. Ajaka et al., *Phys. Lett.* B 475 (2000) 372
[225] O. Bartalini et al., *Phys. Lett.* B 544 (2002) 113
[226] F.V. Adamian et al., *Phys. Rev.* C 63 (2001) 054606
[227] A. Bock et al., *Phys. Rev. Lett.* 81 (1998) 534
[228] R. Workman, R.A. Arndt, I.I. Strakovsky, *Phys. Rev.* C 62 (2000) 048201
[229] C. Gerhardt, *Z. Phys.* C 4 (1980) 311
[230] T. Barnes and F.E. Close, *Phys. Lett.* B 123 (1983) 89
[231] T. Barnes and F.E. Close, *Phys. Lett.* B 128 (1983) 277
[232] R. Beck, priv. com. (2001)
[233] M. Lacombe et al., *Phys. Lett.* B 101 (1981) 139

[234] K.H. Althoff et al., *Z. Phys.* C 1 (1979) 327

[235] Z. Li, R. Workman *Phys. Rev.* C 53 (1996) R549

[236] P.S. Kummer et al., *Phys. Rev. Lett.* 30 (1973) 873

[237] U. Beck et al., *Phys. Lett.* B 51 (1974) 103

[238] J.C. Alder et al., *Nucl. Phys.* B 91 (1975) 386

[239] H. Breuker et al., *Phys. Lett.* B 74 (1978) 409

[240] F.W. Brasse et al., *Nucl. Phys.* B 139 (1978) 37

[241] F.W. Brasse et al., *Z. Phys.* C 22 (1984) 33

[242] F. Tabakin, S.A. Dytman, A.S. Rosenthal, *Proceedings of the Excited Baryons Conf., Troy, New York, USA 4-6 August 1988, Edts. G. Adams, N.C. Mukhopadhyay, P. Stoler, World Scientific* (1989) 168

[243] J.W. Price et al., *Phys. Rev.* C 51 (1995) R2283

[244] B. Schoch, *Prog. Part. Nucl. Phys.* 34 (1995) 43; M. Wilhelm, *PhD thesis, Univ. Bonn* (1993)

[245] B. Krusche et al., *Z. Phys.* A 351 (1995) 237

[246] B. Krusche, N.C. Mukhopadhyay, J.F. Zhang, M. Benmerrouche, *Phys. Lett.* B 397 (1997) 171

[247] S. Homma et al., *J. Phys. Soc. Japan* 57 (1988) 828

[248] F. Renard et al., *Phys. Lett.* B 528 (2002) 215

[249] B. Saghai and Z. Li, *Eur. Phys. J.* A 11 (2001) 217

[250] G.Y. Chen, S.S. Kamalov, S.N. Yang, D. Drechsel, L. Tiator, *nucl-th/0210013* (2002)

[251] M. Batinić, I. Šlaus, A. Švarc, B.M.K. Nefkens, *Phys. Rev.* C 51 (1995) 2310

[252] A.M. Green, S. Wycech, *Phys. Rev.* C 55 (1997) R2167

[253] N.C. Mukhopadhyay, J.F. Zhang, M. Benmerrouche, *Phys. Rev. Lett.* 75 (1995) 3022

[254] R. Thompson et al., *Phys. Rev. Lett.* 86 (2001) 1702

[255] C.S. Armstrong et al., *Phys. Rev.* D 60 (1999) 052004

[256] W. Konen, H.J. Weber, *Phys. Rev.* D 41 (1990) 2201

[257] S. Capstick, B.D. Keister, *Phys. Rev.* D 51 (1995) 3598

[258] J. Ajaka et al., *Phys. Rev. Lett.* 81 (1998) 1797

[259] M. Dugger et al., *Phys. Rev. Lett.* 89 (2002) 222002

[260] C. Bacci et al., *Phys. Lett.* B 28 (1969) 687

[261] R.L. Anderson, R. Prepost *Phys. Rev. Lett.* 23 (1969) 46

[262] B. Krusche et al., *Phys. Lett.* B 358 (1995) 40

[263] P. Hoffmann-Rothe et al., *Phys. Rev. Lett.* 78 (1997) 4697

[264] V. Hejny et al., *Eur. Phys. J.* A 6 (1999) 83

[265] J. Weiss et al., *Eur. Phys. J.* A 11 (2001) 371

[266] V. Hejny et al., *Eur. Phys. J.* A 13 (2002) 493

[267] J. Weiss et al., *Eur. Phys. J.* A 16 (2003) 275

[268] M. Pfeiffer, *PhD thesis, University of Giessen (2002), unpublished* (2002)

[269] A. Fix, H. Arenhövel, *Z. Phys.* A 359 (1997) 427; *Phys. Lett.* B 492 (2000) 32; *Eur. Phys. J.* A 9 (2000) 119; *Phys. Rev.* C 66 (2002) 024002; *Nucl. Phys.* A 697 (2002) 277

[270] A. Sibirtsev et al., *Phys. Rev.* C 64 (2001) 024006

[271] A. Sibirtsev et al., *Phys. Rev.* C 65 (2002) 044007; 067002

[272] N.C. Mukhopadhyay, J.F. Zhang, M. Benmerrouche, *Phys. Lett.* B 364 (1995) 1
[273] F. Ritz, H. Arenhövel, *Phys. Lett.* B 447 (1999) 15
[274] F. Ritz, H. Arenhövel, *Phys. Rev.* C 64 (2001) 034005
[275] ABBHHM-collaboration, *Phys. Rev.* 175 (1968) 1669
[276] G. Gialanella et al., *Nuovo Cimento* A LXIII (1969) 892
[277] A. Piazza et al., *Lett. Nuovo Cimento* III (1970) 403
[278] Cambridge Bubble Chamber group, *Phys. Rev.* 155 (1967) 1477 ; *Phys. Rev.* 163 (1967) 1510
[279] H.R. Crouch et al., *Phys. Rev. Lett.* 13 (1964) 636; 640
[280] H.G. Hilpert et al., *Phys. Lett.* 23 (1966) 707
[281] A. Braghieri et al., *Phys. Lett.* B 363 (1995) 46
[282] F. Härter et al., *Phys. Lett.* B 401 (1997) 229
[283] A. Zabrodin et al., *Phys. Rev.* C 55 (1997) R1617
[284] A. Zabrodin et al., *Phys. Rev.* C 60 (1999) 055201
[285] M. Wolf et al., *Eur. Phys. J.* A 9 (2000) 5
[286] V. Kleber et al., *Eur. Phys. J.* A 9 (2000) 1
[287] W. Langgärtner et al., *Phys. Rev. Lett.* 87 (2001) 052001
[288] F.J. Klein, *PhD thesis, University of Bonn 1996, BONN-IR-96-08* (1996)
[289] E. Hourany, *INPC 2001, AIP Conf. Proc.* 610 (2001) 362
[290] D. Lüke and P. Söding, *Springer Tracts in Modern Physics* 59 (1971) 39
[291] J.A. Gomez Tejedor, E. Oset, *Nucl. Phys.* A 600 (1996) 413
[292] L.Y. Murphy, J.M. Laget, DAPHNIA/SPhN 96-10 (1996)
[293] K. Ochi et al., *Phys. Rev.* C 56 (1997) 1472
[294] J.A. Gomez Tejedor, F. Cano, E. Oset, *Phys. Lett.* B 379 (1996) 39
[295] J.C. Nacher et al., *Nucl. Phys.* A 695 (2001) 295
[296] F. Klingl et al., *Nucl. Phys.* A 624 (1997) 527
[297] J.C. Nacher, E. Oset, *Nucl. Phys.* A 697 (2002) 372
[298] R. Plötzke et al., *Phys. Lett.* B 444 (1998) 555
[299] J. Link, *PhD thesis, University of Bonn, unpublished* (2000)
[300] J. Barth et al. (SAPHIR collaboration), *submitted to Eur. Phys. J. A* (2003)
[301] J. Barth et al. (SAPHIR collaboration), *Eur. Phys. J. A, accepted* (2003)
[302] W. Struczinski et al., *Nucl. Phys.* B 108 (1976) 45
[303] M.Q. Tran et al., *Phys. Lett.* B 445 (1998) 20
[304] ABBHHM collaboration, *Phys. Rev.* 188 (1969) 2060
[305] T. Mart, C. Bennhold, *Phys. Rev.* C 61 (2000) 012201
[306] S. Goers et al., *Phys. Lett.* B 464 (1999) 331
[307] K.-H. Glander et al. (SAPHIR collaboration), *submitted to Eur. Phys. J. A* (2003)
[308] T. Mart, *Phys. Rev.* C 62 (2000) 038201
[309] S. Capstick and W. Roberts, *Phys. Rev.* D 58 (1998) 074011
[310] D.H. Saxon et al., *Nucl. Phys.* B 162 (1980) 522
[311] K.W. Bell et al., *Nucl. Phys.* B 222 (1983) 389
[312] S. Capstick and W. Roberts, *Phys. Rev.* D 57 (1998) 4301
[313] J. Junkersfeld for the CB-ELSA collaboration, *Acta Phys. Pol.* B 33 (2002) 941